

AD-A183 333

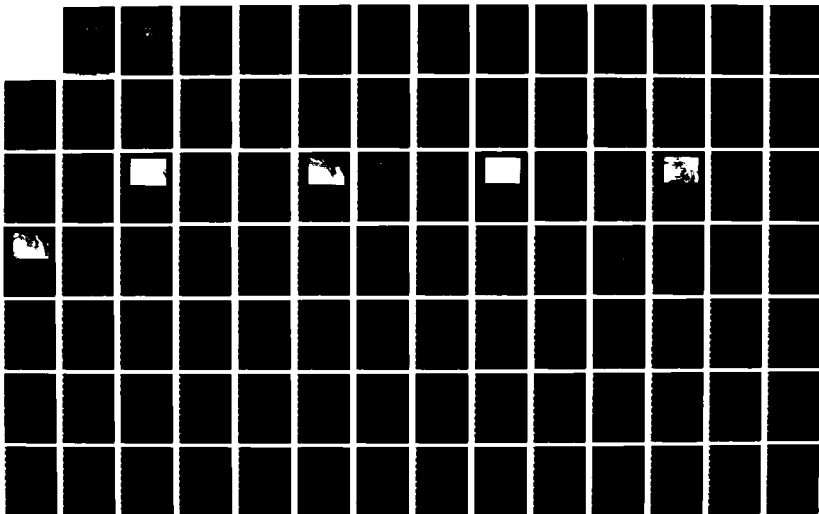
DIAGNOSTIC STUDY OF A GENESIS OF ATLANTIC LOWS
EXPRIMENT (GALE) CYCLOGENESIS EVENT(U) NAVAL
POSTGRADUATE SCHOOL MONTEREY CA D J SOPER MAR 87

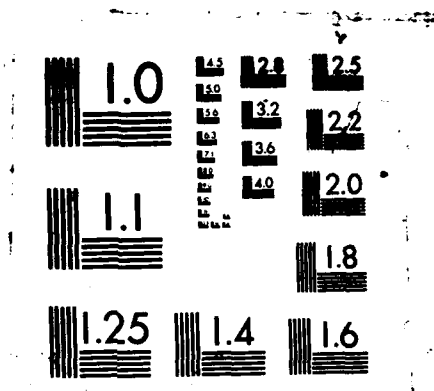
1/2

UNCLASSIFIED

F/G 4/2

NL





MICROCOPY RESOLUTION TEST CHART
NATIONAL BUREAU OF STANDARDS-1963-A

AD-A183 333

DTIC FILE COPY

2

NAVAL POSTGRADUATE SCHOOL
Monterey, California



DTIC
ELECTE
AUG 17 1987
A

THESIS

DIAGNOSTIC STUDY OF A GENESIS OF
ATLANTIC LOWS EXPERIMENT (GALE)
CYCLOGENESIS EVENT

by

Daniel J. Soper

March 1987

Thesis Advisor
Co-Advisor

R. L. Elsberry
C.-S. Liou

Approved for public release; distribution is unlimited.

87 8 13 040

REPORT DOCUMENTATION PAGE

1a REPORT SECURITY CLASSIFICATION UNCLASSIFIED			1b RESTRICTIVE MARKINGS	
2a SECURITY CLASSIFICATION AUTHORITY			3 DISTRIBUTION/AVAILABILITY OF REPORT Approved for public release; distribution is unlimited	
2b DECLASSIFICATION/DOWNGRADING SCHEDULE				
4 PERFORMING ORGANIZATION REPORT NUMBER(S)			5 MONITORING ORGANIZATION REPORT NUMBER(S)	
6a NAME OF PERFORMING ORGANIZATION Naval Postgraduate School		6b OFFICE SYMBOL (if applicable) 63	7a NAME OF MONITORING ORGANIZATION Naval Postgraduate School	
6c ADDRESS (City, State, and ZIP Code) Monterey, California 93943-5000			7b ADDRESS (City, State, and ZIP Code) Monterey, California 93943-5000	
8a NAME OF FUNDING/SPONSORING ORGANIZATION		8b OFFICE SYMBOL (if applicable)	9 PROCUREMENT INSTRUMENT IDENTIFICATION NUMBER	
9a ADDRESS (City, State, and ZIP Code)			10 SOURCE OF FUNDING NUMBERS	
			PROGRAM ELEMENT NO	PROJECT NO
			TASK NO	WORK UNIT ACCESSION NO
11 TITLE (Include Security Classification) DIAGNOSTIC STUDY OF A GENESIS OF ATLANTIC LOWS EXPERIMENT (GALE) CYCLOGENESIS EVENT				
12 PERSONAL AUTHOR(S) Soper, Daniel J.				
13a TYPE OF REPORT Master's Thesis		13b TIME COVERED FROM _____ TO _____	14 DATE OF REPORT (Year, Month, Day) 87 MARCH	15 PAGE COUNT 139
16 SUPPLEMENTARY NOTATION cont. on p. 2				
17 COSATI CODES			18 SUBJECT TERMS (Continue on reverse if necessary and identify by block number)	
FIELD	GROUP	SUB-GROUP	Extratropical Cyclogenesis; Quasi-Lagrangian Diagnostics (QLD).	
19 ABSTRACT (Continue on reverse if necessary and identify by block number) The Navy Operational Regional Atmospheric Prediction System (NORAPS) analyses and forecasts, with 80 km resolution, are used to investigate an explosive cyclogenesis event that occurred in Intensive Observation Period (IOP) 2 during 26-28 January 1986. A synoptic investigation and quasi-Lagrangian diagnostic evaluation of the primary cyclone mass, vorticity, heat and moisture budgets are discussed. Explosive development occurs with the superposition of an upper-level jet streak over a shallow surface system associated with a well-developed coastal front. The advection of shear vorticity aloft in combination with warm advection induces strong low-level convergence and spin-up of the low-level vortex. Significant surface sensible and latent heat fluxes and latent heating maxima are closely correlated with the period of rapid development from 00-12 GMT 27 January 1986.				
20 DISTRIBUTION/AVAILABILITY OF ABSTRACT <input checked="" type="checkbox"/> UNCLASSIFIED/UNLIMITED <input type="checkbox"/> SAME AS RPT <input type="checkbox"/> DTIC USERS			21 ABSTRACT SECURITY CLASSIFICATION UNCLASSIFIED	
22a NAME OF RESPONSIBLE INDIVIDUAL R. L. Elsberry			22b TELEPHONE (Include Area Code) (408)-646-2373	22c OFFICE SYMBOL Code 63Es

Approved for public release; distribution is unlimited.

Diagnostic Study of a Genesis of Atlantic Lows Experiment (GALE)
Cyclogenesis Event

by

Daniel J. Soper
Lieutenant, United States Navy
B.S., University of Massachusetts, 1976

Submitted in partial fulfillment of the
requirements for the degree of

MASTER OF SCIENCE IN METEOROLOGY AND OCEANOGRAPHY


from the

NAVAL POSTGRADUATE SCHOOL
March 1987

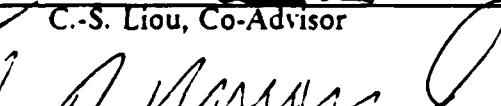
Author:



Daniel J. Soper

Approved by:


R.L. Elsberry, Thesis Advisor


C.-S. Liou, Co-Advisor


R.J. Renard, Chairman,
Department of Meteorology


Gordon E. Schacher,
Dean of Science and Engineering

ABSTRACT

The Navy Operational Regional Atmospheric Prediction System (NORAPS) analyses and forecasts, with 80 km resolution, are used to investigate an explosive cyclogenesis event that occurred in Intensive Observation Period (IOP) 2 during 26-28 January 1986. A synoptic investigation and quasi-Lagrangian diagnostic evaluation of the primary cyclone mass, vorticity, heat and moisture budgets are discussed.

Explosive development occurs with the superposition of an upper-level jet streak over a shallow surface system associated with a well-developed coastal front. The advection of shear vorticity aloft in combination with warm advection induces strong low-level convergence and spin-up of the low-level vortex. Significant surface sensible and latent heat fluxes and latent heating maxima are closely correlated with the period of rapid development from 00-12 GMT 27 January 1986. *Acquainted with the ...*

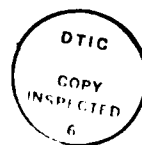


TABLE OF CONTENTS

I.	INTRODUCTION	10
II.	LITERATURE REVIEW	16
	A. THE ROLE OF SYNOPTIC-SCALE FORCING	16
	B. JET STREAK INFLUENCES ON CYCLOGENESIS	17
	C. PLANETARY BOUNDARY-LAYER PROCESSES	18
	D. THE ROLE OF LATENT HEAT RELEASE	20
	E. OROGRAPHIC INFLUENCES ON CYCLOGENESIS	21
	F. SUMMARY	22
III.	SYNOPTIC DESCRIPTION AND EVALUATION OF MODEL FORECAST SKILL	24
	A. GENERAL	24
	B. SYNOPTIC OVERVIEW	24
	C. VERIFICATION OF NORAPS "OPERATIONAL" MODEL FORECASTS	37
	D. VERIFICATION OF NORAPS "FINAL" MODEL FORECASTS	53
IV.	MASS AND VORTICITY BUDGET RESULTS	66
	A. GENERAL	66
	B. DESCRIPTION OF THE MASS BUDGET	66
	C. MASS BUDGET RESULTS	67
	D. DESCRIPTION OF THE VORTICITY BUDGET	68
	E. VORTICITY BUDGET RESULTS	71
	F. SUMMARY	84
V.	HEAT AND MOISTURE BUDGET RESULTS	89
	A. GENERAL	89
	B. DESCRIPTION OF THE HEAT BUDGET	89
	C. HEAT BUDGET RESULTS	90
	D. DESCRIPTION OF THE MOISTURE BUDGET	105

E.	MOISTURE BUDGET RESULTS	109
F.	SUMMARY	119
VI.	CONCLUSIONS AND RECOMMENDATIONS	121
A.	CONCLUSIONS	121
B.	RECOMMENDATIONS	123
APPENDIX A:	NAVY OPERATIONAL REGIONAL ATMOSPHERIC PREDICTION SYSTEM-NORAPS	124
1.	MODEL CHARACTERISTICS	124
2.	MODEL PHYSICS	126
a.	Planetary Boundary Layer	126
b.	Cumulus Parameterization	127
c.	Large-Scale Precipitation	128
d.	Radiation	128
APPENDIX B:	DATA ACQUISITION AND PROCESSING	129
1.	DATA ACQUISITION	129
2.	DESCRIPTION OF WIND ADJUSTMENT	130
3.	CONVENTIONS FOR NORAPS FIELDS AND BUDGET PROGRAMS	131
APPENDIX C:	"OPERATIONAL" NORAPS MODEL SPECIFICATIONS	132
	LIST OF REFERENCES	133
	INITIAL DISTRIBUTION LIST	137

LIST OF FIGURES

3.1a	NORAPS surface analysis at 12 GMT 26 January 1986	26
3.1b	NORAPS 500 mb analysis at 12 GMT 26 January 1986	26
3.1c	NORAPS 300 mb analysis at 12 GMT 26 January 1986	27
3.1d	GOES visible imagery at 1331 GMT 26 January 1986	28
3.2a	NORAPS surface analysis at 00 GMT 27 January 1986	29
3.2b	NORAPS 500 mb analysis at 00 GMT 27 January 1986	29
3.2c	NORAPS 300 mb analysis at 00 GMT 27 January 1986	30
3.2d	GOES IR imagery at 0004 GMT 27 January 1986	31
3.3a	NORAPS surface analysis at 12 GMT 27 January 1986	32
3.3b	NORAPS 500 mb analysis at 12 GMT 27 January 1986	32
3.3c	NORAPS 300 mb analysis at 12 GMT 27 January 1986	33
3.3d	GOES visible imagery at 1330 GMT 27 January 1986	34
3.4a	NORAPS surface analysis at 00 GMT 28 January 1986	35
3.4b	NORAPS 500 mb analysis at 00 GMT 28 January 1986	35
3.4c	NORAPS 300 mb analysis at 00 GMT 28 January 1986	36
3.4d	GOES visible imagery at 1831 GMT 27 January 1986	37
3.5a	NORAPS surface analysis at 12 GMT 28 January 1986	38
3.5b	NORAPS 500 mb analysis at 12 GMT 28 January 1986	38
3.5c	NORAPS 300 mb analysis at 12 GMT 28 January 1986	39
3.5d	GOES visible imagery at 1300 GMT 28 January 1986	40
3.6a	NORAPS surface forecast at 00 GMT 27 January 1986	41
3.6b	NORAPS forecast-analyzed SLP at 00 GMT 27 January 1986	41
3.6c	NORAPS 500 mb forecast at 00 GMT 27 January 1986	42
3.6d	NORAPS forecast-analyzed 500 mb heights at 00 GMT 27 January 1986	42
3.7a	NORAPS surface forecast at 12 GMT 27 January 1986	44
3.7b	NORAPS forecast-analyzed SLP at 12 GMT 27 January 1986	44
3.7c	NORAPS 500 mb forecast at 12 GMT 27 January 1986	45
3.7d	NORAPS forecast-analyzed 500 mb heights at 12 GMT 27 January 1986	45

3.8a	NORAPS surface forecast at 00 GMT 28 January 1986	47
3.8b	NORAPS forecast-analyzed SLP at 00 GMT 28 January 1986	47
3.8c	NORAPS 500 mb forecast at 00 GMT 28 January 1986	48
3.8d	NORAPS forecast-analyzed 500 mb heights at 00 GMT 28 January 1986	48
3.9a	NORAPS surface forecast at 12 GMT 28 January 1986	50
3.9b	NORAPS forecast-analyzed SLP at 12 GMT 28 January 1986	50
3.9c	NORAPS 500 mb forecast at 12 GMT 28 January 1986	51
3.9d	NORAPS forecast-analyzed 500 mb heights at 12 GMT 28 January 1986	51
3.10a	NORAPS forecast vs analyzed primary cyclone track	52
3.10b	NORAPS forecast vs analyzed primary cyclone intensity	53
3.11	NORAPS forecast vs analyzed secondary cyclone track	54
3.12	Location of CLASS sites and dropwindsondes for initial conditions	55
3.13	NORAPS final-operational analysis at 12 GMT 26 January 1986	56
3.14	NORAPS 300 mb final-operational forecasts	57
3.15	NORAPS 850 mb final-operational forecasts	58
3.16	NORAPS SLP final-operational forecasts	61
3.17	NORAPS final vs operational forecast primary cyclone track	62
3.18	NORAPS final vs operational forecast primary cyclone intensity	63
3.19	NORAPS final vs operational forecast secondary cyclone track	65
4.1	Analyzed and forecast horizontal mass transport	69
4.2	Analyzed and forecast vertical velocity (omega)	70
4.3	Analyzed and forecast absolute vorticity time tendency	73
4.4	Analyzed and forecast lateral transport of absolute vorticity	74
4.5	Analyzed and forecast mean mode lateral vorticity transport	76
4.6	Analyzed and forecast eddy mode lateral vorticity transport	77
4.7	Analyzed and forecast vertical transport of absolute vorticity	79
4.8	Analyzed and forecast vorticity divergence term	80
4.9	Analyzed and forecast vorticity tilting term	82
4.10	Analyzed and forecast frictional dissipation of vorticity	83
4.11	Analyzed and forecast residual of absolute vorticity	85
4.12	Analyzed 1000-500 mb average vorticity budget results	86
4.13	Forecast 1000-500 mb average vorticity budget results	87

5.1	Analyzed and forecast quasi-Lagrangian temperature tendency	91
5.2	Analyzed and forecast horizontal temperature advection	93
5.3	Analyzed and forecast vertical temperature advection	94
5.4	Analyzed and forecast area-averaged temperature field	96
5.5	Analyzed and forecast energy conversion term	97
5.6	Analyzed and forecast adiabatic cooling	98
5.7	Forecast surface sensible heat flux	100
5.8	NORAPS forecast surface sensible heat fluxes for eastern U.S.	101
5.9	Analyzed and forecast heat budget residual	103
5.10	NORAPS predicted heating rate vs forecast budget residual	104
5.11	Analyzed 1000-300 mb average heat budget results	106
5.12	Forecast 1000-300 mb average heat budget results	107
5.13	Area and column-averaged heat budget results	108
5.14	Quasi-Lagrangian forecast moisture tendency	111
5.15	NORAPS predicted 6 h total precipitation	112
5.16	Forecast horizontal and vertical moisture fluxes	113
5.17	Forecast surface moisture flux	115
5.18	NORAPS forecast latent heat fluxes for eastern U.S.	116
5.19	Moisture budget residual and NORAPS predicted moistening rate	117
5.20	Moisture budget residual minus NORAPS predicted moistening rate	118
5.21	Area and column-averaged moisture budget results	120

ACKNOWLEDGEMENTS

I would like to thank Dr. Rich Hodur of NEPRF who kindly provided the NORAPS system for this research. I also would like to express my deepest appreciation and gratitude to my co-advisor, Prof. C.-S. Liou, who provided the NORAPS analyses and forecast fields and developed most of the data acquisition and processing programs utilized in this study. His knowledgeable insight of computer programming and guidance were invaluable. I sincerely appreciate the time and efforts of Stacy Heikkinen who incorporated the GALE data into the initial NORAPS analysis. I am greatly indebted to my co-advisor, Prof. R. Elsberry, for his critical review and constructive criticism of this thesis. From my co-advisors I have gained a sound appreciation of the effort and dedication required to achieve quality scientific research. They have my lifelong respect and admiration. Additionally, I would like to thank my professors at the Naval Postgraduate School, who have provided me with a solid background in Meteorology and Oceanography. I would also like to thank the courteous and helpful computer operators at the W. R. Church computer center. Finally, my love and heart-felt thanks to my wife Jeanne, whose support and understanding were invaluable.

I. INTRODUCTION

The explosive deepening of some maritime extratropical cyclones and the inability of current operational numerical models to predict accurately this rapid intensification presents a significant forecast problem. Explosive cyclogenesis has been characterized by Sanders and Gyakum (1980) as a surface central pressure fall, adjusted for latitude by the factor $(\sin\phi/\sin 60^\circ\text{N})$, of at least 1 mb/hr over a 24-h period. Sanders and Gyakum called this critical deepening rate 1 *bergeron*. At 40°N , this critical deepening rate is approximately 18 mb/day. This rapid deepening results in the generation of high surface winds and sea states that pose a serious threat to all maritime activities. The damage sustained to the oceanliner Queen Elizabeth II (Gyakum, 1983 a,b) and the sinking of the oil rig Ocean Ranger (LeMoyne, 1982) are dramatic examples of the destructive nature of such rapidly developing systems. A climatological study of 267 cases of explosive cyclogenesis by Sanders and Gyakum (1980) showed that explosive cyclogenesis is primarily a maritime cold-season event with maximum frequency of occurrence in the western North Pacific and North Atlantic Oceans. Their study indicates that these cyclones tend to occur in the vicinity of the western boundary currents (Gulf Stream and Kuroshio) where strong sea-surface temperature (SST) gradients enhance the low-level baroclinicity.

The failure of current numerical models to accurately forecast the rapid intensification of these explosive systems is well documented in several studies, including those of Sanders and Gyakum (1980), Bosart (1981) and Gyakum (1983b). Sanders and Gyakum's verification of the National Meteorological Center (NMC) six- and seven- layer primitive equation (PE) model predictions demonstrated that the coarse-mesh, six-layer PE model forecast only about 25% of the observed 12-hour central pressure tendencies during the explosive stage of cyclogenesis. The use of the higher resolution seven-layer PE model resulted in a slight improvement, as it captured approximately 33% of the central pressure tendencies. Both models dramatically underforecast these oceanic cyclogenesis events. Bosart (1981) documented the failure of the Limited-area Fine Mesh II (LFM-II) model to adequately forecast cyclogenesis in the 1979 Presidents' Day storm. The model underforecast the storm central pressure by an average of 8-16 mb. Gyakum (1983b) found that the LFM-II model

underforecast the 12-hour explosive deepening of the 1978 Queen Elizabeth II storm by as much as 55 mb. Calland (1983) also discovered forecast errors in both storm intensity and storm track in his evaluation of the NMC and Fleet Numerical Oceanography Center (FNOC) coarse-mesh primitive equation model predictions for a western North Pacific Ocean explosive cyclogenesis event.

Possible reasons advanced for the failure of the models include initial analysis deficiencies, improper boundary-layer and convective precipitation physics (Bosart, 1981; Gyakum, 1983b), and inadequate model spatial and temporal resolution. Deficiencies in the model initial state, particularly in the planetary boundary layer (PBL), could have a significant effect on any model parameterized convective processes. Bosart (1981) suggests that the apparent boundary-layer analysis deficiencies in the Presidents' Day storm might have been due to the omission of significant level sounding data in the initial analysis cycle. Anthes and Keyser (1979) have shown that variations in the PBL structure can exert a significant impact on short-range forecasts of cyclogenesis. Anthes *et al.* (1980) demonstrated the importance of proper PBL resolution for realistic numerical model forecasts of cases with differentially heated baroclinic boundary layers. Bosart (1981) also noted that the LFM-II model parameterizes oceanic sensible heat flux but ignores latent heat flux. The net result is that boundary-layer air is simultaneously warmed and dried accompanying a cold offshore flow above a warm sea surface as opposed to warming and moistening in the real atmosphere. Anthes and Keyser (1979) show that the surface pressure evolution in a fine-mesh model is rather sensitive to the choice of cumulus parameterization scheme and the resulting distribution of latent heat. By studying numerical simulations of the QE II storm, Anthes *et al.* (1983) conclude that PBL simulations initialized with high-resolution data are considerably superior to those initialized with only the NMC analysis. The supplementary data produce conditions that are slightly more moist and less stable along the track of the storm, as well as an enhanced cyclonic circulation in the PBL, which creates a lower troposphere that is more favorable for development. Gyakum (1983b) compared the operational performance of the NMC LFM-II model (horizontal resolution - 120 km) versus the FNOC operational model (horizontal resolution - 381 km). He observed that both models were similarly deficient in forecasting the intensity of the Queen Elizabeth II storm and concluded that the increase in horizontal resolution with the trend to finer mesh models does not represent the sole solution to the problem.

In the past 10 years, significant advances in our understanding of the dynamics and evolution of extratropical explosive cyclogenesis has occurred. Although the development of extratropical explosive cyclones is associated with the synoptic-scale upper-level wave pattern, numerous other factors such as land-sea temperature contrasts, surface sensible and latent heat fluxes, an environment favorable for latent heat release and smaller-scale wave features in the upper and lower levels are also important in modulating the growth rate. According to the available evidence, the basic mechanisms occurring during explosive cyclogenesis are on sub-synoptic space and time scales that are not resolved by the existing synoptic network that has a 12-hour sampling period. The limited amount of data available over data-sparse oceanic regions is also of primary concern.

The Genesis of Atlantic Lows Experiment (GALE) completed in 1986 was the first cooperative mesoscale experiment to be devoted to winter cyclogenesis. The objectives of GALE included the study of a variety of mesoscale phenomena and air-sea interaction processes indigenous to the east coast of the United States. Utilizing an impressive array of observational facilities, data were collected with spatial and temporal resolution adequate to resolve most meso-alpha and meso-beta features. Horizontal resolution to 5 km, vertical resolution to 100-200 m and temporal resolution to 5 min were obtained through the use of several special observing systems. These observational facilities included research aircraft, ground-based and airborne scanning doppler, a portable automated mesonet (PAM), rawinsondes, mini-radiosondes, meteorological buoys, research vessels, naval ships, and coastal-marine automated platforms (C-MAN). Satellite data from the Geostationary Earth Satellite (GOES) and TIROS systems of the National Oceanographic and Atmospheric Administration (NOAA), and from the Defense Meteorological Satellite Program (DSMP) platforms were also collected in support of the GALE objectives. Some of the most useful satellite products included temperature and moisture profiles, sea-surface temperatures (SST's), cloud-drift winds, precipitable water and moisture mapping, and thickness and geopotential height observations. The net result of this cooperative collection effort was the generation of a research-quality data base that could be applied to the study of the sub-synoptic aspects of east coast cyclogenesis. High quality analyses derived from this data base should lead to improved 48-72 h forecasts and a better understanding of the physical mechanisms controlling the formation and rapid development of east coast storms. The location of the GALE observational

network, which was centered on the eastern Carolinas, and the period of the field experiment (15 January - 15 March 1986), encompass the general location and time of year most favorable for cyclogenesis on the east coast, based on studies by Colucci (1976) and others.

The cyclogenesis event selected for this study occurred during Intensive Observation Period (IOP) 2 of GALE. The initial coastal cyclone formed over Georgia on 12 GMT 26 January 1986 and moved rapidly off the Carolina coast by 00 GMT 27 January 1986. Explosive deepening occurred during the next 12-h period and a secondary cyclogenesis event developed in the cold air. Both cyclones deepened explosively according to the Sanders and Gyakum criterion, but they moved northward to Hudson Bay too fast to give more than modest snowfall. This event includes the cold air damming and coastal front characteristic of "Type B" cyclogenesis as described by Austin (1941) and Miller (1946). Type B cyclogenesis is often preceded by a wedge of cold continental air and high pressure on the east slopes of the Appalachians, which has been termed "cold air damming" by Forbes *et al.* (1984). The coastal cyclone often forms along the associated "coastal front" (Bosart *et al.*, 1972), which concentrates the baroclinicity associated with the land-sea temperature contrast.

Quasi-Lagrangian Diagnostics (QLD), as originally developed by Johnson and Downey (1975), are applied to examine the heat, moisture, mass and vorticity budgets of the storm. Application of QLD techniques in studying cyclone development (Wash, 1978) has proven valuable in diagnoses of poorly forecast storms. Several previous theses (Conant, 1982; Cook, 1983; Calland, 1983) have used QLD techniques in detailed analyses of east-coast cyclogenesis, rapid cyclogenesis in the polar airstream, and explosive cyclogenesis in the North Pacific Ocean respectively. The budget studies investigate the mean properties of the cyclone both spatially and temporally, and determine the relative contributions of the terms at various stages of cyclone growth. Inherent in this technique is a significant amount of areal, vertical, and time averaging over the budget volume. The QLD technique uses an isobaric spherical coordinate system that translates with the storm. Since the radius of the storm is small compared to the radius of the earth, the budget volume can be approximated by a cylinder. With the cylindrical budget volume centered on and translating with the cyclone center, aspects of cyclone development associated with the storm motion are effectively removed. Vertical distributions, lateral exchanges and sources and sinks of cyclone properties resulting from purely developmental processes are then analyzed.

This thesis is part of a larger investigation into the nature and physical mechanisms underlying maritime explosive cyclogenesis, which has the overall objective of improving numerical weather prediction capability over the oceans. The two main objectives of this thesis will be a determination whether the enhanced data sources provided by GALE will allow diagnostic studies to provide new insight into the physical processes important in maritime explosive cyclogenesis and an assessment of the impact that enhanced initial conditions have on model forecast skill. The Navy Operational Regional Atmospheric Prediction System (NORAPS) model, with a horizontal resolution of 80 km and 12 σ levels, will be utilized in this study. A base time of 12 GMT 26 January 1986 will be used for the model forecast. NORAPS analyses are available at 12-h intervals from 12 GMT 26 January 1986 to 12 GMT 28 January 1986. NORAPS forecasts are available at 6-h intervals during this same period (48 h). The "operational" NORAPS analyses serve as the "control" study. Available dropwindsondes and Cross-chain Loran Atmospheric Sounding Systems (CLASS) from IOP-2 of GALE will be added to the initial "operational" data set to create an enhanced "final" analysis with increased spatial coverage.

The specific objectives of this thesis are:

- Assess the impact of the additional GALE data on forecast skill by verifying the NORAPS "final" forecast against the "operational" forecast;
- Compute mass and vorticity budgets during the cyclone's evolution to determine the vertical structure and dynamical contributions to rapid cyclogenesis;
- Document the mean thermal and moisture structure of this explosive cyclogenesis case using QLD for both the analyses and forecasts;
- Assess the relative contribution of the terms in the thermodynamic and moisture budget equations at various stages of cyclone development, and the horizontal and vertical distribution of those terms;
- Compare the moisture budget estimates of the diabatic heating rates with the heat budget for the forecast case; and
- Identify properties of the NORAPS model that do not realistically represent the real atmosphere.

A survey of the literature on maritime explosive cyclogenesis is given in Chapter II. A synoptic overview of the IOP-2 coastal cyclogenesis event and a discussion of the results of both the "operational" and "final" NORAPS analyses and forecasts is presented in Chapter III. The results of the mass, vorticity, heat and moisture budgets for the NORAPS "operational" analyses and forecasts is given in Chapter IV and Chapter V. Conclusions and recommendations for future study are outlined in Chapter

VI. Appendix A provides a discussion of the characteristics and important parameterizations in the NORAPS model. Appendix B covers data acquisition and processing procedures. Appendix C discusses the modifications made to the original NORAPS model to correct for errors in the heating and moistening rates and changes incorporated into the "operational" NORAPS model that were necessary to correctly represent realistic air-sea interactions.

II. LITERATURE REVIEW

Typical mid-latitude cyclogenesis is initiated and maintained by synoptic-scale trough/ridge patterns. However, mesoscale forcing provided by upper- and lower-level jet streaks, enhanced land-sea thermal contrast and coastal frontogenesis, and oceanic sensible and latent heat fluxes are the extra ingredients that modulate the growth rate of maritime cyclones and help focus rapid cyclogenesis along the coast. Maritime explosive cyclogenesis must then be viewed as a scale-interaction problem in which both synoptic and mesoscale processes play important roles. During the past decade, numerous studies of explosive cyclones have identified a number of potential dynamical processes responsible for rapid intensification.

A. THE ROLE OF SYNOPTIC-SCALE FORCING

Sanders and Gyakum's (1980) climatological study emphasized the importance of the synoptic weather pattern in combination with the oceanic influences in identifying regions where explosive cyclogenesis is likely to occur. Their results indicate that maritime explosive cyclones tend to occur over large gradients of sea-surface temperature associated with the western boundary currents (Gulf Stream and Kuroshio). Very few cyclones explosively developed in regions without significant sea-surface temperature gradients. A statistical analysis and updated climatology of explosive cyclones by Roebber (1984) also indicated that baroclinic zones are preferred regions of explosive cyclogenesis. His climatological and statistical evidence suggests that the explosive mechanism is a combination of the baroclinic process and some other mechanism. Sanders and Gyakum (1980) found that, on the average, surface low-pressure systems experience rapid deepening when a mobile 500 trough was approximately 400 n mi west-southwest of the surface center. In more than 75 percent of their cases, a mobile upper trough was located in the southwest quadrant from the surface system. In over 90 percent of the cases, the nearest 500 mb trough was positioned in the western semi-circle. This is consistent with Petterssen's development theory as positive vorticity advection (PVA) in advance of the upper trough can lead to upper-level divergence over the surface low and a positive surface vorticity tendency. Petterssen (1956) defined cyclone intensification as the change in geostrophic surface vorticity, which he related to the change in upper-level vorticity and the change in

thickness between the upper-level pressure surface and 1000 mb. Kocin and Uccellini (1984) show that for nearly two-thirds of the east coast cyclone cases reviewed in their study, a general amplification of the upstream trough and an increase of the magnitude of the jet winds were observed 12 to 24 h prior to cyclogenesis. Bosart (1981) and Uccellini *et al.* (1985) found that a mid-tropospheric short-wave trough and low-level tropospheric warm advection were associated with the rapid deepening of the Presidents' Day storm of 18-19 February 1979. Similarly, Chen *et al.* (1985) identified the importance of coupling between an upper-level trough and an existing surface disturbance prior to explosive deepening.

B. JET STREAK INFLUENCES ON CYCLOGENESIS

Kocin and Uccellini's (1984) climatological survey of 18 major east coast storms also showed that upper- and lower-tropospheric jet streaks embedded within a variety of synoptic trough/ridge configurations contributed to the development of surface cyclones and associated severe winter weather in every case reviewed. Upper-level jet streaks enhance surface cyclogenesis by creating an area of upper-level divergence in the left quadrant of the exit region with associated upward vertical motion, and by providing a source of potential vorticity upstream of the developing cyclone through tropopause folding. Additionally, the lower branch of the ageostrophic transverse circulation in the exit region of the upper-level jet streak can induce a low-level jet (LLJ) that transports warm, moist air into the convective region. This low-level jet is termed the "conveyor belt" by Harrold (1973) because of its role in transporting momentum and latent and sensible heat. Shapiro (1983) suggested that proper coupling of the upper and lower jets can facilitate deep convection and link the low-level system to the jet-level processes. With the upper-level jet advecting cooler, drier air aloft and the LLJ advecting warm, moist air into the area at lower levels, the lapse rate can become convectively unstable. If the ascent branches of the upper and lower secondary circulations become aligned, deep convection is possible.

Diagnostic studies by Uccellini *et al.* (1985) and Bosart and Lin (1984) of the 1979 Presidents' Day storm isolated mesoscale circulation patterns associated with the upper-level jet streak that extruded high potential vorticity from the stratosphere downward toward the lower troposphere 1,500 km upstream of the east coast and 12 to 24 h prior to the rapid development phase of this storm. In the 12 h preceding rapid cyclogenesis, the stratospheric air descended toward the 800 mb level to a position just

upstream of the area where explosive cyclogenesis occurred. The stratospheric air mass was nearly co-located with the storm center as explosive deepening and vortex development commenced, which suggests that the stratospheric extrusion toward the PBL and the associated vortex stretching contributed to the explosive development. During this same storm, Uccellini *et al.* (1984) were able to isolate three jet streaks that appeared to play important roles in the development of two separate areas of heavy snowfall. One area of heavy snow developed prior to rapid deepening and was linked to an increasingly unstable subtropical jet streak (STJ) and a noticeably ageostrophic LLJ. The second area of heavy snowfall developed in conjunction with explosive cyclogenesis off the east coast as a polar jet streak (PFJ) and a mid-tropospheric short-wave trough propagated toward the coastal region.

In a comparative diagnostic study of weak versus strong synoptic-scale forcing, Pagnotti and Bosart (1984) suggest that in addition to latent heating and thermal advection, differential cyclonic vorticity advection is crucial to deeper, more intense development. Commenting on their study, Uccellini (1984) points out that the advection of shear vorticity associated with a jet streak plays the same role as the positive vorticity advection associated with a short-wave trough. Calland's (1983) study of an explosive cyclogenesis event under straight 500 mb flow supported this argument. A quasi-Lagrangian vorticity analysis indicated that horizontal vorticity advection was important, even in the absence of a short-wave trough aloft. The large eddy vorticity flux into the volume at upper levels was associated with advection of cyclonic shear vorticity by an intense jet streak. Rapid intensification occurred as the surface low moved under the region of upper-level divergence aloft. In a similar study, Cook (1983) attributed the spin-up of a maritime extratropical cyclone to the presence of an upper-level jet maximum and reduced low-level static stability.

C. PLANETARY BOUNDARY-LAYER PROCESSES

Other studies have identified the importance of cold air damming and coastal frontogenesis prior to rapid cyclogenesis. Kocin and Uccellini (1984) identified cold-air damming and coastal frontogenesis in 12 of 15 cases that eventually qualified as explosive deepeners. Cold-air damming and associated coastal frontogenesis create a low-level thermally direct circulation with upward vertical motion on the seaward side of the frontal zone and enhanced precipitation over the cold air. The thermal gradients observed in the coastal frontal zone, combined with large oceanic sensible and latent

heat fluxes, create a lower troposphere characterized by enhanced low-level baroclinicity and reduced static stability. This combination of reduced static stability and a potential for latent heating creates an environment that is exceedingly conducive to rapid cyclogenesis. In the Presidents' Day storm, Bosart (1981) showed how cyclogenesis was initiated along a coastal front without evident upper-level support. However, Uccellini *et al.* (1984) link coastal frontogenesis with increased thermal and moisture advections from the LLJ that forms in the lower branch of the indirect circulation associated with the STJ. The coastal front steered the shallow cyclone parallel to the coast until it eventually acquired a favorable phase relationship for deepening in advance of a vigorous short-wave trough. Bosart and Lin (1984) also emphasize that the initial growth of cyclonic vorticity in the lower troposphere is driven primarily by convergence along the Carolina coastal front during this same storm, which demonstrates that planetary boundary layer processes may be vital to incipient storm development.

Still other studies have discussed the importance of sensible and latent heat fluxes as significant contributors to cyclogenesis. The climatological study by Budyko (1974) of the flux of latent and sensible heat from the ocean to the overlying atmosphere shows that these fluxes reach a local maximum off the mid-Atlantic states during the winter months. The mean latent heat flux for December was reported to be 355 W/m^2 , while the sensible heat flux was 97 W/m^2 . These values greatly exceed the corresponding warm-season values. These cold-season maxima are caused by the increased temperature and specific humidity differences between the air and the sea, and by higher oceanic mean wind speeds. The effect of sensible and latent heat fluxes on the Presidents' Day storm is discussed by Bosart (1981). His results show that the thermal contrast between the nearshore and offshore waters was about 2° C higher than the climatological average, due to the presence of high SST's about 200 km from the coast. Over a 12-h period, the total heat flux averaged 600 W/m^2 with the latent heat flux about double the sensible heat flux. The latent, sensible and total heat fluxes peaked about 150-200 km offshore. Warming and moistening of the PBL also appeared to be important in other studies. Investigations of separate cyclogenesis cases by Cook (1983) and Calland (1983) based on data from the First GARP Global Experiment (FGGE) noted a dramatic decrease in low-level static stability during the early stages of cyclogenesis. Chen *et al.* (1985) indicated that sensible and latent heat flux from the Kuroshio was instrumental in destabilizing the lower layer of the polar air mass in his synoptic study of explosive cyclogenesis northeast of Taiwan.

Many studies have proposed that the bulk effects of convective processes, including the vertical transport of mass and vorticity, and the release of latent heat are important in explosive cyclogenesis. The sensible, latent heat fluxes and increased convective instability in the PBL greatly favor the development of deep convection. Bosart (1981) points to boundary-layer processes and the bulk effects of convective-scale processes as the fundamental physical mechanisms leading to explosive cyclogenesis in the Presidents' Day cyclone. Preceding and accompanying the onset of deepening, convection was observed to break out near and to the east of the incipient storm center where cold polar air was being rapidly warmed, moistened and destabilized by oceanic sensible and latent heat fluxes. Explosive deepening and transformation of the cyclone to a vortex with hurricane-like characteristics subsequently occurred. Convective processes have also been associated with the vertical advection of vorticity, which was identified as a key factor in this same storm (Bosart and Lin, 1985).

D. THE ROLE OF LATENT HEAT RELEASE

Based on quasi-geostrophic diagnostic calculations, Gyakum (1983b) concluded that the latent heating associated with cumulus convection was crucial to the rapid intensification of the QE II storm. According to his results, the initial development occurred as a result of baroclinic instability in the lower troposphere. As the cyclone intensified, the lifting of potentially unstable air triggered deep convection, and the associated latent heat release led to further deepening through a positive feedback mechanism similar to convective instability of the second kind (CISK). Using composites constructed from weather ship rawinsonde data, Rogers and Bosart (1986) concluded that explosively deepening cyclones are basically baroclinic phenomena whose development may be strongly enhanced in some cases by the bulk effects of cumulus convection. A case study of a very intense cyclone revealed deep layers of conditional instability near the low center. Pagnotti and Bosart (1984) show that warm thermal advection and latent heat release are both of nearly equal importance to low-level convergence and vorticity generation for weak, shallow cyclones prior to the explosive deepening period. Numerical simulations of the QE II storm by Anthes *et al.* (1983) confirmed that latent heating produces a stronger storm with a warmer core, as suggested by Gyakum (1983 a,b). They also indicated that the vertical distribution of convective heating was important with a more intense storm occurring when the

maximum heating occurred in the lower troposphere. The lower maximum in heating produces an associated lower maximum in vertical velocity, which leads to stronger convergence and vorticity generation in the low levels of the storm. Chang *et al.* (1984) investigated latent heat induced energy transformations during cyclogenesis. Using real-data numerical simulation experiments, they found that the maximum latent heat release occurred in the middle-upper troposphere, but the most significant response to the heating appeared in the lower troposphere. They also concluded that the growth of the cyclone did not depend on the short-term generation of available potential energy by condensation processes to provide a source of energy. Rather, the latent heat aided in the conversion of pre-existing potential energy to kinetic energy. Liou and Elsberry (1985) used the QLD technique to investigate an explosive maritime cyclogenesis case over the western North Pacific Ocean using a research version of the University of California at Los Angeles (UCLA) General Circulation Model (GCM). Their study identified area-averaged heating rates of 25-30° C/day at 600-700 mb. Diabatic heating was due primarily to latent heat release from stable condensation and middle-level convection. Additionally, they found that the sea-level pressure (SLP) deepening rate was highly correlated with the diabatic heating rate. Elsberry *et al.* (1985) found similar results for this case with heat budgets derived from the FGGE analyses.

E. OROGRAPHIC INFLUENCES ON CYCLOGENESIS

Orographic influences on rapid intensification may be either indirect or direct. Cold air trapped by the Appalachians will tend to enhance the near-shore temperature gradient. In addition, the cross-isobaric flow in the damming pressure ridge to the east of the Appalachians, combined with a geostrophic easterly wind over the ocean regions, promotes coastal frontogenesis (Bosart, 1975). Thus, cold-air damming serves to sharpen the coastal baroclinic zone while the cold continental air flowing out over high SST's maximizes the fluxes of sensible and latent heat. The enhanced region of low-level baroclinicity and reduced static stability creates a PBL that is favorable for a shallow cyclogenesis event. East of the Appalachians, lee cyclogenesis processes also may be important. Since east coast cyclogenesis is displaced from the mountains, it is not obvious that lee-slope processes are involved. However, Baker (1970) suggests that the cold dome on the east slopes in Type B cases effectively extends the mountains eastward to the coastline. Adiabats slope downward to the east in this region, so that

westerlies that emerge aloft may have a "downslope" component. More study is required to determine if lee cyclogenesis plays a role in east coast explosive cyclogenesis events.

F. SUMMARY

From these studies, it is hypothesized that maritime explosive cyclogenesis occurs when there is favorable superposition of significant upper-level forcing over a low-level disturbance in conjunction with an environment that is conducive to rapid intensification. The upper-level dynamical forcing can be caused by either intense short waves aloft, embedded jet streaks or a combination of both. The vorticity advection aloft will then force upward vertical motion and convergence at the lower levels. During the cold season, continental cold air flowing over warm oceans with strong SST gradients will gain heat and moisture through strong upward fluxes of sensible and latent heat. The effect of this upward energy flux is to destabilize the PBL. Sensible heating warms the well-mixed boundary layer and decreases the static stability of the lower troposphere. Latent heat flux moistens the PBL and increases the convective instability of the lower troposphere. The upper-level forcing provides a third possible mechanism for contributing to low-level instability through dynamically-forced vertical ascent and adiabatic cooling. The sensible and latent heat fluxes, combined with the effects of cold-air damming, land-sea thermal contrasts and strong SST gradients promote the development of a region of enhanced low-level baroclinicity that leads to coastal frontogenesis. The coastal front will develop a thermally direct mesoscale circulation as the horizontal thermal gradient strengthens. Release of baroclinic instability in combination with latent heat release, as warm, moist air ascends on the warm side of the frontal zone can trigger an incipient low or wave perturbation along the front. This shallow cyclonic system will be effectively steered by the coastal front, and will parallel the coast until it moves into a region of dynamically forced vertical ascent due to strong upper-level PVA. This large-scale ascent can lead to large amounts of latent heat release through the bulk effects of cumulus convection. The net heating of the storm volume can lead to a warm core structure over the storm center with an accompanying rapid decrease in SLP, increase in surface winds and sea state, and convective features typical of a tropical cyclone.

It could be argued that some or all of these features could be present in cyclogenesis events that do not undergo rapid intensification. The goal of future

research should be to determine which of these physical processes are "essential" for explosive cyclogenesis to occur. The long-term objective of future research also could be the establishment of "minimal" conditions and "optimal" conditions for explosive cyclogenesis, so that useful operational forecast rules may developed.

From this literature review, the importance of emphasizing explosive cyclogenesis as a scale-interaction problem is apparent. Diagnostic studies of explosive cyclogenesis must have the capability to resolve the dynamical forcing due to mesoscale features and PBL processes to be useful in expanding our present understanding. The effects of jet streaks, pre-existing lows, frontogenesis, mesoscale precipitation bands and the effects of sensible and latent heat flux must be quantitatively understood before "minimal" and "optimal" conditions for explosive cyclogenesis can be defined. Studies by Kaplan *et al.* (1982) and Uccellini *et al.* (1983) point to the existence of complex interactions between the jet streak and diabatic processes, which can occur within areas of 1500 to 2000 km and within 6 to 9 h. The net result of these nonlinear interactions is rapid changes in the evolution of east coast storms that cannot be properly resolved with existing operational analyses. The enhanced initial conditions possible with the GALE data set will help increase our understanding of the dynamical scale interactions and will provide the basis for this study.

III. SYNOPTIC DESCRIPTION AND EVALUATION OF MODEL FORECAST SKILL

A. GENERAL

The storms selected for this study occurred during IOP-2 of GALE, which encompassed the period 12 GMT 23 January to 04 GMT 29 January 1986. Cold-air damming and coastal frontogenesis were present early in the period and had a definite influence on the subsequent cyclogenesis. Two separate cyclogenesis events occurred. Offshore cyclogenesis developed in association with the coastal front over the period 26 - 27 January 1986, while a secondary cyclogenesis event developed within the colder air on 27 - 28 January 1986.

In this study, the NORAPS analyses are used to describe the development of the cyclogenesis events. The weather synopsis of IOP-2 provided in the GALE Field Program Summary is also utilized in this discussion for completeness. A base time of 12 GMT 26 January 1986 is selected for the model forecasts and analyses. Sea-level pressure (SLP) analyses are used to provide a description of the storm track and intensification. Upper-level analyses (500 and 300 mb) are presented to identify the synoptic mesoscale dynamical forcing evident in the development of the cyclone. NORAPS analyses are also used to verify the corresponding NORAPS forecasts and to provide a measure of forecast skill. Significant deviations between the model "operational" forecasts and the verifying analyses will be highlighted. The "final" forecast is then verified against the "operational" forecast to identify possible improvements in forecast skill due to the enhanced initial conditions provided by a small portion of the GALE data set. The NORAPS surface analysis utilizes an 89 x 89 hemispheric grid (268 km) to interpolate to the higher resolution (80 km) NORAPS grid. For this case, the update cycle uses the Navy Operational Global Atmospheric Prediction System (NOGAPS) analyzed fields as the "first guess" for the NORAPS upper-air analysis.

B. SYNOPTIC OVERVIEW

Cold-air damming was well established east of the Appalachians by 18 GMT 24 January 1986 (not shown). The cold air was deep (up to 3 km) and had an easterly component along the east slopes at all levels except in the lowest few hundred meters.

A coastal front formed around 08 GMT 25 January 1986 just onshore near Cape Hatteras, where the highly ageostrophic winds in the lowest levels over land were confluent with the easterly, quasi-gradient winds at the coast. The cold air dome just inland was only about 200 m deep. Considerable precipitation occurred due to the thermally direct circulation of the coastal front and because of dynamically-forced vertical ascent associated with a mid-tropospheric short wave that began entering the region from the southwest. The coastal front was drawn offshore around 00 GMT 26 January 1986 by a "premature" coastal low, so that the major cyclogenesis on the 27th was offshore. As the coastal front moved offshore, considerable convection developed along it, and lightning strikes were frequent.

The disturbance that ultimately became the first major cyclone was present at 12 GMT 25 January 1986 as a minor frontal wave in extreme southeastern Texas. The initial NORAPS surface analysis (Fig. 3.1a) at 12 GMT 26 January 1986 indicates that the surface disturbance was located in Georgia (32.4°N , 81.7°W) and was still weak (1009 mb). A strong anticyclone center (1048 mb) was observed over the North Atlantic at 47°N , 48°W . The corresponding 1000-500 thickness pattern reveals a distinct baroclinic zone located along the east coast of the U.S. with moderate to strong cold advection across the southeastern U.S. and Gulf Coast and moderate warm advection across New England. Cold advection over the southeastern U.S. weakens with height and changes to warm advection at 250 mb (not shown). The 500 mb height and vorticity analysis depicts a long-wave trough centered along 89°W with an associated absolute vorticity maximum over Louisiana (Fig. 3.1b). Although vorticity advection aloft is strong over the Gulf Coast, it is much weaker over the southeastern U.S. The 300 mb height and isotach analysis locates the long-wave trough axis along 90°W (Fig. 3.1c). This observed westward tilt with height of the trough axis is consistent with the baroclinic instability development process. Intense jet maxima of greater than 60 m/s are located both upstream and downstream of the 300 mb trough axis. The developing surface disturbance is located in proximity of the right-rear quadrant of the downstream jet, which creates a favorable situation for surface development due to upper-level divergence and dynamically-forced vertical ascent. The Geostationary Operational Environmental Satellite (GOES) visible imagery valid at 1331 GMT 26 January 1986 depicts the cloud patterns associated with the quasi-stationary coastal front and developing wave over Georgia (Fig. 3.1d).

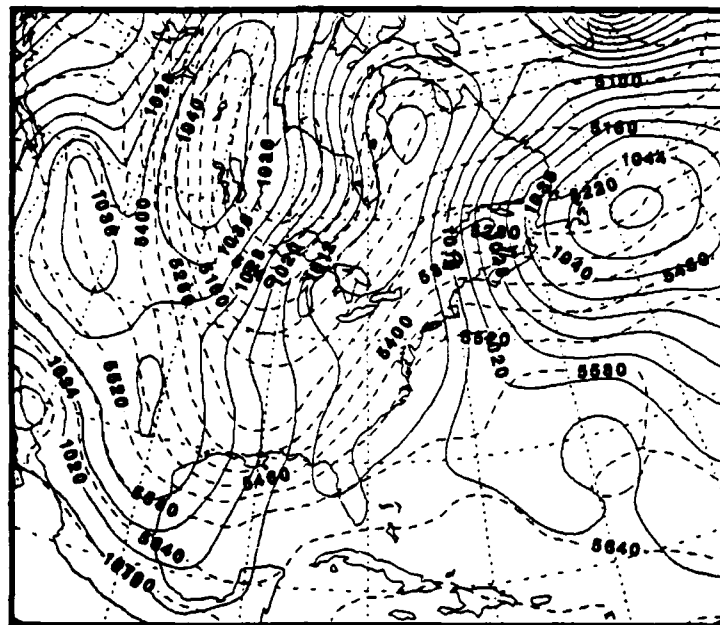


Figure 3.1a NORAPS surface pressure analysis (solid) in mb and 1000-500 mb thickness (dashed) in gpm at 12 GMT 26 January 1986. Contour interval is 4 mb (isobars) and 60 gpm (thickness).

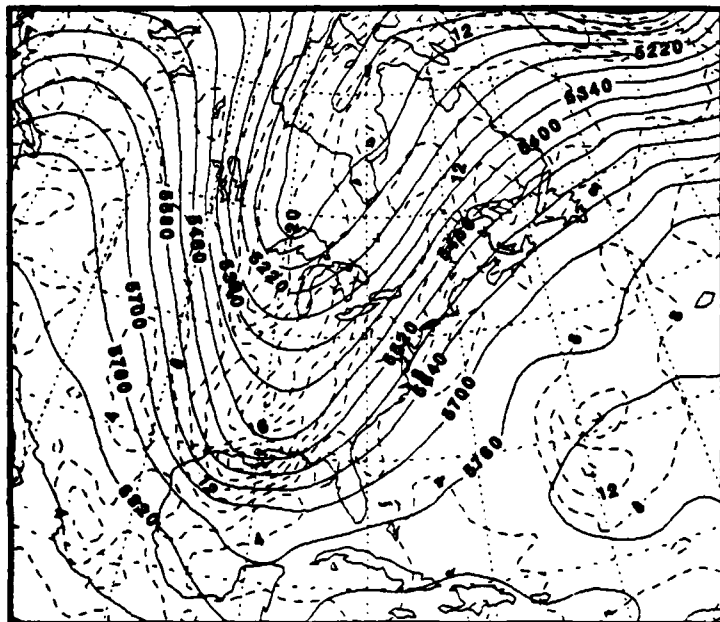


Figure 3.1b NORAPS 500 mb geopotential heights (solid) in gpm and absolute vorticity (dashed) in units of 10^{-5} s^{-1} at 12 GMT 26 January 1986. Contour interval is 60 gpm (heights) and $4 \times 10^{-5} \text{ s}^{-1}$ (vorticity).

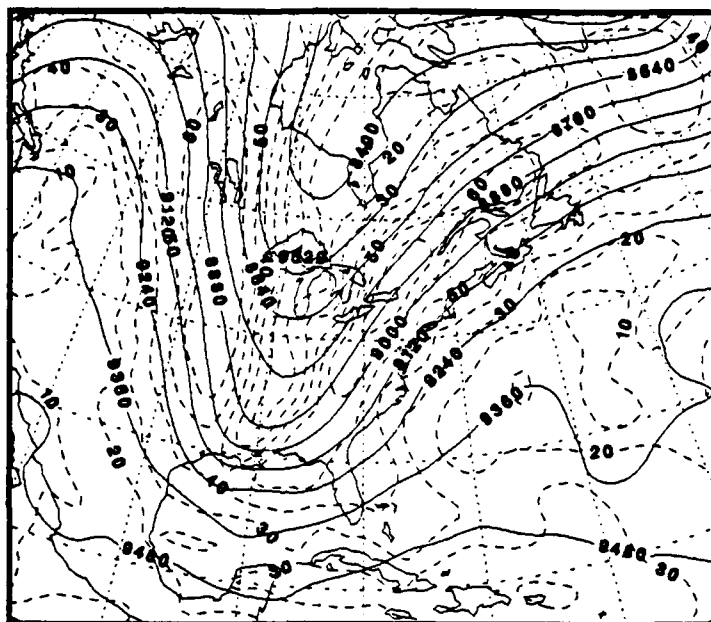


Figure 3.1c NORAPS 300 mb geopotential heights (solid) in gpm and isotach analysis (dashed) in m/s at 12 GMT 26 January 1986. Contour interval is 120 gpm (heights) and 10 m/s (isotachs).

Although upper-level forcing due to positive vorticity advection (PVA) is present over the storm center, significant cold advection in the lower troposphere provides a "braking effect" that inhibits rapid development of the surface disturbance. Consequently, the surface disturbance experienced only moderate deepening as it moved toward the Carolina coastline, in spite of the well-defined wave and jet streak aloft.

By 00 GMT 27 January 1986 (Fig. 3.2a), the surface low deepened to 1000 mb as it moved northeastward to a position approximately 80 n mi northeast of Cape Hatteras (36.7°N , 74.5°W). The North Atlantic anticyclone continued to move southeastward to 46°N , 41°W with little change of intensity but an increase in areal extent. The 1000-500 mb thickness pattern depicts increased baroclinicity in the lower troposphere as the thermal gradients along the east coast of the U.S. become stronger. Strong cold advection extends from the Carolinas to Florida with moderate warm advection evident from New Jersey northward to the Canadian maritime provinces. A cold front extends from the low southward to the tip of Florida and the associated SLP trough is clearly depicted in the surface analysis. Relatively weak warm advection is found over the storm center at low- and mid-tropospheric levels and significant warm

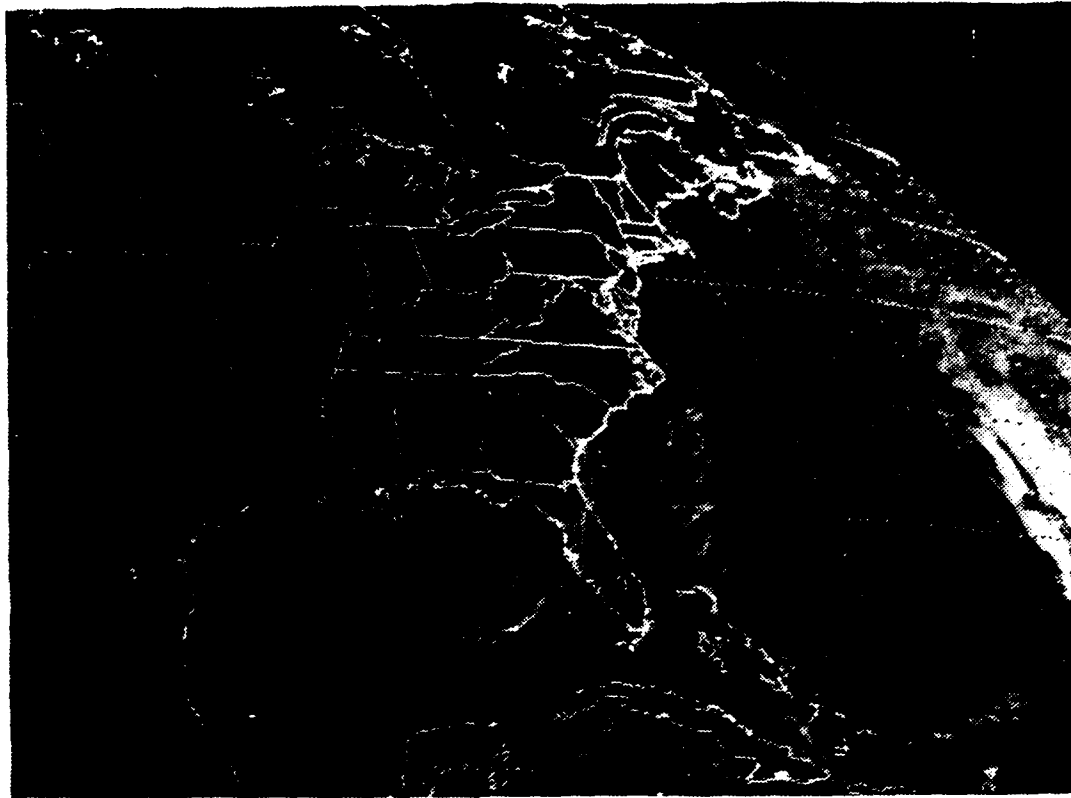


Figure 3.1d GOES visible imagery at 1331 GMT 26 January 1986.

advection occurs at 250 mb (not shown). The 500 mb trough axis (Fig. 3.2b) has translated eastward to 83°W and deepened approximately 60 m along its base. The horizontal tilt of the axis has shifted from NE-SW to NW-SE in response to the strong cold surge across the southeastern states. Absolute vorticity maxima associated with the base of the trough have also translated eastward to the Florida coast and created a region of strong PVA over the storm center. The 300 mb isotachs continue to show extensive 70 m/s jet streak maxima upstream and downstream from the trough axis (Fig. 3.2c). The storm center is now located under the right-rear quadrant of the downstream jet streak. The GOES Infrared (IR) imagery at 0004 GMT 27 January 1986 continues to depict the deep cloud patterns associated with the developing coastal low (Fig. 3.2d). Although the rate of cyclogenesis was only moderate prior to 00 GMT 27 January 1986, the enhanced lower-level baroclinicity, warm advection over the storm center and strong upper-level PVA aloft create an environment favorable for rapid development in the ensuing 12-h period.

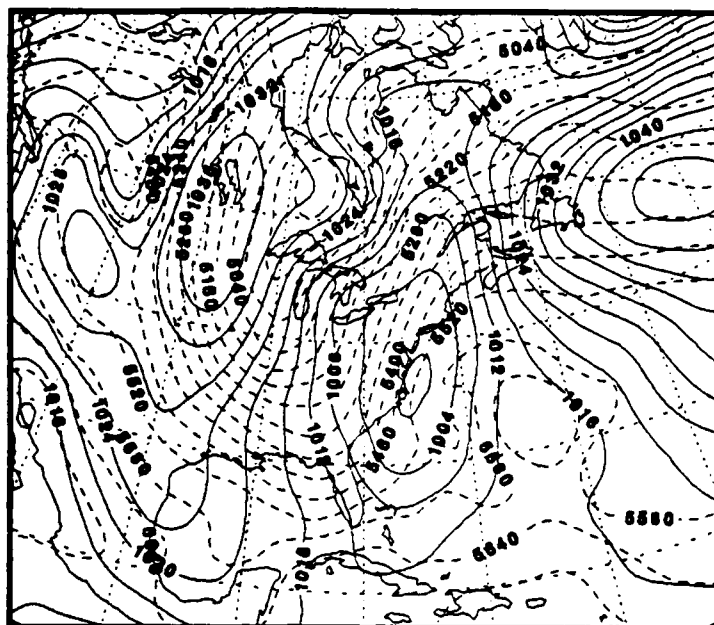


Figure 3.2a NORAPS surface pressure analysis (solid) in mb and 1000-500 mb thickness (dashed) in gpm at 00 GMT 27 January 1986. Contour interval is 4 mb (isobars) and 60 gpm (thickness).

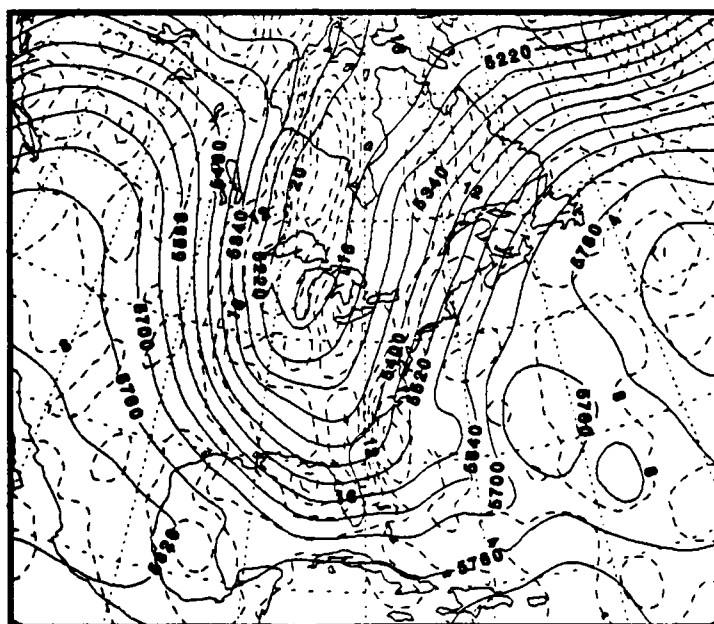


Figure 3.2b NORAPS 500 mb geopotential heights (solid) in gpm and absolute vorticity (dashed) in units of 10^{-5} s^{-1} at 00 GMT 27 January 1986. Contour interval is 60 gpm (heights) and $4 \times 10^{-5} \text{ s}^{-1}$ (vorticity).

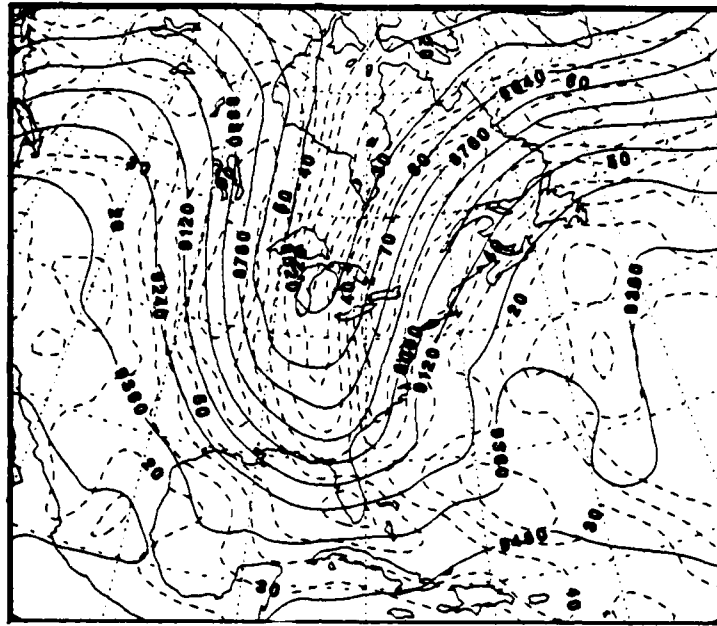


Figure 3.2c NORAPS 300 mb geopotential heights (solid) in gpm and isotach analysis (dashed) in m s at 00 GMT 27 January 1986. Contour interval is 120 gpm (heights) and 10 m s (isotachs).

By 12 GMT 27 January 1986 (Fig. 3.3a), the coastal cyclone moved north-northeast into New Hampshire (43.2°N , 71.8°W) after having rapidly deepened to 986 mb. The North Atlantic anticyclone continued to move eastward to 45°N , 35°W and remained at 1048 mb. A strong baroclinic zone existed along the east coast of the U.S. as the thermal gradient continued to be strengthened by the synoptic-scale flow associated with the coastal low. Strong cold advection occurred from south of New England to Florida and moderate warm advection existed across the Canadian maritime provinces. The original cold front extended from the surface low southward to Cuba and a secondary cold front along the coast was also now evident in the surface analysis. Over the storm center, the low- to mid-level (850, 700 and 500 mb) temperature advection continued to be weak while strong warm advection was observed at 250 mb (not shown). The 500 mb trough axis has shifted slightly eastward to 81°W and deepened about 120 gpm along the base of the trough (Fig. 3.3b). An upper-level vortex is well-defined at 500 mb and 300 mb (Fig. 3.3c), with very strong jet streaks at 300 mb to the west and northeast. The associated strong absolute vorticity centers over the southeastern U.S created a region of significant PVA over the

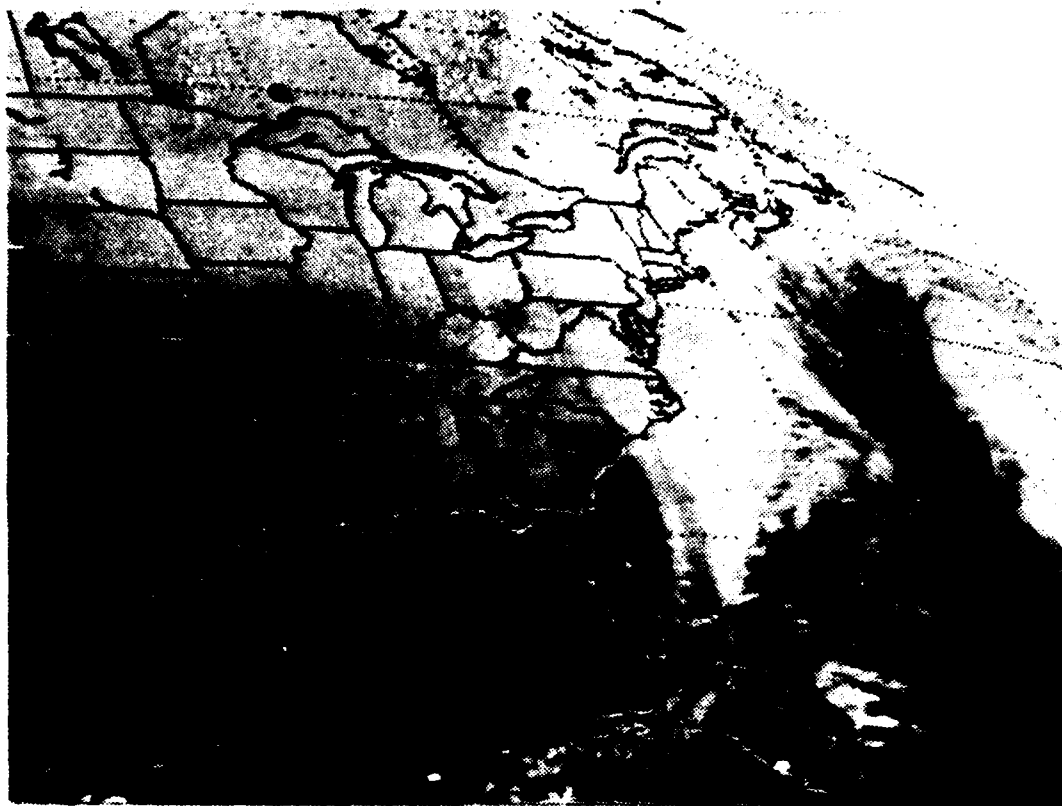
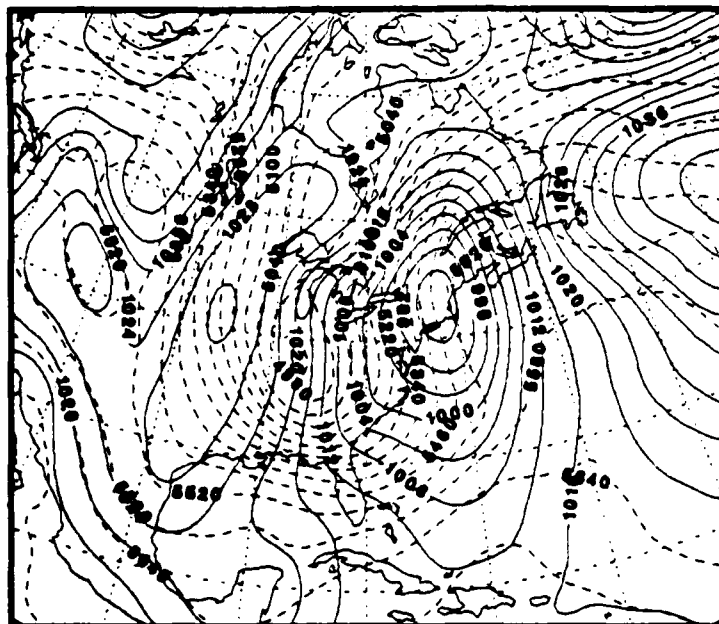


Figure 3.2d GOES IR imagery at 0004 GMT 27 January 1986.

Carolinas with much weaker PVA located over the storm center. The surface cyclone remained in proximity to the right-rear quadrant of the downstream jet streak. Deep convection associated with the original cold front as well as shallow cloudiness in the cold air behind the front are depicted in GOES visible imagery at 1330 GMT 27 January 1986 (Fig. 3.3d).

The reduced upper-level forcing due to weakened PVA aloft and movement of the storm center over land created conditions less favorable for continued intensification of the coastal cyclone. The storm had been expected to produce 1-2 feet of snow from West Virginia across Pennsylvania and into east-central New York. However, snowfalls of only 6-8 inches were observed in most locations. The strong surge of cold polar arctic air over the warm waters along the western edge of the Gulf Stream, combined with the strong upper-level forcing aloft over the Carolina coastal area, created conditions very favorable for development of cyclogenesis within the cold air.



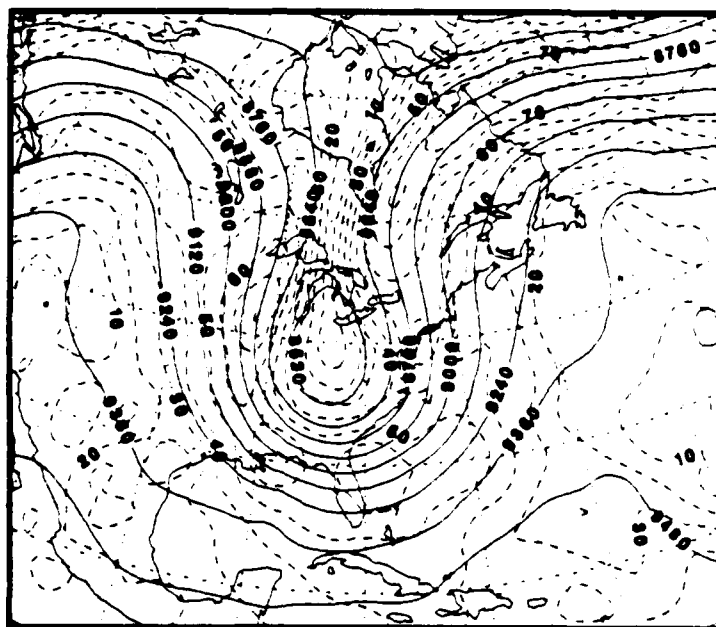


Figure 3.3c NORAPS 300 mb geopotential heights (solid) in gpm and isotach analysis (dashed) in m/s at 12 GMT 27 January 1986. Contour interval is 120 gpm (heights) and 10 m/s (isotachs).

Two distinct surface lows appear in the 00 GMT 28 January 1986 NORAPS surface analysis (Fig. 3.4a). The original coastal cyclone has deepened to 985 mb as it continued to track northward into Quebec, Canada. A secondary cyclogenesis event has also developed off Cape Hatteras (39.0°N , 70.5°W) in the cold continental offshore flow and deepened to 991 mb. The corresponding 1000-500 thickness pattern indicates that strong advection offshore continued to occur south of New Jersey as far as Florida. Negligible thermal advection is occurring over the original surface cyclone in the low- to mid-troposphere with weak warm advection at 250 mb (not shown). Weak thermal advection in the low- to mid troposphere is occurring over the secondary cyclone with strong warm advection at 250 mb. A lobe in the 500 mb vorticity analysis that is associated with the mid-tropospheric vortex has resulted in strong PVA over the secondary cyclone center (Fig. 3.4b). The 500 mb long-wave trough along 79°W has amplified considerably due to the southeast push of cold polar air in the lower troposphere. Three separate intense (70 m/s) jet streaks are translating through the long-wave trough (Fig. 3.4c). The jet streak previously located at the base of the trough 12 h earlier has moved slightly downstream so that the secondary cyclone continues to be positioned under the left exit region of the jet. The 1831 GMT 27

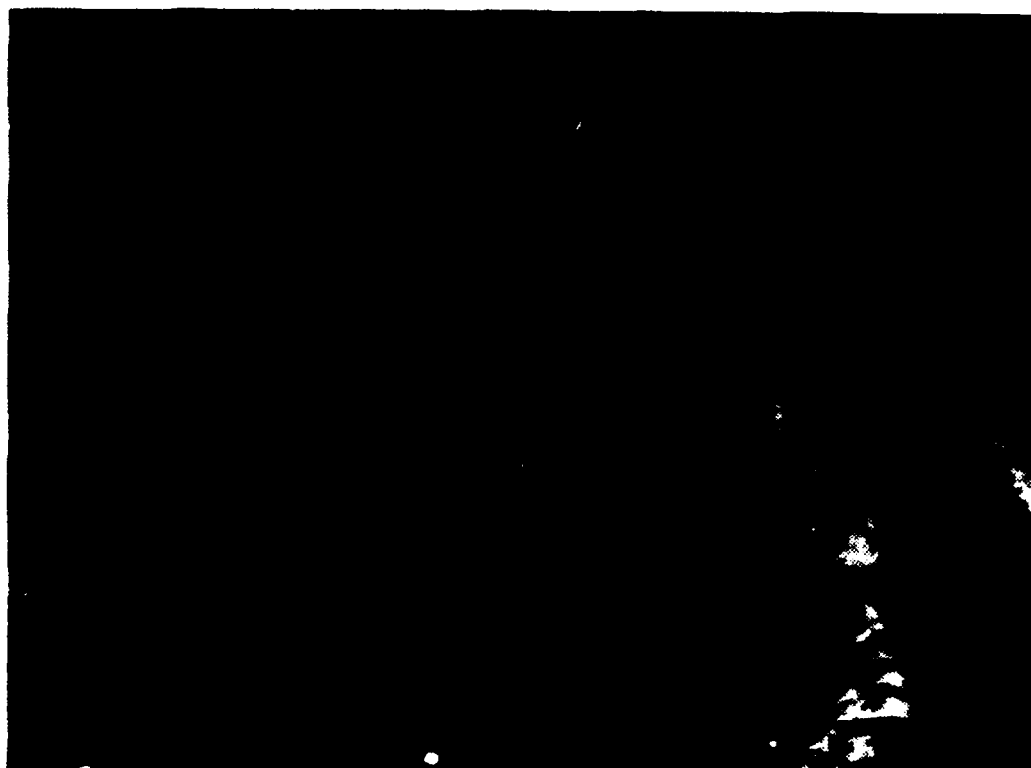


Figure 3.3d GOES visible imagery at 1330 GMT 27 January 1986.

January GOES visible imagery indicates extensive cloudiness in the cold air with a distinct cloud band associated with the incipient secondary system (Fig. 3.4d).

Because the original coastal cyclone now located in Canada has insignificant upper-level forcing and weak thermal advection, no further development of this system is anticipated. However, the secondary cyclogenesis event has very strong upper-level jet streak forcing and its position offshore creates conditions favorable for significant deepening.

By 12 GMT 28 January 1986 (Fig. 3.5a), both cyclones have moved rapidly northward. The original coastal cyclone is east of Hudson Bay (57.2°N , 69.2°W) and has deepened slightly to 984 mb. The secondary cyclone center is in New Brunswick, Canada (45.8°N , 67.1°W) and has undergone rapid deepening to 983 mb over the previous 12 h period. A pronounced baroclinic zone that is associated with the cold air surge is offshore in the wake of the secondary cyclone. Very strong cold advection in

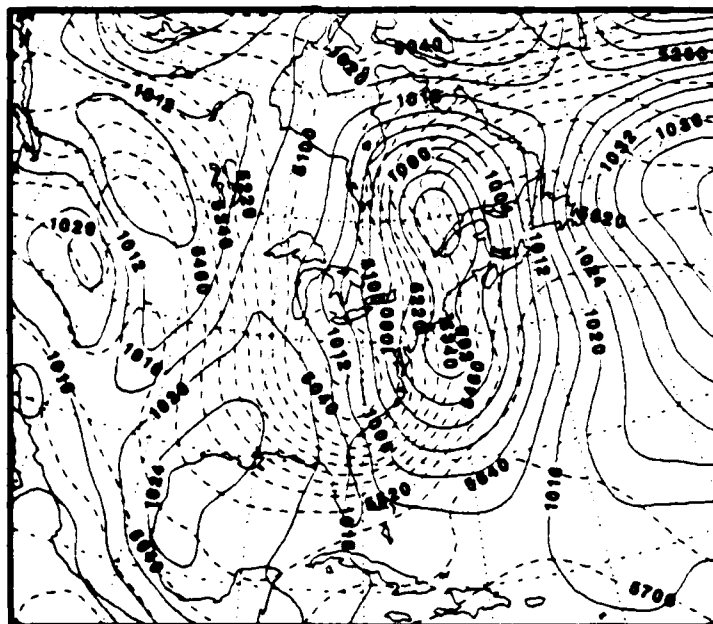


Figure 3.4a NORAPS surface pressure analysis (solid) in mb and 1000-500 mb thickness (dashed) in gpm at 00 GMT 28 January 1986. Contour interval is 4 mb (isobars) and 60 gpm (thickness).

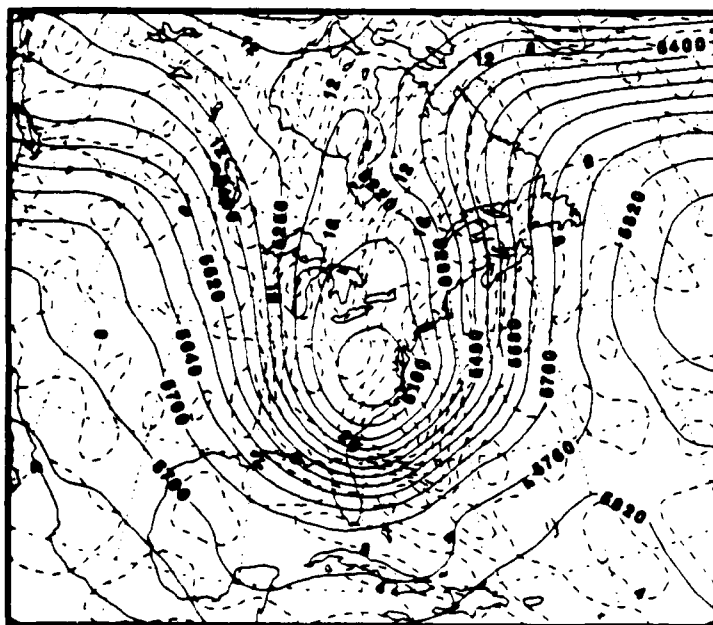


Figure 3.4b NORAPS 500 mb geopotential heights (solid) in gpm and absolute vorticity (dashed) in units of 10^{-5} s^{-1} at 00 GMT 28 January 1986. Contour interval is 60 gpm (heights) and $4 \times 10^{-5} \text{ s}^{-1}$ (vorticity).

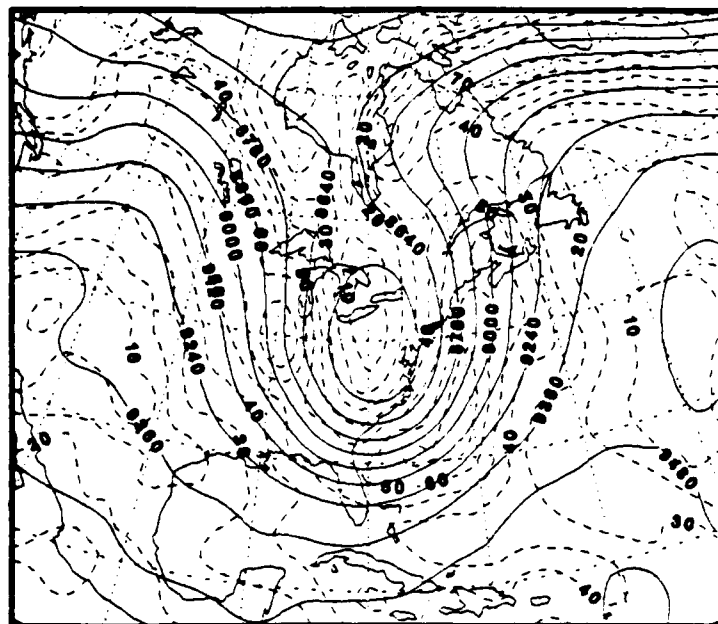


Figure 3.4c NORAPS 300 mb geopotential heights (solid) in gpm and isotach analysis (dashed) in m/s at 00 GMT 28 January 1986. Contour interval is 120 gpm (heights) and 10 m/s (isotachs).

the lower troposphere is evident from Maine to Florida. The temperature analyses at 850, 700, 500 and 250 mb indicate weak thermal advection at all levels over the primary system and strong cold advection (850 and 700 mb) with moderate warm advection (250 mb) over the secondary cyclone center (not shown). Continued eastward translation of the long-wave axis to 75°W with significant (120 gpm) deepening of the mid-tropospheric vortex is shown in Fig. 3.5b. The PVA aloft is weak over both cyclone centers. Due to the continued downstream translation of the intense 70 m/s jet streak along the east coast of the U.S., the secondary cyclone center remained under the left exit region of the jet (Fig. 3.5c). Both frontal cloudiness and an extensive cloud deck associated with the cold outbreak over the ocean (Fig. 3.5d) are depicted in the GOES IR satellite imagery at 1300 GMT 28 Jan 1986.

Although both of these cyclones deepened at rates that Sanders and Gyakum (1980) characterized as "explosive deepeners", they were not classical winter storms because their snow shields were not sufficient to paralyze the east coast. The major cold outbreak following the second cyclone into the southeast was particularly impressive. Temperatures at 500 mb were -40°C, as low as -27°C at 850 mb and temperatures below freezing were measured near the sea surface along the west edge of



Figure 3.4d GOES visible imagery at 1831 GMT 27 January 1986.

the Gulf Stream, where SST's were at least 18°C . The resulting convection was vigorous, although capped at about 3 km, and contained lightning and thousands of steam devils. This cold air surge coincided with the space shuttle Challenger tragedy.

C. VERIFICATION OF NORAPS "OPERATIONAL" MODEL FORECASTS

At 00 GMT 27 January 1986, the NORAPS 12-h surface forecast depicts a 999 mb low center at 36.3°N , 74.1°W (Fig. 3.6a), whereas the corresponding surface analysis has a 1000 mb center about 30 n mi to the northeast at 36.7°N , 74.5°W (Fig. 3.2a). Although the storm intensity and location verifies well, other significant differences exist. The forecast tends to underestimate the size of the storm and includes ridging across Virginia that is not indicated in the analysis. The SLP forecast minus analysis field depicts several regions with 2-4 mb forecast errors (Fig. 3.6b). Overprediction of the intensity of the upstream ridges along 98°W and 110°W leads to areas with 2-4 mb differences west of the coastal low. Similarly, the forecast ridging

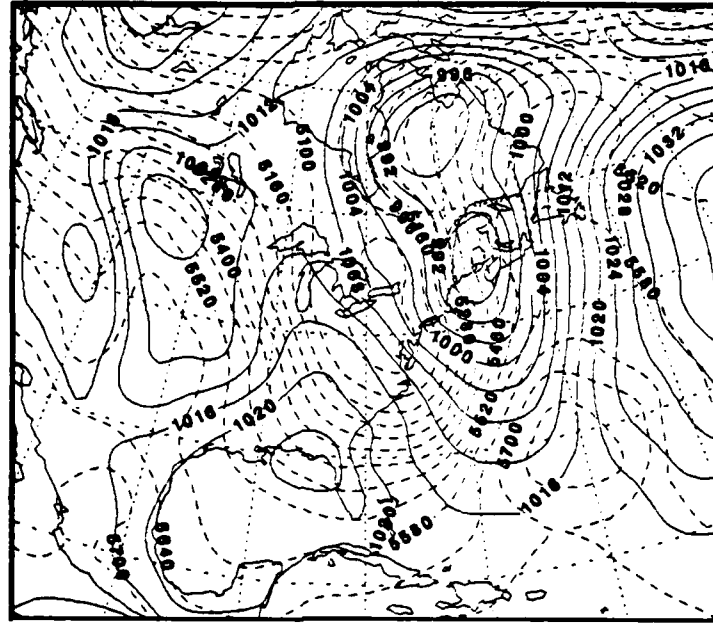


Figure 3.5a NORAPS surface pressure analysis (solid) in mb and 1000-500 mb thickness (dashed) in gpm at 12 GMT 28 January 1986. Contour interval is 4 mb (isobars) and 60 gpm (thickness).

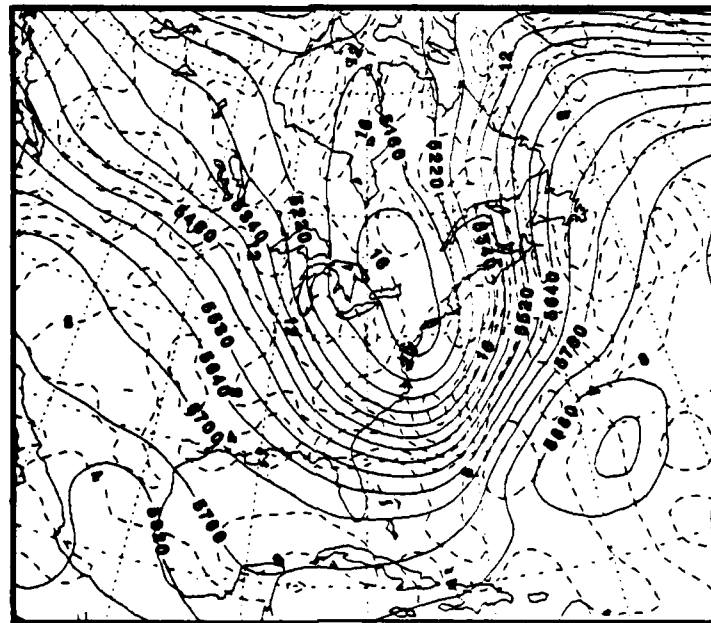


Figure 3.5b NORAPS 500 mb geopotential heights (solid) in gpm and absolute vorticity (dashed) in units of 10^{-5} s^{-1} at 12 GMT 28 January 1986. Contour interval is 60 gpm (heights) and $4 \times 10^{-5} \text{ s}^{-1}$ (vorticity).

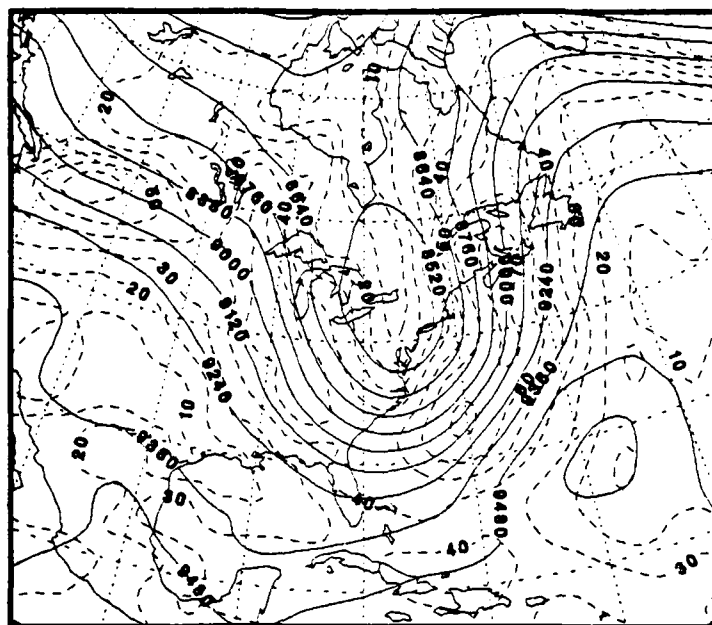


Figure 3.5c NORAPS 300 mb geopotential heights (solid) in gpm and isotach analysis (dashed) in m/s at 12 GMT 28 January 1936. Contour interval is 120 gpm (heights) and 10 m/s (isotachs).

across Virginia and underestimation of the intensity of the North Atlantic anticyclone are also associated with areas of 2-4 mb differences. Both forecast and analysis 1000-500 thickness patterns have regions of enhanced baroclinicity along the eastern seaboard with strong cold advection from the Carolinas southward and moderate warm advection across New England. In the 500 mb forecast (Fig. 3.6c), the long-wave trough is narrower and displaced slightly west of the analyzed position. Additionally, the analyzed 500 mb short-wave (Fig. 3.2b) just downstream of the long-wave axis is not clearly depicted in the forecast. As a result, the absolute vorticity maxima are forecast to the west of the corresponding analysis positions. Forecast 500 mb heights also tend to underestimate the intensity of the long-wave trough by 30-90 gpm off the Florida coast eastward to 65°W (Fig. 3.6d), due to the absence of this short-wave feature. Therefore, the model tends to predict weaker PVA aloft over the storm center than is indicated in the analysis. The 300 mb forecast (not shown) verifies well with the analysis, and depicts intense jet streaks greater than 70 m/s both upstream and downstream of the trough axis. The 850, 700 and 500 mb forecasts include moderate cold advection in the low- to mid-troposphere, whereas the corresponding analyses have weak warm advection. The forecast warm advection at 250 mb is stronger than indicated in the analysis (not shown).

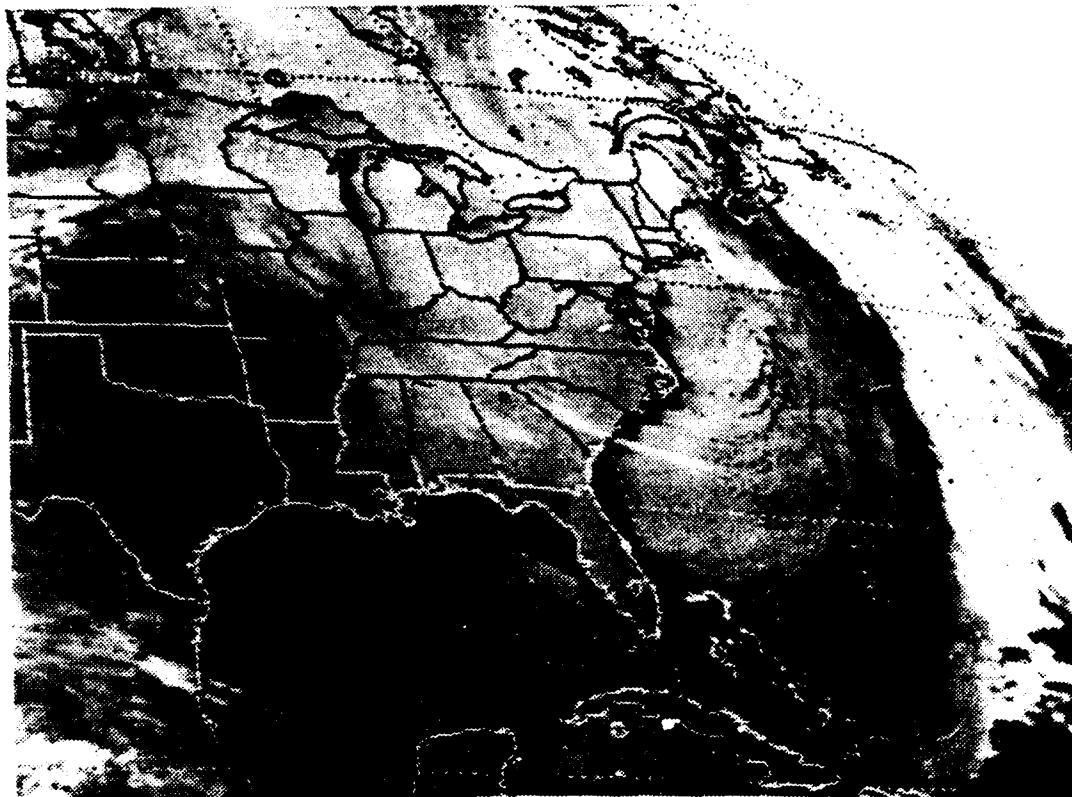


Figure 3.5d GOES visible imagery at 1300 GMT 28 January 1986.

Overall, the NORAPS 12-h "operational" forecast fields are in agreement with the corresponding analysis fields. Significant differences can be attributed to the error in the predicted position of the coastal low (30 n mi) and the greater low-level surge of cold air off the Florida coast. The forecast 500 mb heights do not indicate the presence of a short-wave aloft and the predicted 500 mb long-wave trough is too narrow.

The NORAPS 24-h surface forecast verifying at 12 GMT 27 January 1986 has the storm center over Long Island (41.0°N , 72.6°W) with a deepening to 982 mb (Fig. 3.7a). The corresponding surface center in the analysis is in New Hampshire (43.2°N , 71.8°W) with an intensity of 986 mb (Fig. 3.3a). This 4 mb forecast error in storm intensity in combination with a positional error of approximately 130 n mi is significant. The surface forecast still depicts a high pressure ridge west of Chesapeake Bay. The surface trough associated with the secondary cold front is located offshore in

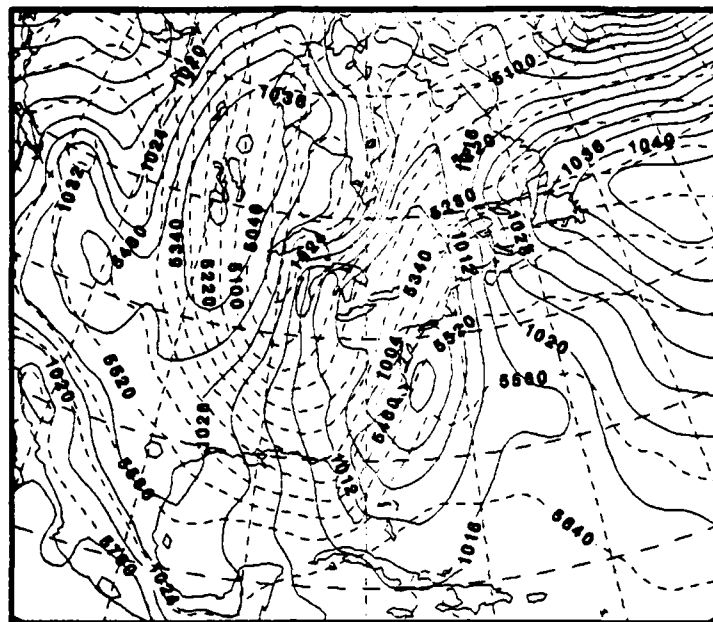


Figure 3.6a NORAPS operational forecast SLP (solid) in mb and 1000-500 mb thickness (dashed) in gpm at 00 GMT 27 January 1986. Contour interval is 4 mb (isobars) and 60 gpm (thickness).

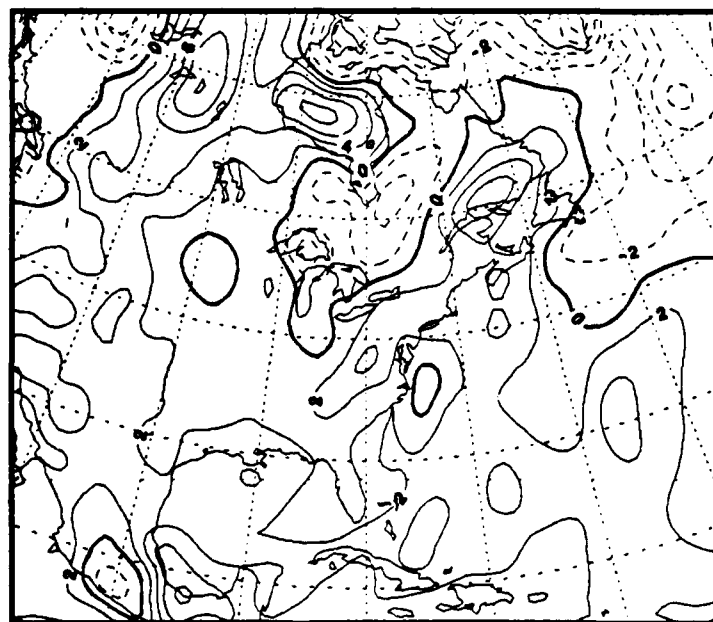


Figure 3.6b NORAPS operational forecast SLP minus verifying analysis (contour interval of 2 mb) at 00 GMT 27 January 1986. Positive, negative differences are solid, dashed, and the zero contour is enhanced.

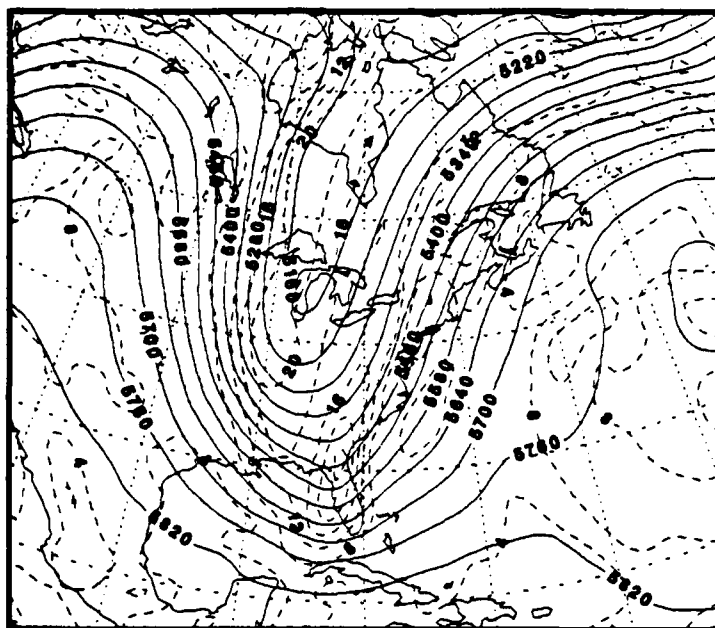


Figure 3.6c NORAPS operational forecast 500 mb heights (solid) in gpm and absolute vorticity (dashed) in units of 10^{-5} s^{-1} at 00 GMT 27 January 1986. Contour interval is 60 gpm (heights) and $4 \times 10^{-5} \text{ s}^{-1}$ (vorticity).

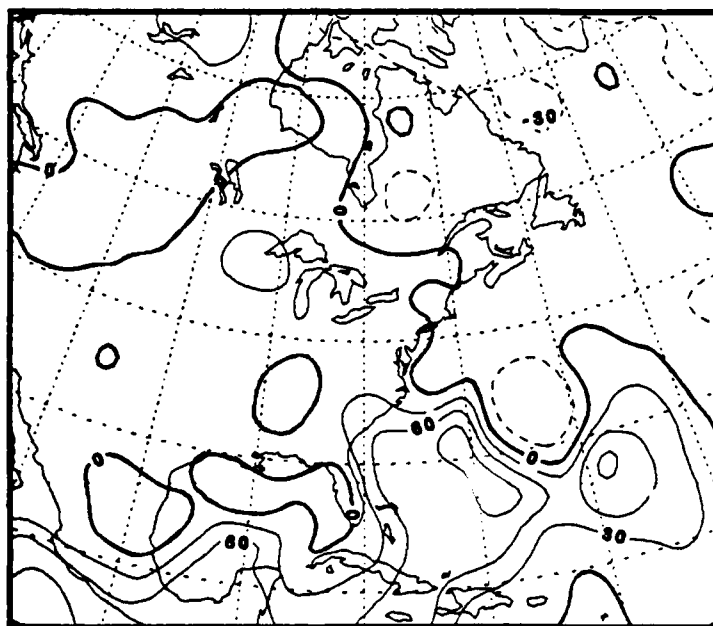


Figure 3.6d NORAPS operational forecast 500 mb heights minus verifying analysis (contour interval of 30 gpm) at 00 GMT 27 January 1986. Positive, negative differences are solid, dashed, and the zero contour is enhanced.

the forecast, which is east of the position in the analysis. The coastal low is too deep by 4-6 mb across most of its southern extent (Fig. 3.7b). This may be due to excessive low-level heating of the air in the cold outbreak over the Gulf Stream. The SLP forecast errors upstream of the surface low have increased dramatically with typical values ranging from 4-16 mb in the Northwest and Midwest regions of North America. These appear to be due to poor handling of the surface processes in the cold air over land. Surface highs in these areas tend to be overpredicted (too high) while the lows are underpredicted (too high) over this range of values. Both the forecast and analyzed 1000-500 thickness patterns indicate that the lower-tropospheric baroclinic zone along the eastern seaboard is strengthening. The forecast 500 mb height and absolute vorticity (Fig. 3.7c) are in general agreement with the 500 mb analysis. The location of the mid-tropospheric closed vortex is shifted slightly to the east of the analysis position. The absolute vorticity centers verify well and the prediction of relatively weak PVA over the storm center is supported by the analysis. The forecast 500 mb heights are too high by 30-60 gpm off the Carolina coast due to the absence of the translating short-wave trough (Fig. 3.7d). West of the closed vortex and along the upstream ridge, the 500 mb heights are also too high by 30-60 gpm. At 300 mb, a 60 m/s jet streak is predicted upstream of the trough axis (not shown), while the same jet is analyzed at 70 m/s. This is consistent with the weaker gradient to the west of the low at 500 mb mentioned above. Both the 850, 700, 500 and 250 mb forecasts and analyses have moderate cold advection in the lower troposphere and moderate warm advection at upper levels over the storm center (not shown).

By 00 GMT 28 January 1986, two surface systems are evident in both the forecast and analysis. The forecast indicates that the primary cyclone has tracked northwest into southern Quebec, Canada (47.1°N , 74.5°W) at a speed of about 14 kts (Fig. 3.8a), whereas the analyzed location is in northern Quebec (49.8°N , 69.6°W) and the translation speed is 18 kts (Fig. 3.4a). Although the forecast intensity of 984 mb verifies very well with the analyzed intensity of 985 mb, there is a large positional error of approximately 240 n mi in the predicted storm track. The forecast secondary cyclogenesis in the cold air at (39.6°N , 73.3°W) and predicted intensity of 990 mb verifies fairly well with the corresponding position (39.0°N , 70.5°W) and intensity (991 mb) in the analysis. The error in the predicted storm position is approximately 80 n mi. The forecast 1000-500 thickness pattern depicts a strong offshore cold surge south of the secondary system, with a deeper SLP trough than is indicated in the analysis.

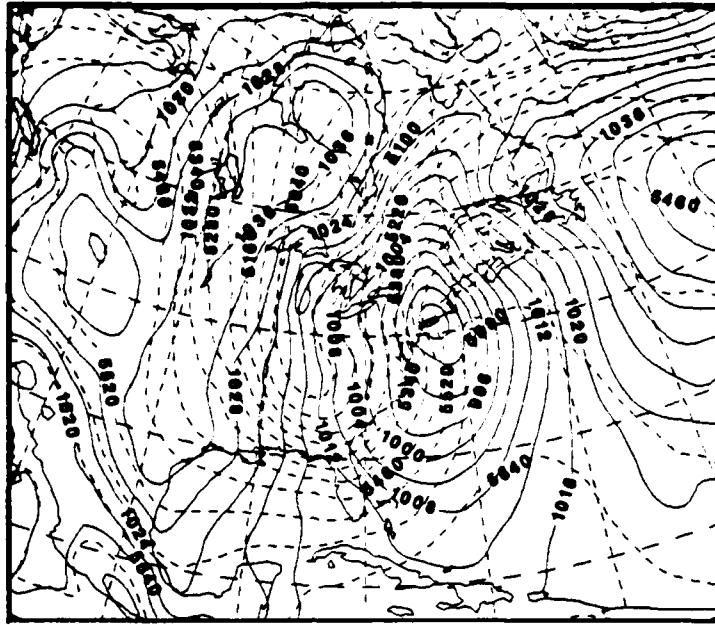


Figure 3.7a NORAPS operational forecast SLP (solid) in mb and 1000-500 mb thickness (dashed) in gpm at 12 GMT 27 January 1986. Contour interval is 4 mb (isobars) and 60 gpm (thickness).

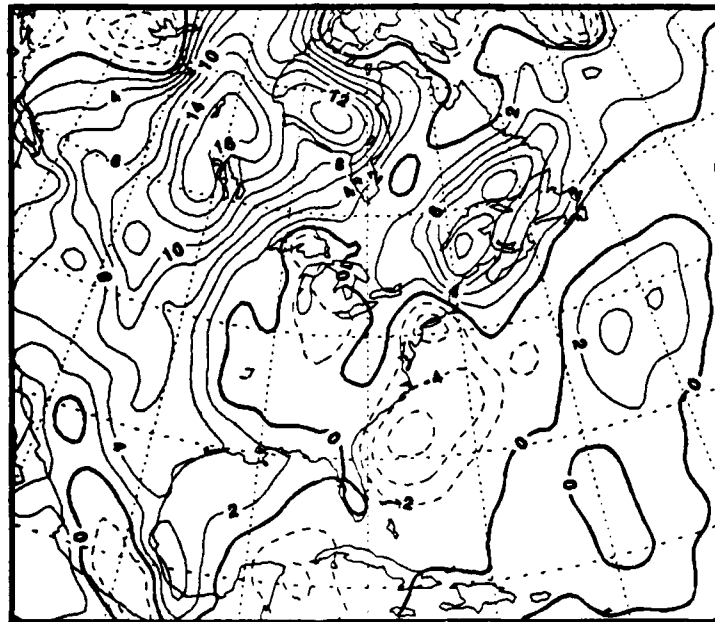


Figure 3.7b NORAPS operational forecast SLP minus verifying analysis (contour interval of 2 mb) at 12 GMT 27 January 1986. Positive negative differences are solid dashed, and the zero contour is enhanced.

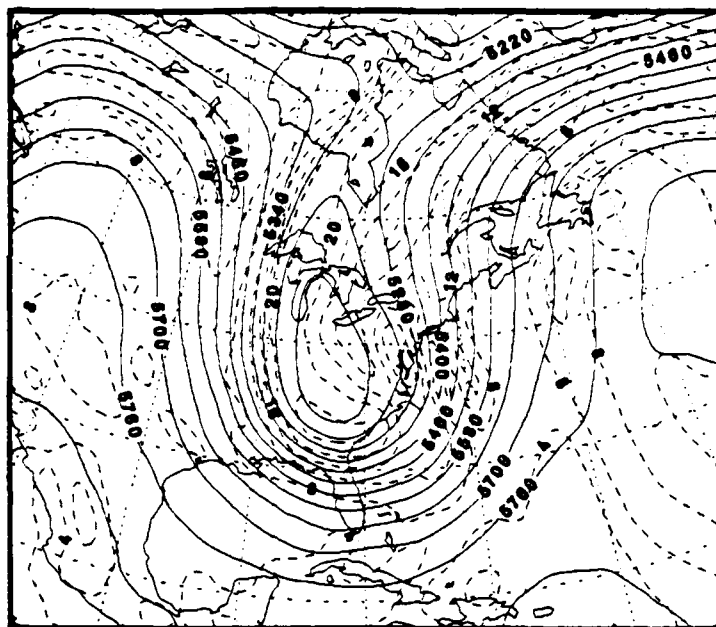


Figure 3.7c NORAPS operational forecast 500 mb heights (solid) in gpm and absolute vorticity (dashed) in units of 10^{-5} s^{-1} at 12 GMT 27 January 1986. Contour interval is 60 gpm (heights) and $4 \times 10^{-5} \text{ s}^{-1}$ (vorticity).

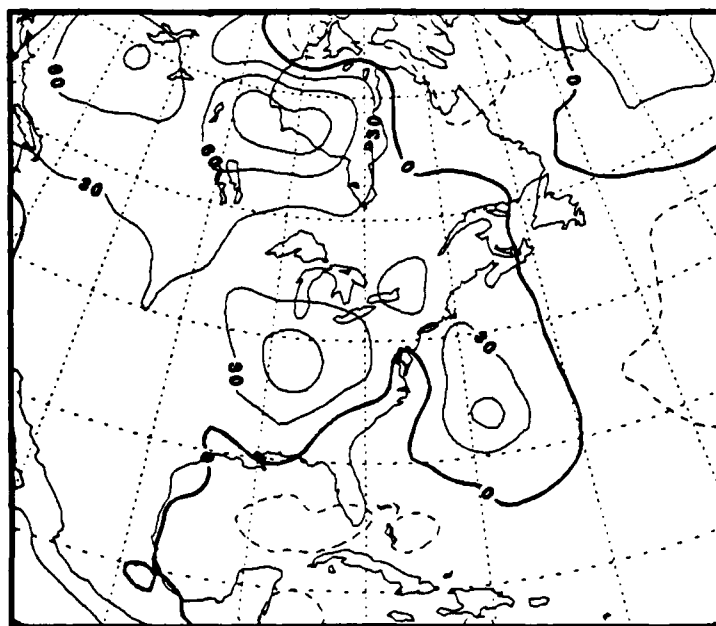


Figure 3.7d NORAPS operational forecast 500 mb heights minus verifying analysis (contour interval of 30 gpm) at 12 GMT 27 January 1986. Positive negative differences are solid dashed, and the zero contour is enhanced.

Increasingly larger SLP forecast errors are indicated in the verification fields in Fig. 3.8b. The lower forecast SLP's off the Carolina coast continue to be evident where the cold air streams over the region of high SST's. The large forecast errors associated with the upstream synoptic pattern remain significant (4-16 mb) and appear to be stationary over the cold land surfaces. Some of the significant SLP forecast errors (12-20 mb) in the region north of the primary low may be due to the large positional error of the forecast storm track. However, much of the error appears to be associated with excessive SLP over the cold land surface. Additionally, the strong North Atlantic anticyclone to the east is now overpredicted by 4-6 mb. The 500 mb forecast (Fig. 3.8c) of strong PVA over the secondary system verifies well with the analysis. Overprediction of the mid-tropospheric vortex heights by 60 gpm and underestimation of the trough heights at the base by 0-30 gpm can be identified in the 500 mb verification field (Fig. 3.8d). The ridge over southern Canada is overpredicted by 60-120 gpm. The 300 mb isotach forecast (not shown) also does not verify with the corresponding analysis. Three separate jet streaks with intensities of 60 m/s in the forecast (not shown) are associated with the long-wave trough, whereas the analysis has only two jet streaks with intensities of 70 m/s. The location of the forecast jet streaks is also quite different from that of the analysis. The secondary cyclone in the analysis is under the left-exit region of the downstream jet streak, whereas the forecast has the primary cyclone in this position.

The 48-h prognosis at 12 GMT 28 January 1986 continues to depict the two surface lows but their positions and intensities are both poorly forecast. The initial coastal low was forecast to be southeast of Hudson Bay at 51.7°N, 77.6°W with an intensity of 994 mb (Fig. 3.9a), whereas the actual storm track has the low approximately 350 n mi to the northeast at 57.2°N, 69.2°W with an intensity of 984 mb (Fig. 3.5a). This difference of 10 mb constitutes the largest forecast error that occurs over the 48-h period, as the model continues to fill the low when in fact it is still deepening slightly. Similarly, the secondary cyclone is predicted at 40.0°N, 69.3°W and has filled to 992 mb, whereas the actual storm moved northward into New Brunswick, Canada (45.8°N, 67.1°W) and has undergone rapid intensification to 983 mb. The SLP verification field includes several areas with large forecast errors (Fig. 3.9b). The intensity of the North Atlantic anticyclone continues to be overpredicted by 4-12 mb west of the ridge axis. The SLP trough along the east coast of the U.S. is predicted to be much deeper (4-10 mb) than in the corresponding analysis. Similarly, the high

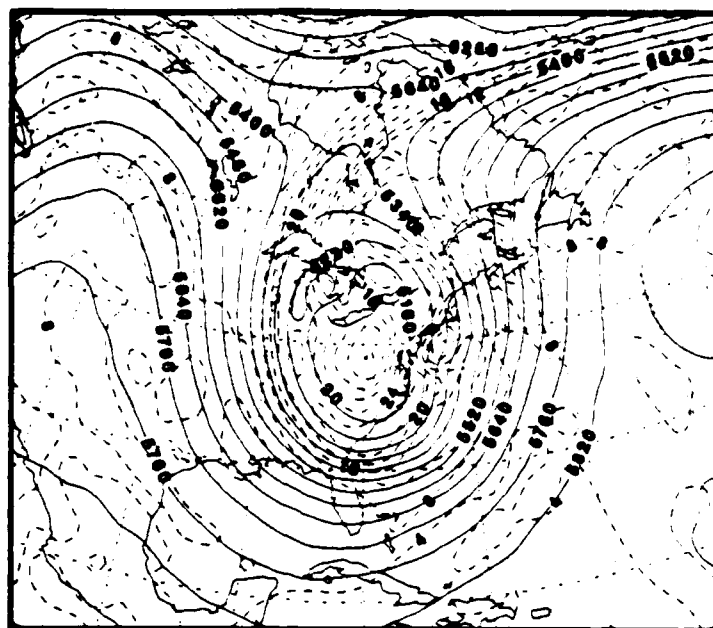


Figure 3.8c NORAPS operational forecast 500 mb heights (solid) in gpm and absolute vorticity (dashed) in units of 10^{-5} s^{-1} at 00 GMT 28 January 1986. Contour interval is 60 gpm (heights) and $4 \times 10^{-5} \text{ s}^{-1}$ (vorticity).

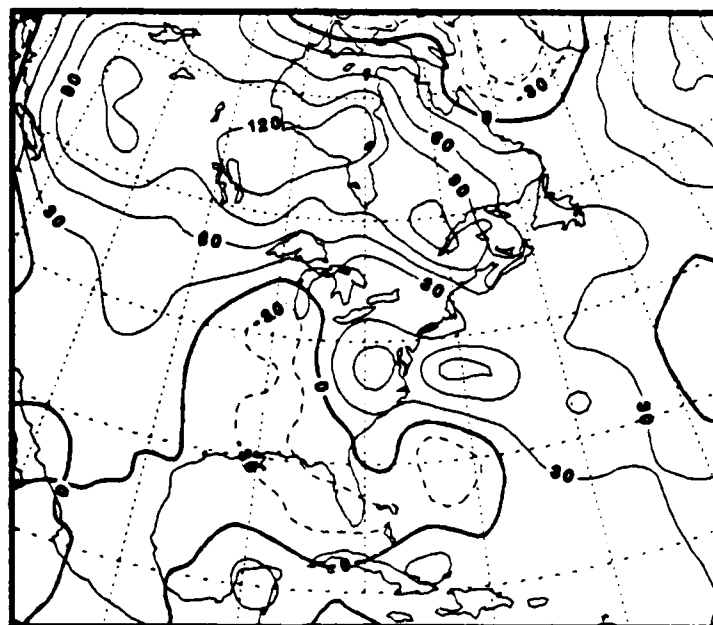


Figure 3.8d NORAPS operational forecast 500 mb heights minus verifying analysis (contour interval of 30 gpm) at 00 GMT 28 January 1986. Positive, negative differences are solid, dashed, and the zero contour is enhanced.

pressure system over and to the east of the Rockies continues to be over-predicted by 8-20 mb. Forecast errors of as much as 36 mb north of the primary low appear to be due to the large positional errors in the forecast storm track and excessive SLP over the cold land surface. The forecast 1000-500 thickness pattern shows a weaker thermal gradient in the lower troposphere than the verifying analysis. The forecast 500 mb height and absolute vorticity fields (Fig. 3.9c) also have extensive errors. The forecast 500 mb heights along the upstream ridge are too high by 60-210 gpm and the forecast heights near the base of the trough are too low by 30-150 gpm, which results in significant distortion of the 500 mb field. The mid-tropospheric vortex is still underforecast by 60-90 gpm. As anticipated, the associated absolute vorticity fields verify poorly. The 300 mb forecast (not shown) includes a 60 m/s jet streak upstream and a 70 m/s jet streak downstream, whereas the 300 mb analysis (Fig. 3.5c) indicates that the upstream jet streak intensity is only 50 m/s.

The tracks of the primary coastal cyclone for both the NORAPS "operational" forecast (every 6 h) and analysis (every 12 h) from 12 GMT 26 January 1986 until 12 GMT 28 January 1986 are presented in Fig. 3.10a. The forecast track errors increase in time. After only 24 h, the center lags the observed low by approximately 130 n mi. Beyond the 24 h period, the forecast track is to the west of the observed cyclone track. The NORAPS "operational" forecast and analyzed intensities at each 12-h verification time starting from 12 GMT 26 January 1986 are given in Fig. 3.10b. The predicted intensity agrees quite well with the analyzed intensity to 12 h, but overpredicts (too deep) the cyclone intensity by 4 mb at 12 GMT 27 January 1986. Beyond 24 h, the low is predicted to fill, while the analysis indicates that the low is still deepening slightly. Therefore, the small error at 00 GMT 28 January 1986 (36 h) should be regarded as somewhat coincidental. At 12 GMT 28 January 1986 (48 h), the forecast error has reached a maximum at 10 mb.

The NORAPS "operational" forecast versus analyzed track for the secondary system from 00 GMT 28 January 1986 to 12 GMT 28 January 1986 is depicted in Fig. 3.11. The initial track error is approximately 125 n mi and increases to about 300 n mi after only 12 hours. The model-predicted cyclone intensity of 990 mb verifies well with the analyzed intensity of 991 mb at 00 GMT 28 January 1986 (not shown). By 12 GMT 28 January 1986 (12 h), the forecast SLP of 992 mb is much higher than the analyzed value of 983 mb. As in the primary system, the tendency of the NORAPS model to fill the low center prematurely is noted.

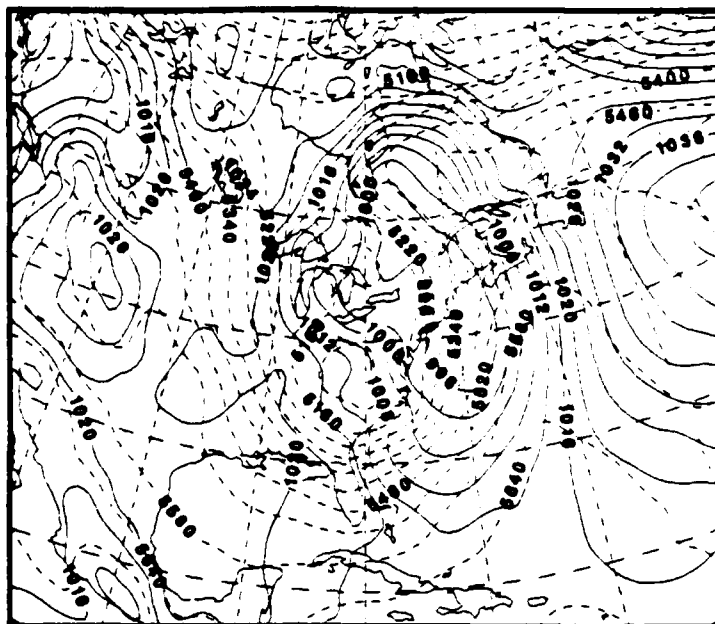


Figure 3.9a NORAPS operational forecast SLP (solid) in mb and 1000-500 mb thickness (dashed) in gpm at 12 GMT 28 January 1986. Contour interval is 4 mb (isobars) and 60 gpm (thickness).

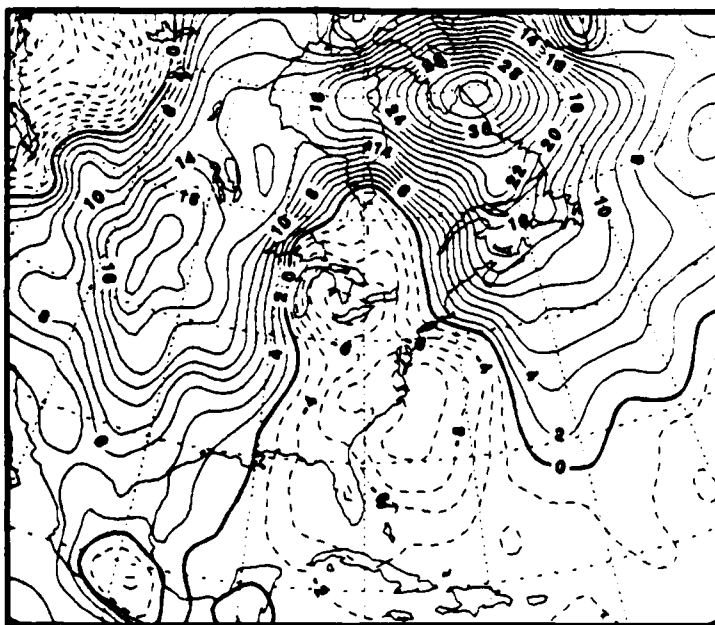


Figure 3.9b NORAPS operational forecast SLP minus verifying analysis (contour interval of 2 mb) at 12 GMT 28 January 1986. Positive negative differences are solid dashed, and the zero contour is enhanced.

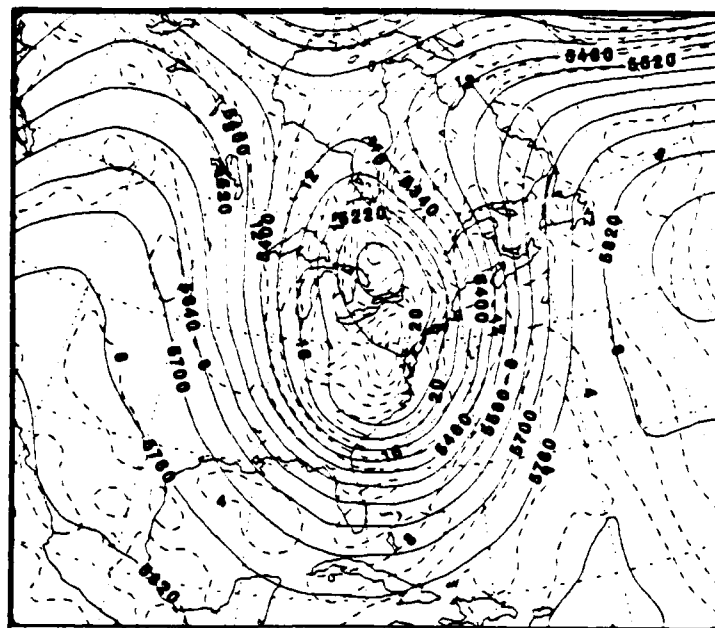


Figure 3.9c NORAPS operational forecast 500 mb heights (solid) in gpm and absolute vorticity (dashed) in units of 10^{-5} s^{-1} at 12 GMT 28 January 1986. Contour interval is 60 gpm (heights) and $4 \times 10^{-5} \text{ s}^{-1}$ (vorticity).

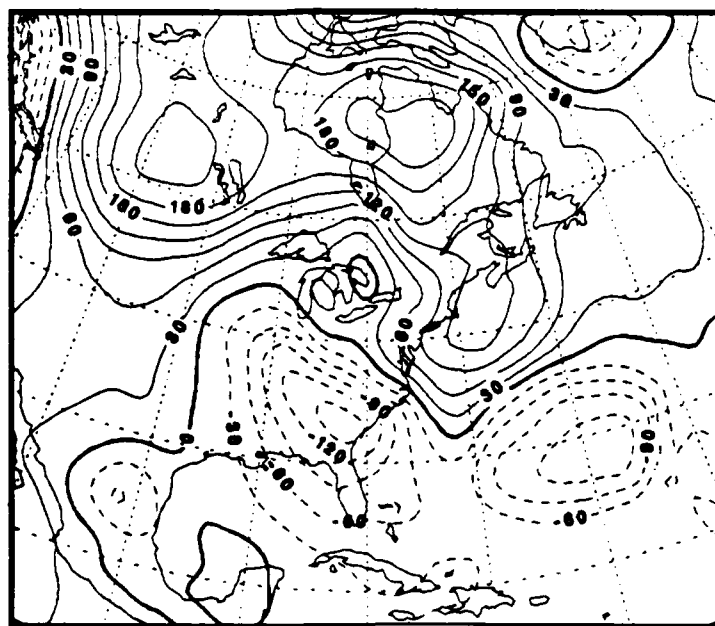


Figure 3.9d NORAPS operational forecast 500 mb heights minus verifying analysis (contour interval of 30 gpm) at 12 GMT 28 January 1986. Positive negative differences are solid dashed, and the zero contour is enhanced.

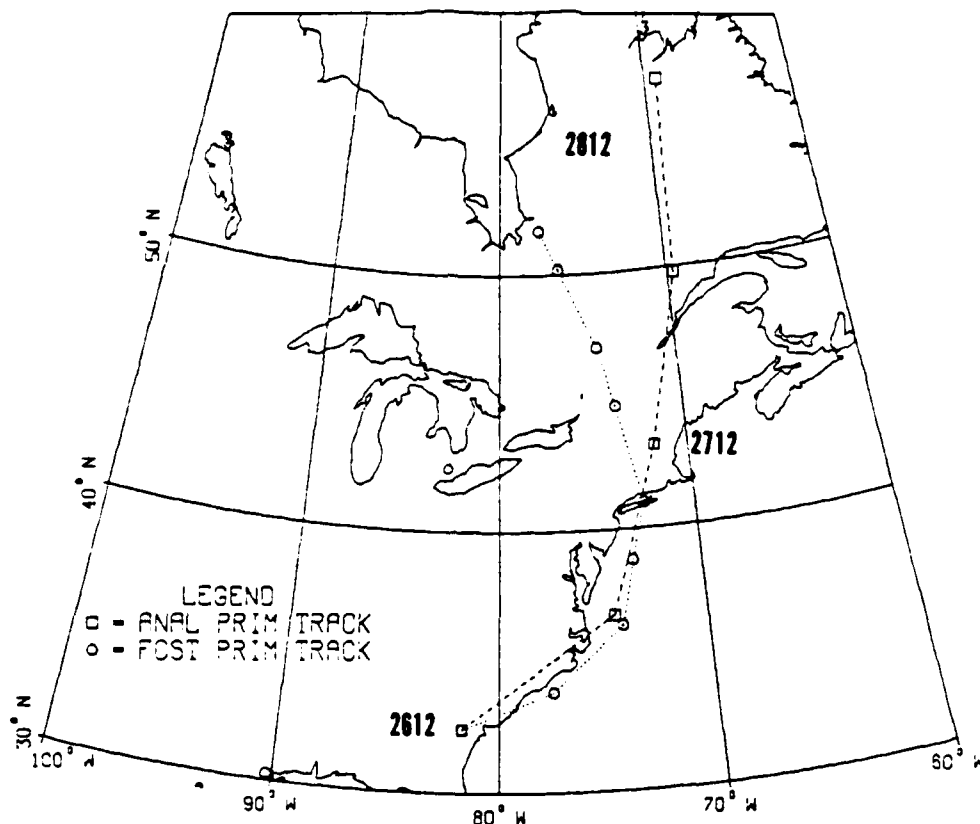


Figure 3.10a NORAPS "operational" forecast positions (circles) each 6h and analyzed positions (boxes) each 12 h for the primary coastal cyclone from 12 GMT 26 January to 12 GMT 28 January 1986.

The forecast minus analyzed cyclone track and intensity differences identified at the 36 and 48-h verification times appear to be associated with several factors. The influence of the lateral boundaries may be linked to these observed differences. As suggested above, the poor surface forecasts over the cold land regions and off the east coast of the U.S. in the cold outbreak region also may contribute to the errors. The SLP and 500 mb verifications indicate that the model overpredicts (too high) SLP's and heights upstream of the surface low and 500 mb trough respectively. At each successive verification time, these forecast errors increase in magnitude and areal extent. By the 36 and 48-h verification times, the model tendency to overpredict SLP had propagated into the area of the surface low centers and the low centers were predicted to fill instead of continuing to deepen. Additionally, the intense North Atlantic anticyclone that was underforecast at 12 h, was significantly overpredicted by

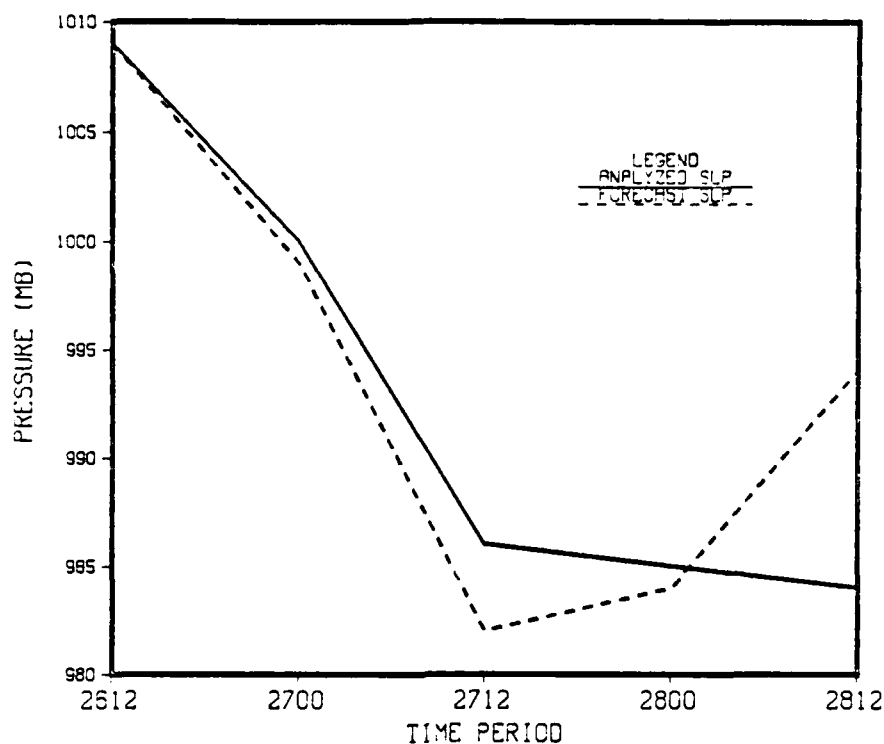


Figure 3.10b NORAPS "operational" forecast SLP (dashed) and analyzed SLP (solid) for primary coastal cyclone from 12 GMT 26 January 1986 to 12 GMT 28 January 1986.

4-12 mb at the later verification times (36 and 48 h). The forecast North Atlantic anticyclone was probably inhibited from translating eastward by the specification of the lateral boundary conditions. This high-pressure system could then act to steer the predicted storm tracks to the west of the analyzed tracks by restricting movement of the storms to the north and east. Also, the excessive SLP's over the cold land surfaces may have prevented the forecast low from penetrating into these areas (i.e. northern Quebec), which caused the 36 to 48-h forecasts to be significantly degraded.

D. VERIFICATION OF NORAPS "FINAL" MODEL FORECASTS

The initial "operational" analysis at 12 GMT 26 January 1986 is enhanced using a small subset of the data collected during GALE to begin addressing the question of data impact on NORAPS forecasts. The off-time National Weather Service (NWS) soundings and other GALE data prior to the initial time have not been assimilated because of the 12-h update cycle being used. This "final" analysis is then utilized to create a "final" forecast run that has the advantage of additional GALE area data in

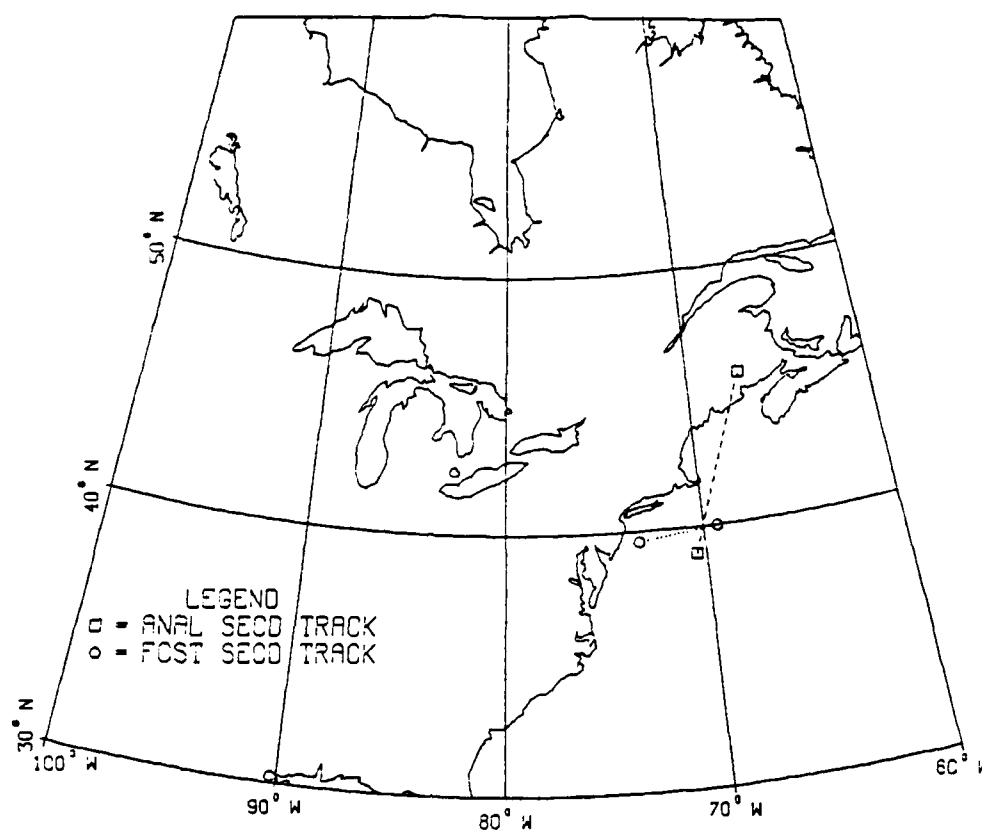


Figure 3.11. NORAPS "operational" forecast positions (circles) and analyzed positions (boxes) for the secondary cyclone at 00 GMT 28 January and 12 GMT 28 January 1986.

the initial conditions. Only 14 Omega dropwindsondes (ODW) and seven NCAR Cross-chain Loran Atmospheric Sounding System (CLASS) soundings are added to the initial analysis at 12 GMT 26 January 1986. The CLASS sites are located across North and South Carolina while the dropwindsondes are over the Atlantic coastal areas from North Carolina to Florida and in the Gulf of Mexico (Fig. 3.12). Notice that the initial storm center tends to be located upstream of the CLASS sites and positions of dropwindsonde launches. By virtue of Loran-C balloon tracking and special processing, the CLASS soundings provide more accurate and frequent winds than the NWS network. Soundings to 100 mb are provided at 3-h and 1.5 h intervals. The ODW's were launched from the NOAA Citation CE-500 and Air Force (Air Weather Service) aircraft. The ODW is a system that translates (retransmits) Omega navigation signals to a computer onboard the aircraft, which computes winds as the

sonde descends to the surface. Winds are integrated over 2-min intervals to smooth the noise in the Omega location data.

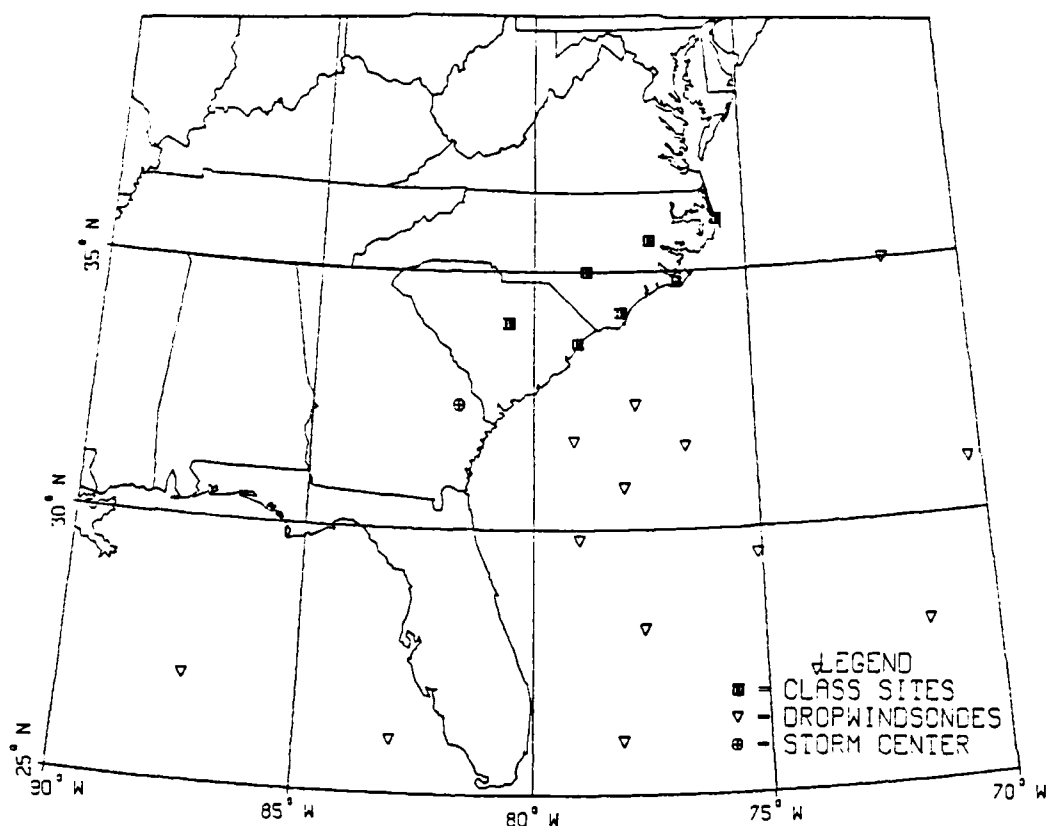


Figure 3.12 Locations of the NCAR Cross-chain Loran Atmospheric Sounding Systems (CLASS) sites (squares) and Omega Dropwindsondes (ODW) utilized in the 12 GMT 26 January 1986 enhanced analysis.

The difference between the NORAPS "final" analysis and the "operational" analysis is provided in Fig. 3.13. Geopotential heights are observed to be higher by 5-20 gpm over the Carolinas and adjacent coastal areas at both 850 and 300 mb. Over this same region, geopotential heights are lower by 10-20 gpm at the 500 mb level. This implies a colder lower troposphere and warmer upper troposphere in the "final" analysis.

Differences between the "final" forecast and the "operational" forecast at two representative levels (300 mb and 850 mb) are depicted in Fig. 3.14 and Fig. 3.15 for the period 00 GMT 27 January 1986 to 12 GMT 28 January 1986. At the 300 mb

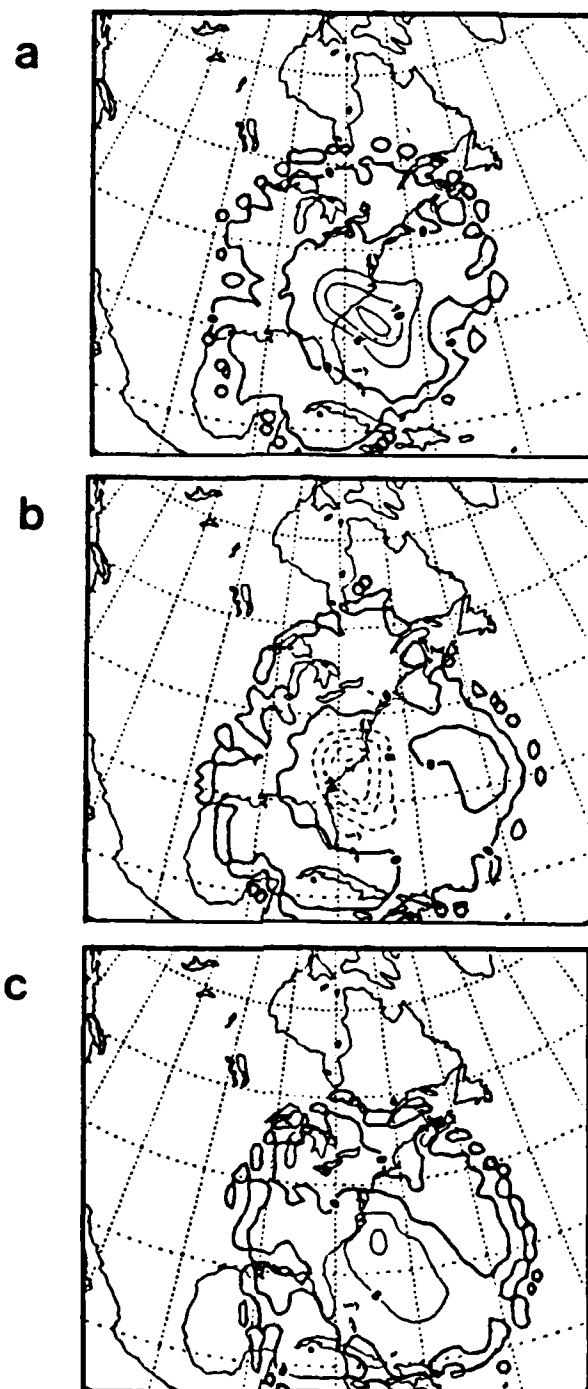


Figure 3.13 NORAPS "final" minus "operational" analysis for the
 (a) 300 mb, (b) 500 mb and (c) 850 mb level at 12 GMT
 26 January 1986. Contour interval is 5 gpm.

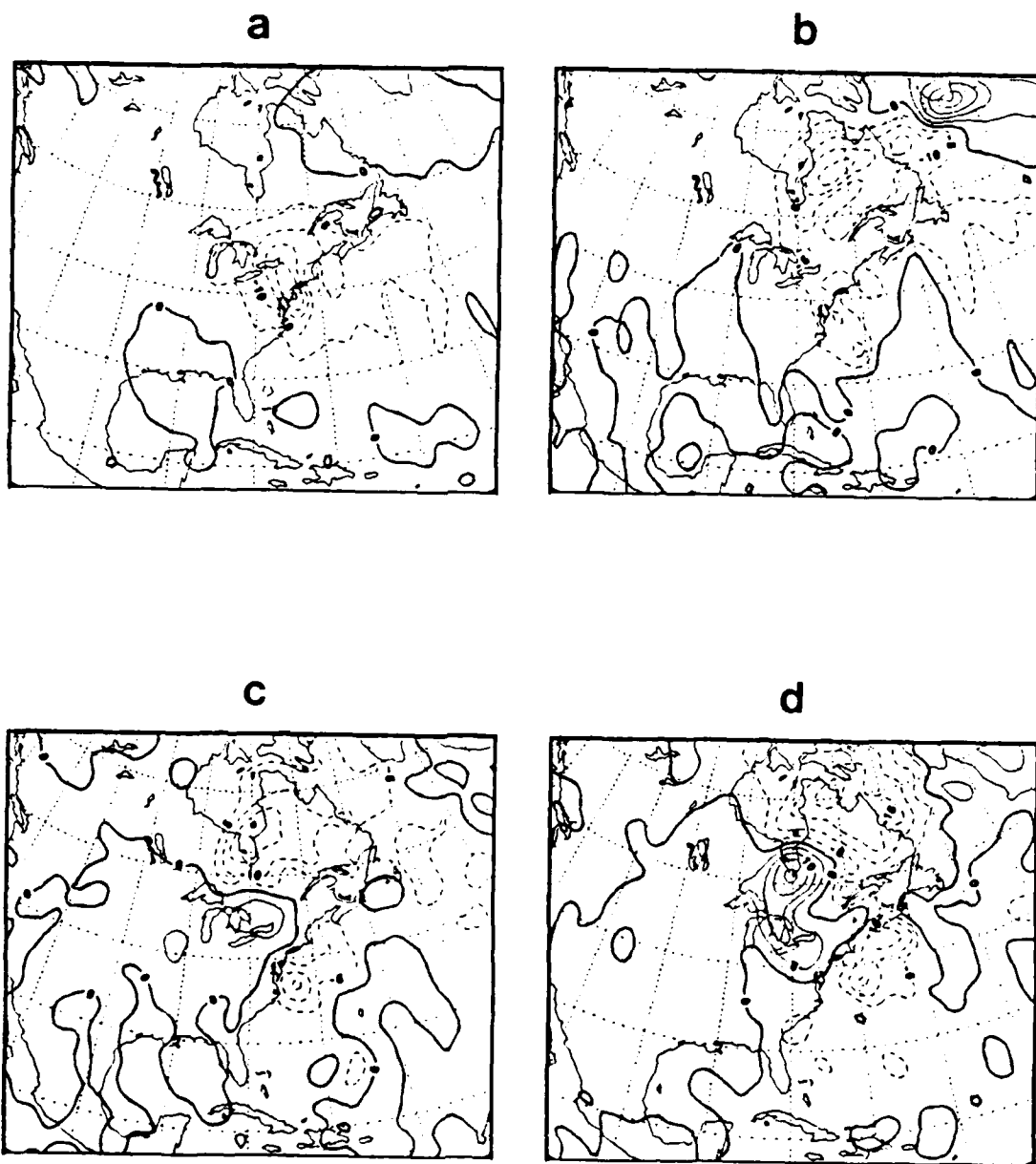


Figure 3.14. NORAPS 300 mb "final" minus "operational" forecast at (a) 00 GMT 27 January, (b) 12 GMT 27 January, (c) 00 GMT 28 January, and (d) 12 GMT 28 January 1986. Contour interval is 5 gpm.

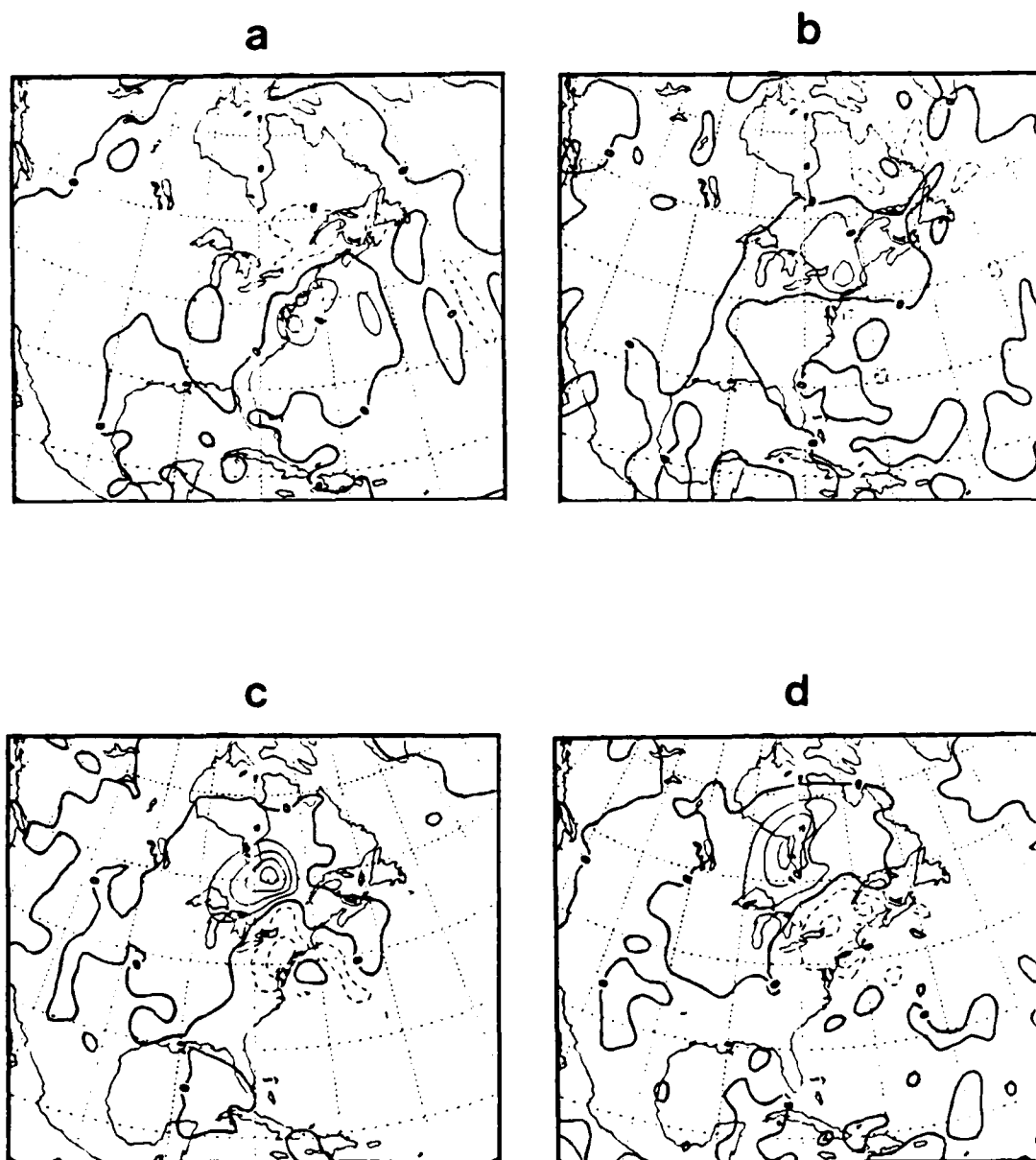


Figure 3.15 NORAPS 850 mb "final" minus "operational" forecast at (a) 00 GMT 27 January, (b) 12 GMT 27 January, (c) 00 GMT 28 January, and (d) 12 GMT 28 January 1986. Contour interval is 5 gpm.

level, the differences identified in the initial conditions appear to translate significantly ahead of the storm during the first 24-h period. Geopotential heights are 10-20 gpm lower over the northeastern U.S. at 00 GMT on the 27th and in eastern Canada at 12 GMT on the 27th, when the heights are 10-20 gpm higher near Greenland. During the following 24-h period, differences in the 300 mb heights are found both north and south of the forecast surface low center. The heights are lower by 15 gpm to the east of Hudson Bay and off the New Jersey coast at 00 GMT on the 28th. Height differences again exceed 20 gpm at 12 GMT 28 January 1986, with lower heights evident along the New England coastal areas and east of Hudson Bay, and higher heights extending south of Hudson Bay to the Great Lakes. At the 850 mb level (Fig. 3.15), the geopotential height differences are also observed to propagate downstream with maximum values generally to the northwest of the surface low forecast position. During the first 24-h period, height differences of 10 gpm are found east of Chesapeake Bay and over upstate New York and New England. At 00 GMT 28 January 1986, the largest forecast height differences occur with heights higher by 10-20 gpm southeast of Hudson Bay and lower by 10 gpm over New York and New Jersey. Four distinct areas of 10 gpm differences are observed at 12 GMT 28 January 1986 with the higher heights over Hudson Bay and lower heights over the northeastern U.S.

The difference between the "final" and "operational" forecast SLP is illustrated in Fig. 3.16. At 00 GMT 27 January 1986, a positive SLP difference of 1 mb is observed from Cape Cod westward and ahead of the forecast storm center position. This difference is due to a strong high-pressure ridge that is forecast across the mid-Atlantic states east of the Chesapeake Bay (not shown). This high-pressure ridge is almost non-existent in the surface analysis. Consequently, this 1 mb difference results in greater forecast SLP errors in the "final" run than in the "operational" run at this time. The new forecast position of the primary coastal cyclone center is approximately 60 n mi south of the "operational" forecast position and 80 n mi south of the analyzed position. The "final" forecast storm intensity of 1000 mb is in agreement with the initial forecast intensity of 999 mb and verifies exactly with the analysis (Fig. 3.10b). SLP differences of 1-2 mb are depicted west and northwest of the storm center at 12 GMT 27 January 1986. The forecast pressure ridging west of Chesapeake Bay and differences in the forecast positions of the surface low center can be related to these positive difference areas. Negative 1 mb areas are located south of the surface low and northeast of Newfoundland, Canada. The "final" forecast storm intensity of 982 mb agrees with the

"operational" forecast, as both overdeepen the low center by 4 mb. At 00 GMT 28 January 1986, four deviation centers can be identified. Positive differences of 1-3 mb are located southeast of Hudson Bay ahead of the primary low center. Behind the primary low position, a negative 1 mb area is found in Ontario, Canada. The "final" forecast intensity of 982 mb agrees favorably with the "operational" forecast intensity of 984 mb. Based on an analyzed intensity of 985 mb, this represents a slightly poorer forecast. Another negative 1 mb center southeast of Cape Cod can be related to the predicted differences in the secondary cyclone position. The "final" forecast intensity of 990 mb of this cyclone agrees exactly with the "operational" forecast and is close to the analyzed value of 991 mb. Three deviation centers of 1-2 mb are evident at 12 GMT 28 January 1986. Positive 1-2 mb areas across the southern extent of Hudson Bay and negative 1-2 mb areas across Quebec, Canada are both related to the forecast positional differences in the primary cyclone center of 120 n mi, which is the largest difference during the 48 hour forecast period. The "final" primary storm intensity of 994 mb agrees exactly with the "operational" forecast and both are 10 mb higher than the analyzed intensity of 984 mb. The negative 1-2 mb difference areas across southern New England and New York are attributed to forecast position differences for the secondary cyclone of approximately 90 n mi. The "final" forecast intensity of the secondary system agrees exactly with the control forecast intensity of 992 mb, but is much higher than the analyzed intensity of 983 mb.

The original differences between the "final" and "operational" analysis due to the enhanced initial conditions appear to affect the "final" forecast in several ways. Differences in the initial wind field at 12 GMT 26 January 1986 should be felt relatively soon (0-12 h) and may be linked to the 60 n mi difference in forecast storm position at 00 GMT 27 January. Differences in the initial temperature and height fields should persist over a much longer period (12-48 h) and may partially explain why the "final" forecast begins to deviate significantly from the "operational" forecast beyond 30 h. The original deviation fields (Fig. 3.13) also appear to exhibit growth at subsequent forecast times (Fig. 3.14, Fig. 3.15 and Fig. 3.16), possibly due to baroclinic processes. They do not simply translate with the mean flow.

The tracks of the primary cyclone for the NORAPS "final" forecast and the "operational" forecast at 6-h intervals from 12 GMT 26 January 1986 to 12 GMT 28 January 1986 are presented in Fig. 3.17. The first significant difference in the surface low position occurs at 00 GMT 27 January 1986, when the "final" forecast storm

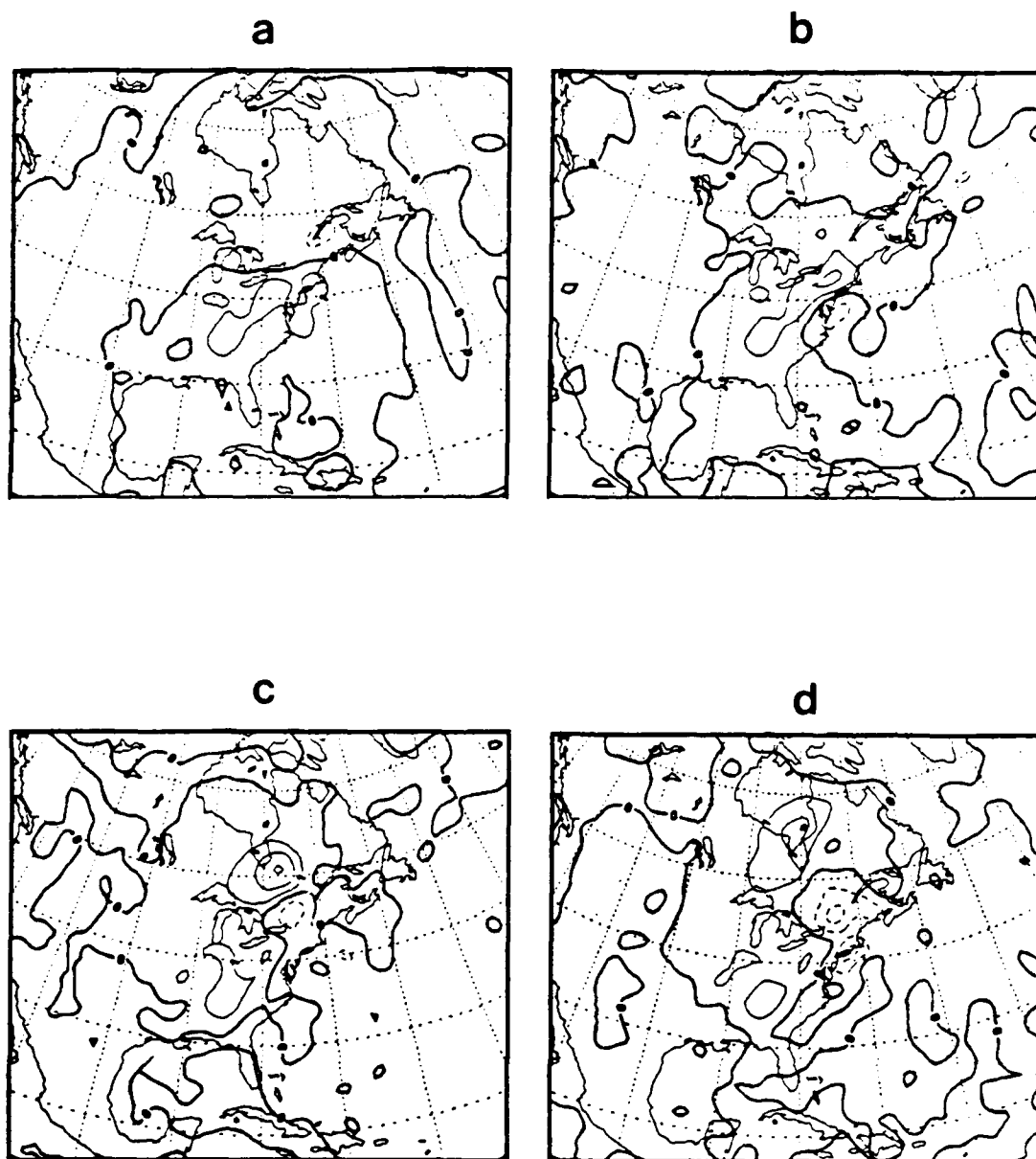


Figure 3.16 NORAPS SLP "final" minus "operational" forecast at
 (a) 00 GMT 27 January, (b) 12 GMT 27 January, (c) 00 GMT 28 January,
 and (d) 12 GMT 28 January 1986. Contour interval is 1 mb.

center is approximately 60 n mi south of the "operational" forecast position. The differences in forecast position tend to be insignificant over the next 24 hour period, in view of the 80 km model spatial resolution. At 06 GMT 28 January 1986, the forecast storm centers again start to deviate significantly. By 12 GMT 28 January 1986, the storm centers are separated by 90 n mi with the "final" forecast center southeast of the "operational" forecast position. The NORAPS "final" and "operational" forecast primary cyclone intensities each 12-h starting from 12 GMT 26 January 1986 are depicted in Fig. 3.18. The "final" predicted intensities agree with the initial forecast intensities with only a 1 mb difference at 00 GMT 27 January 1986 and a 2 mb difference at 00 GMT 28 January 1986.

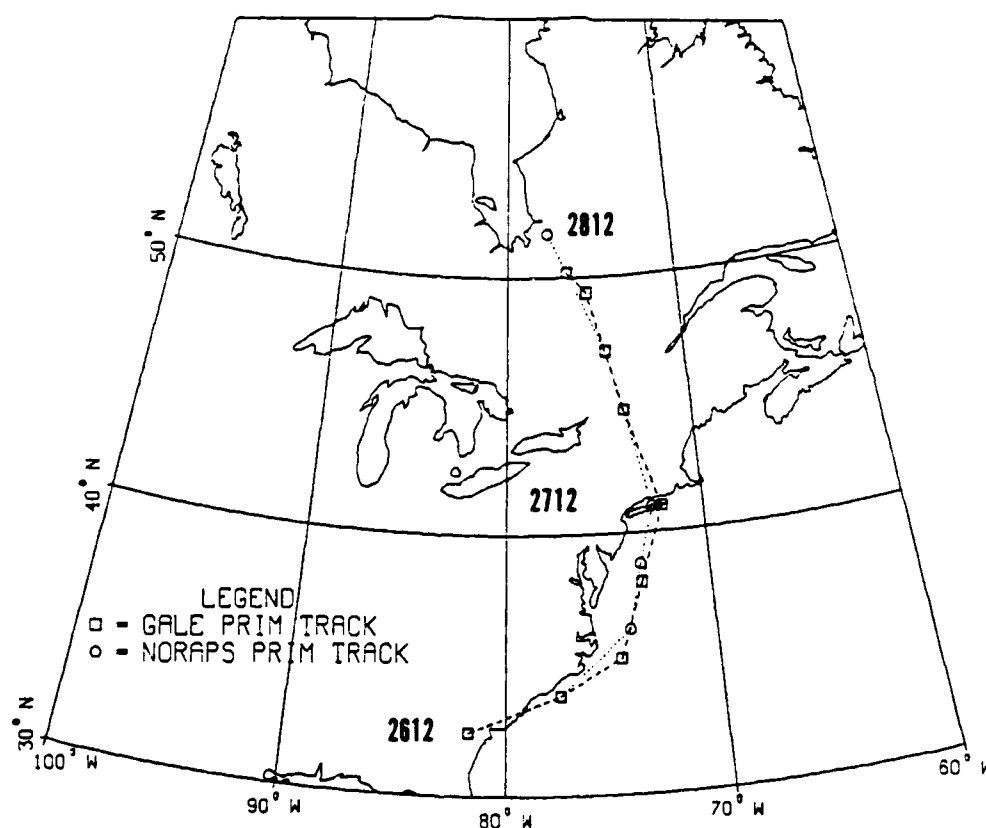


Figure 3.17 NORAPS "final" forecast positions (boxes) and "operational" forecast positions (circles) each 6 h for the primary coastal cyclone from 12 GMT 26 January to 12 GMT 28 January 1986.

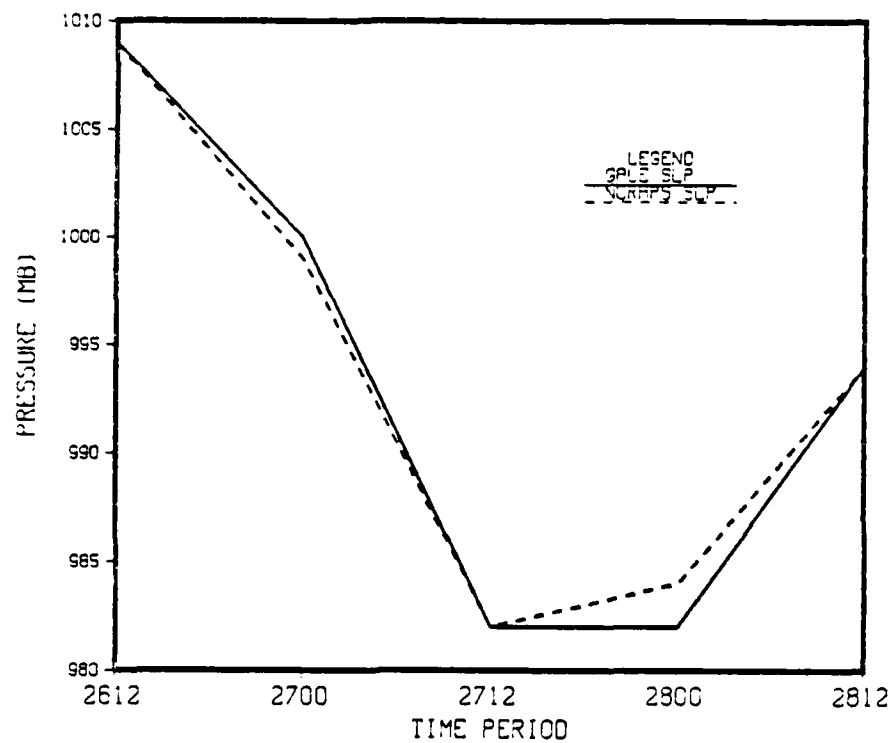


Figure 3.18 NORAPS "final" forecast SLP (solid) and "operational" forecast SLP (dashed) for primary coastal cyclone from 12 GMT 26 January 1986 to 12 GMT 28 January 1986.

The NORAPS "final" versus "operational" forecast tracks for the secondary system at 00 GMT 28 January 1986 and 12 GMT 28 January 1986 are presented in Fig. 3.19. The initial difference of approximately 30 n mi increases to about 100 n mi after 12 hours. Although this is an improvement over the initial forecast secondary track, the positional error between the "final" predicted storm center and the verifying analysis is still large (approximately 2-40 n mi). The "final" predicted storm intensity of 990 mb at 00 GMT 28 January 1986 and 992 mb at 12 GMT 28 January 1986 agrees exactly with the "operational" forecast. However, the analyzed storm intensity at 12 GMT 28 January 1986 is still much deeper at 983 mb.

Based on these results, one can reasonably conclude that the small set of GALE data added to the initial conditions in this case has provided no significant improvement in forecast skill over the "operational" control forecast. The "final" forecast primary storm track is significantly different at only two time periods, and actually verified poorer than the control forecast. Similarly, the primary storm forecast intensities are not significantly improved. These same conclusions can also be applied to the "final" forecast of the secondary low. The "final" forecast secondary storm intensities were virtually identical and the slight improvement in storm position was not significant. The lack of improvement in forecast skill can be related to the fact that the additional sounding data provided from GALE is downstream of the storm center at 12 GMT 26 January 1986, rather than upstream. At the 850 mb and 300 mb levels, the difference centers are usually located downstream (ahead) of the forecast surface low position (Fig. 3.14 and Fig. 3.15) and therefore have little impact on the upstream surface disturbance. Finally, it should be noted that this was a very limited data impact study. No attempt has been made to improve upon the original 12-h update cycle to utilize GALE soundings that are available every 3 h. Therefore, no firm conclusions concerning the effectiveness of enhanced spatial and temporal resolution in the initial conditions can be stated with confidence. Further research in this area is clearly necessary.

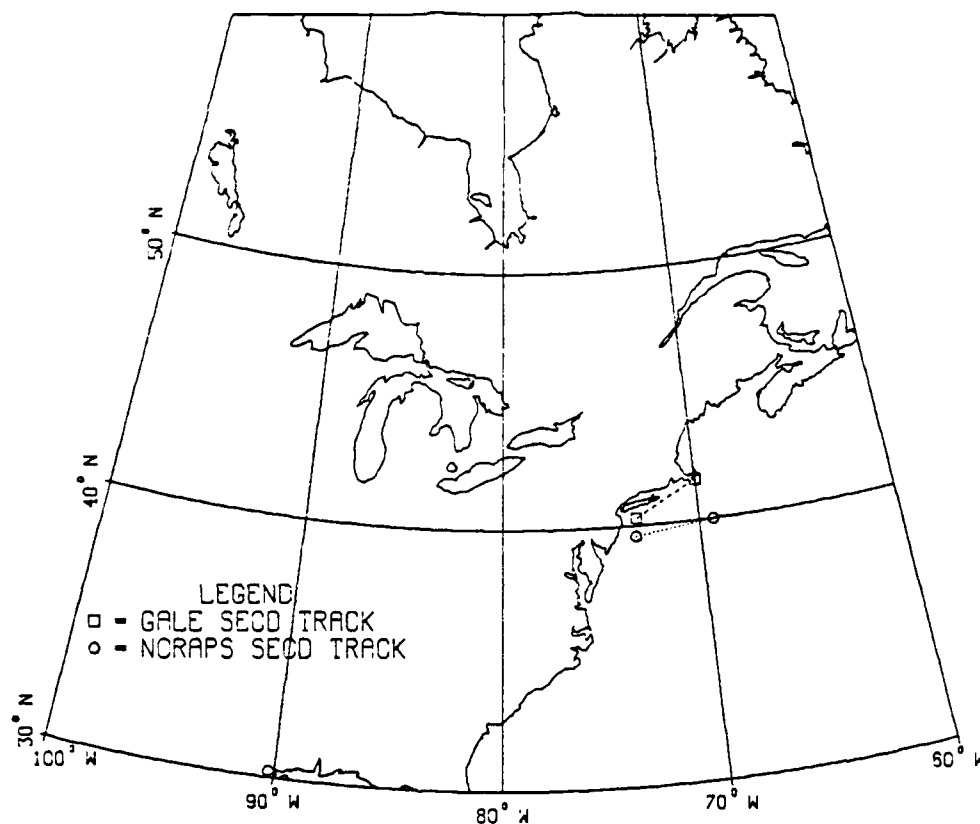


Figure 3.19 NORAPS "final" forecast positions (boxes) and "operational" forecast positions (circles) each 6 h for the secondary cyclone at 00 GMT 28 January and 12 GMT 28 January 1986.

IV. MASS AND VORTICITY BUDGET RESULTS

A. GENERAL

Through the use of the QLD technique, a quantitative evaluation of the physical processes most important in extratropical cyclogenesis can be determined. The QLD budget volume is defined by ten mandatory pressure levels in the vertical and by a variable radius in the horizontal. This budget volume is then centered over the sea-level pressure minimum and is moved with the system to account for translational effects in the lateral transport and advection terms in the budget equation. A radius of four degrees latitude was selected to focus on the inner storm processes that are important in the dynamical forcing of the surface disturbance.

The generalized budget equation relates the time rate of change of a meteorological property within the budget volume to lateral flux transport, vertical flux transport and sources, sinks of the property within the volume. This equation is applicable to the storm budget volume in spherical coordinates. The QLD study presented in the following two chapters will focus on the primary coastal cyclone only. Because the "final" forecast provided no significant improvement in forecast skill, only the "operational" forecast and analysis will be evaluated. Budgets of mass and vorticity will be discussed in this chapter. Heat and moisture budget results will be considered in Chapter V.

B. DESCRIPTION OF THE MASS BUDGET

The mass budget is computed using the finite difference form of the continuity equation in pressure coordinates. Vertical velocities (ω) are computed kinematically and interpolated to the budget volume. Horizontal winds are also interpolated to the budget volume and converted to normal and tangential wind components for use in the budget computations. The horizontal and vertical winds are then adjusted to achieve mass balance using O'Brien's (1970) linear correction scheme. The net horizontal flux at each level for a particular radius is calculated using the line integral method. The horizontal fluxes are then summed in the vertical, which results in a vertically-integrated horizontal mass flux for each radius. This vertically-integrated horizontal mass flux is then adjusted to balance the net vertical mass flux between the top (100 mb) and an arbitrarily chosen bottom level (1000 mb). The forecast uses the

model-predicted values of omega at the upper and lower boundaries, while omega is set equal to zero at both boundaries in the analysis case. The forecast employs a constant correction factor to adjust the horizontal divergence at each level. The analysis employs a weighting function that linearly decreases with pressure to account for the larger error in the wind field with height.

Based on the adjusted divergences, the normal winds are evenly corrected for all 36 points at each level. The adjusted horizontal divergences lead to vertical velocities that satisfy mass continuity and the boundary conditions at the top and bottom. This adjustment process is necessary to account for the effects of observational and interpolation errors in the analysis and forecast fields. Truncation errors can arise from the finite differencing schemes used in the budget. Interpolations from the model sigma levels to the budget pressure levels and from the Lambert conformal grid to the cylindrical budget volume are also potential sources of error.

C. MASS BUDGET RESULTS

Applying the principle of conservation of mass results in a mass budget equation with no sources or sinks. The mass budget equation relates the mass time tendency (dM/dt) to the sum of the lateral (horizontal) transport (flux) and vertical transport (flux) terms. The lateral transport term represents the net horizontal mass convergence divergence within a particular layer. The vertical mass transport term is inferred from the vertical velocity field.

The NORAPS "operational" forecast horizontal and vertical mass transports are compared with the corresponding transport terms calculated from the analysis. The forecast fields are available every 6 h from 12 GMT 26 January 1986 until 12 GMT 28 January 1986. The corresponding analysis fields are available every 12 h during the same 48-h period. Time periods generally refer to the period between synoptic times. For example, the time 2618 in the analyzed omega field represents the period 12 GMT 26 January 1986 to 00 GMT 27 January 1986.

The analyzed and forecast horizontal mass transports (divergence, convergence) presented in Fig. 4.1 have a two-layer vertical structure that consists of strong low-level mass influx associated with convergence into the budget volume and a layer of mass outflow associated with middle and upper-level divergence. The level of non-divergence (LND) is located at approximately 600 mb in the analysis but occurs around 500 mb in the forecast. A low LND as in the analysis is consistent with the findings of other

investigations of explosive maritime cyclogenesis (Sanders and Gyakum, 1980; Rau, 1986). The shallow inflow layer combined with the deeper outflow layer results in a net vertically-integrated mass loss within the atmospheric column that is consistent with the surface pressure falls of the developing phase of the cyclone. The strength of the mass flux increases until 06 GMT 27 January 1986 with a distinct inflow maximum near 950 mb in both the analysis and the forecast. The corresponding outflow maxima occur at 200 mb (analysis) and 250 mb (forecast). Concurrent with the intensification of the storm is the small vertical growth of the convergent layer in both the analysis and forecast cases. Growth of the convergent layer during cyclogenesis is in agreement with Calland (1983). The height of the forecast LND falls off rapidly after 18 GMT 27 January 1986 as the storm begins to dissipate.

The area-averaged vertical velocities for the analysis and forecast cases is presented in Fig. 4.2. The omega fields represent the vertical mass transport and because of mass continuity necessarily reflect periods of significant horizontal mass transport. Although the elevation of the absolute maximum near 500 mb at 03 GMT 27 January 1986 agrees with the corresponding analysis, the magnitude of the upward vertical motion in the forecast is significantly greater than in the analysis. Again, this is consistent with the greater predicted deepening over the period 00-12 GMT 27 January. These vertical velocity maxima are correlated directly with the low-level convergence and upper-level divergence maxima during the period of rapid surface deepening from 00-12 GMT 27 January 1986.

D. DESCRIPTION OF THE VORTICITY BUDGET

The flux form of the vorticity equation is

$$\overline{\delta \zeta_a} / \delta t = -1/A \oint \zeta_a (V_n - V_o) dl - \partial / \partial p (\overline{\omega \zeta_a}) \quad (4.1)$$

$$- \overline{\zeta_a (\nabla \cdot V)} + k \cdot (\partial V / \partial p \times \nabla \omega) + \overline{Fr} + \overline{R},$$

where ζ_a is the absolute vorticity, A is the horizontal area, V_n is the wind component normal to the line integral, V_o is the cyclone velocity component normal to the line integral, ω is the vertical velocity, Fr denotes the frictional term, R is the residual and the overbar denotes the area-average of the particular term. The term on the left side of (4.1) is the quasi-Lagrangian time tendency of the absolute vorticity. The first term on the right side of (4.1) represents the horizontal transport (flux) of absolute vorticity,

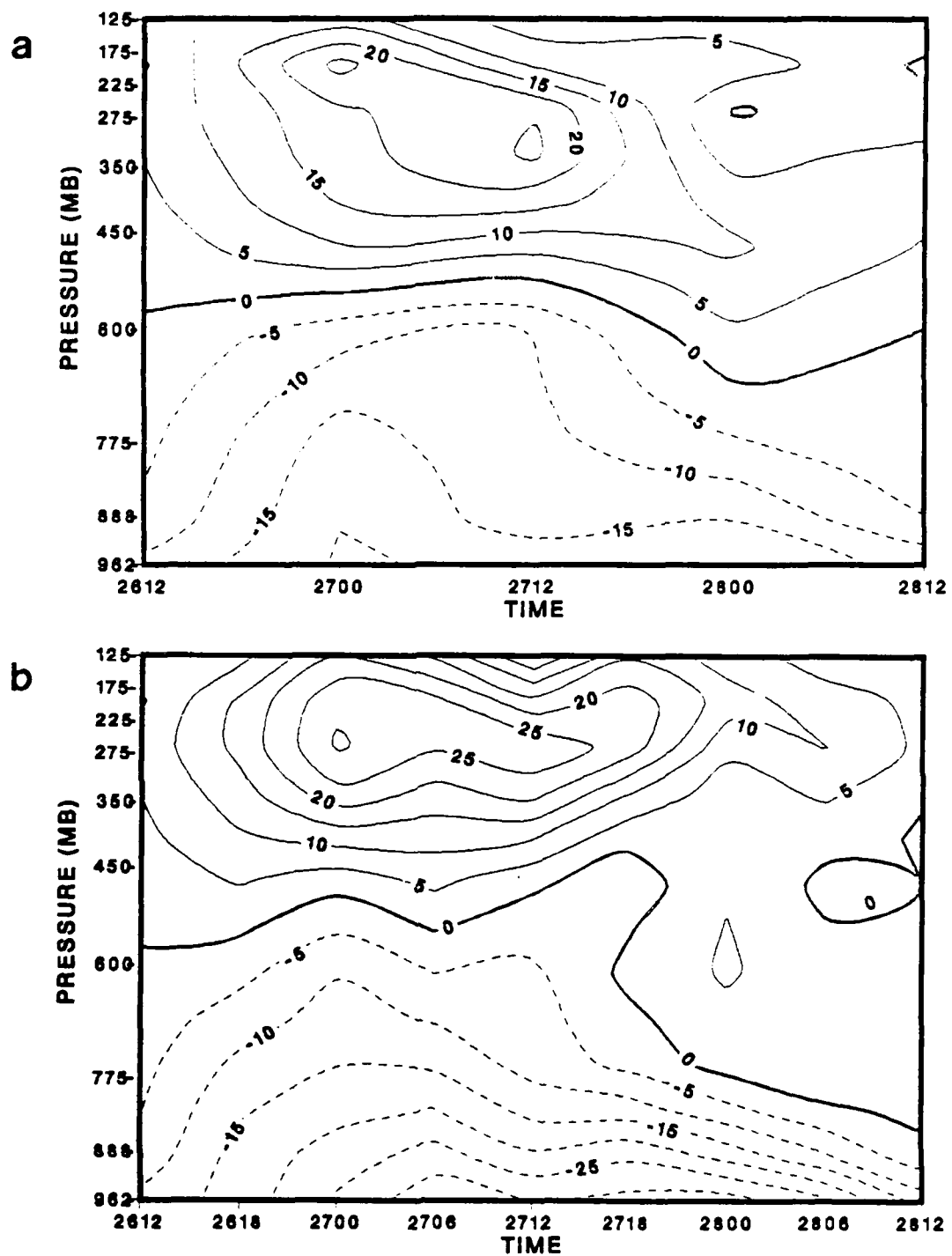


Figure 4.1 Horizontal convergence divergence (flux) for 4° lat. radius in the (a) analysis and (b) forecast. Negative positive values denote mass flux into out of budget volume. Contours are $5 \times 10^{-6} \text{ s}^{-1}$.

while the second term is the vertical transport. The third term represents the source sink of absolute vorticity due to convergence divergence within the budget volume. The fourth term on the right side is the tilting term and the fifth term represents the effects of frictional dissipation of vorticity. The last term on the right side is a residual that includes the sources and sinks not explicitly resolved by the other terms and the effects of truncation and interpolation errors. If all the sources and sinks that contribute to the vorticity tendency have been accounted for and the interpolation and truncation errors are negligible, the magnitude of the residual should be relatively small. Interpolation and truncation errors constitute a significant source of error in budget studies involving numerical integration. The analysis also has the additional problem of uncertainty due to incomplete observational data sets.

The lateral transport of absolute vorticity term can be partitioned into mean and eddy modes, which may also be considered as the symmetric and asymmetric components. Alternately, the transport terms can be partitioned into divergence and advection contributions by the use of vector identities to provide a different insight into these physical processes. Calland (1983) shows that the eddy mode of the lateral transport of absolute vorticity is similar to the advection of absolute vorticity. Jet streaks and short-wave troughs are two mechanisms that contribute to the eddy mode component. Similarly, the mean mode of the lateral transport is analogous to the vorticity divergence term and represents the effects due to mean cyclone convergence/divergence. The vertical flux term can also be separated into mean and eddy contributions.

The vertical component of vorticity is calculated from the horizontal wind field using a finite difference form of relative vorticity in cylindrical coordinates and adding the appropriate value of the Coriolis parameter at the grid point. The NORAPS forecast and analyzed wind fields are smoothed using a 25-point filter eight times for display purposes. This smoothing also creates a source of error in the budget computations.

E. VORTICITY BUDGET RESULTS

The quasi-Lagrangian time tendency of absolute vorticity is calculated with a centered time difference that applies at the mid-point of the two time periods. Thus, the other terms are averaged over two time periods to present all the terms in the budget at a common time. For the forecast case, 15 GMT 26 January includes the

period 12-18 GMT 26 January 1986. The analysis times apply to the 12-h period between synoptic times (00 and 12 GMT). The absolute vorticity budget results are presented in vertical time sections at a 4° lat. radius for both the NORAPS forecast and analysis.

The area-averaged absolute vorticity time tendency for the analysis (Fig. 4.3a) features a strong positive tendency pattern in the middle troposphere at 06 GMT 27 January during the period of rapid storm development. The weak vorticity tendency pattern in the low and middle levels beyond 12 GMT 27 January is consistent with the onset of the occlusion phase and dissipation of the storm. In the forecast (Fig. 4.3b), the general vorticity pattern is similar to the analyzed case, although the magnitudes of the positive negative tendencies are significantly larger as expected from the greater forecast deepening and filling rates. The forecast vorticity time tendency includes a negative tendency at the initial period, a positive tendency maximum in the upper troposphere (350 mb) at 21 GMT 27 January 1986 and negative tendencies in the low to middle troposphere after 15 GMT 27 January 1986. Notice that this positive vorticity tendency maximum occurs during a period when the storm is predicted to fill. Thus, the upper-level forcing is not being transported to the surface, perhaps due to the effects of frictional dissipation as the forecast storm is well inland (Fig. 3.10a).

The lateral transport of absolute vorticity (Fig. 4.4) represents one of the most important forcing terms in the vorticity budget equation. Transport into the budget volume arises from the mean convergent flow (mean mode) and from asymmetries in the cyclonic flow (eddy mode). In the analysis (Fig. 4.4a), an inward transport of vorticity occurs through all time periods in the lower and upper troposphere, with outward vorticity transport in the middle troposphere. The strong inward transport of vorticity below 775 mb reaches a maximum at 18 GMT 27 January that coincides with the mature stage of the cyclone. The horizontal vorticity transport in the forecast (Fig. 4.4b) exhibits general agreement with the analysis in the lower and upper troposphere, although the magnitude of the inward transport is significantly greater. In the middle and upper levels, an alternating pattern of outward and inward transport is depicted which agrees fairly well with the analysis. During the period 03-21 GMT 27 January 1986, the forecast has inward lateral vorticity transport in the middle troposphere, whereas the analysis has small outward lateral transport. This outward transport of vorticity can be related to the overriding contribution of divergence over advective processes to the total lateral vorticity transport. An examination of the mean and eddy modes of the lateral vorticity transport term will clarify this relationship.

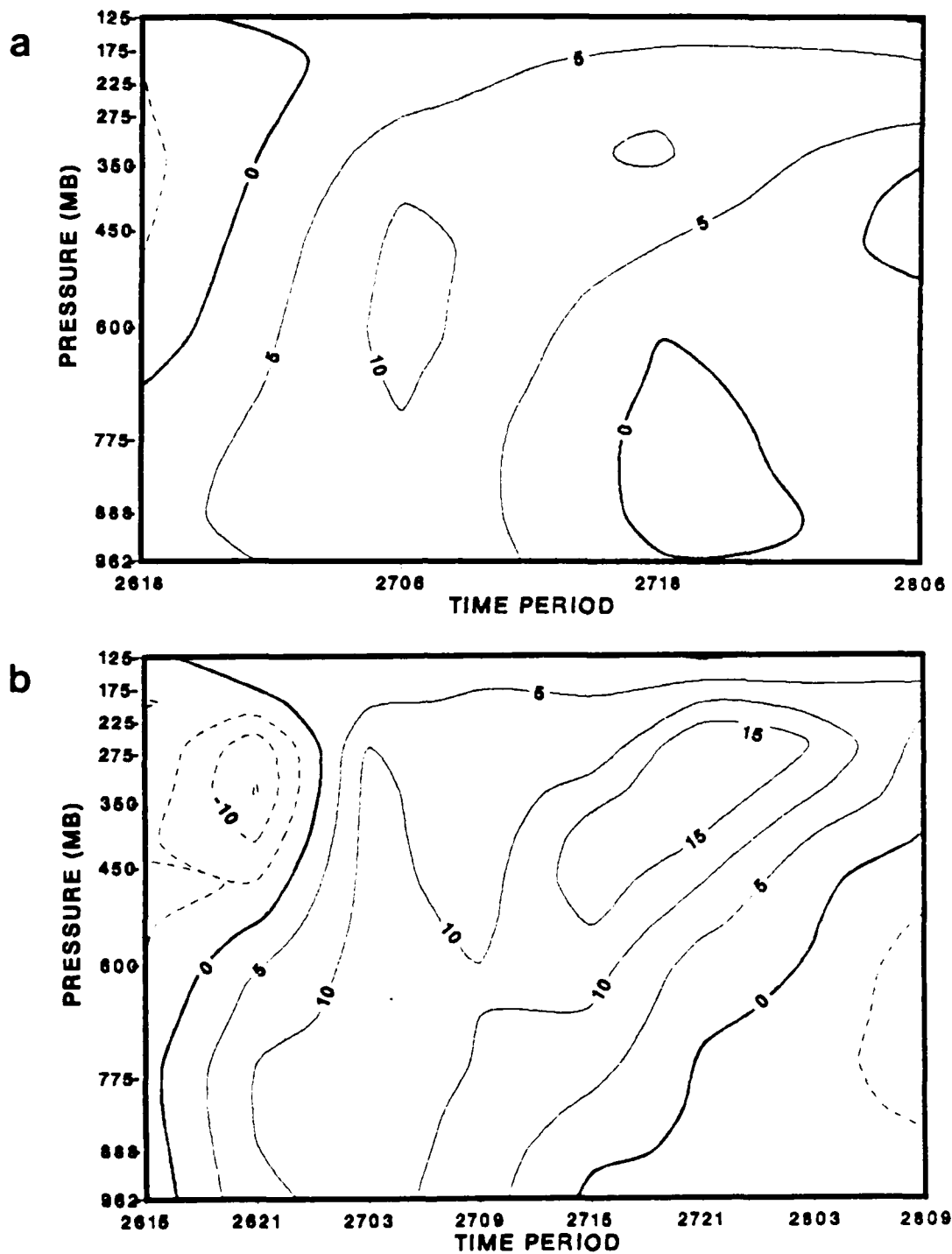


Figure 4.3 Area-averaged absolute vorticity time tendency for 4° lat. radius in the (a) analysis and (b) forecast. Solid dashed contours indicate vorticity increases decreases. Contours are $5 \times 10^{-10} - 10 \text{ s}^{-2}$.

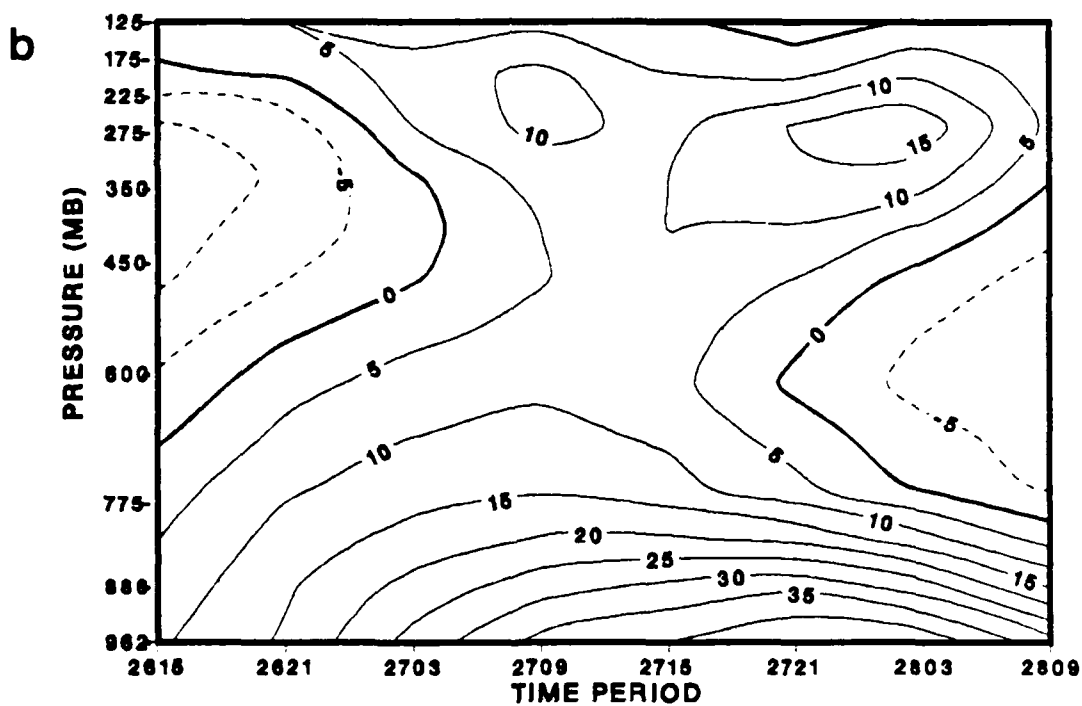
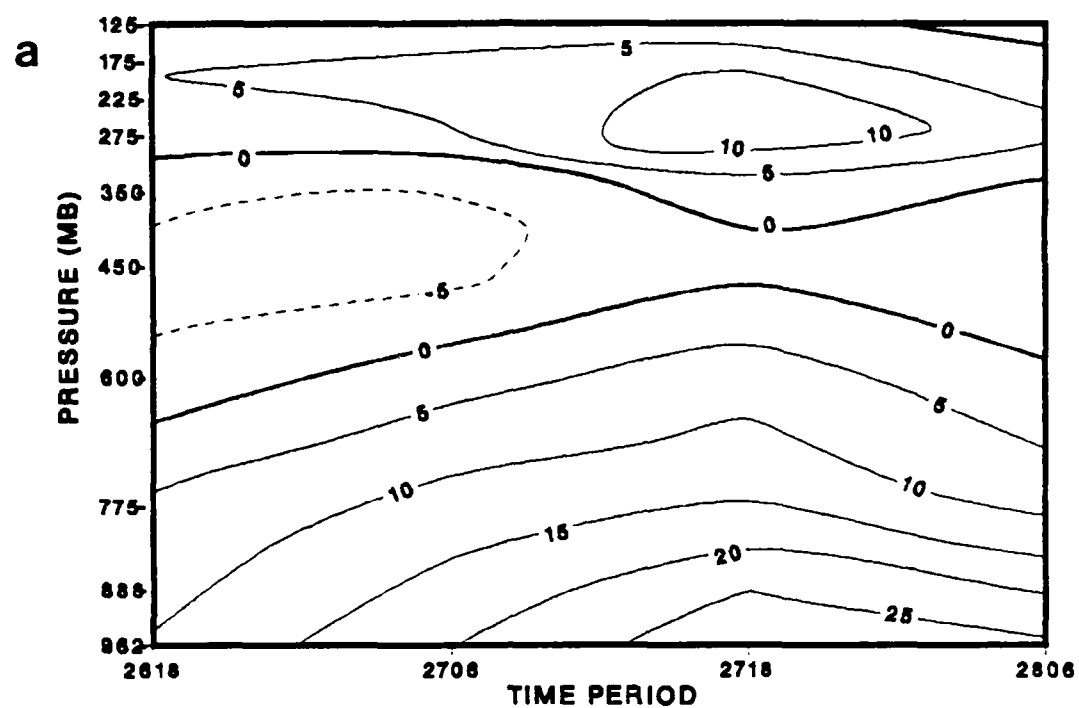


Figure 4.4 Lateral transport of absolute vorticity for 4° lat. radius in the (a) analysis and (b) forecast. Solid dashed contours indicate inward outward vorticity transport. Contours are $5 \times 10^{10} \text{ s}^{-2}$.

The mean mode component of the lateral vorticity transport is associated with the mean low-level inflow and upper-level outflow of vorticity. In both the analysis (Fig. 4.5a) and forecast (Fig. 4.5b), strong low-level inward vorticity transport changes to strong upper-level outward vorticity transport, with a level of transition at approximately the 500 mb level. As anticipated, these inward outward horizontal transport patterns by the mean flow agree remarkably well both temporally and spatially with the lateral mass transport fields (Fig. 4.1). In particular, the upper-level outflow maxima are consistent with the strong divergence maxima evident during the period of rapid storm development. The strong inflow maxima in the lower levels occur approximately 6 h after the period of maximum deepening, and coincide with the mature stage of the storm (maximum intensity). The significantly larger magnitudes of the mean mode transports in the forecast versus the analysis are also consistent with the results in the lateral mass transport fields.

The eddy mode component of the total lateral vorticity transport represents the horizontal transport due to asymmetries in the wind field that are correlated with vorticity deviations. It is analogous to the transport of vorticity by advective processes (Calland, 1983) and provides insight into the upper-level vorticity increases that ultimately affect the low-level circulation tendencies. The analyzed (Fig. 4.6a) and forecast (Fig. 4.6b) eddy components have strong inward vorticity transport maxima in the upper troposphere, with greater magnitudes in the forecast. The low and middle levels have outward vorticity transport or weak inward transport by the eddy component. The upper-level maximum in the analysis correlates very well with the period of rapid storm deepening, which suggests that cyclonic shear vorticity input to the budget volume from the upper-level jet streak (Fig. 3.2c) is an important factor in the storm development. The PVA aloft leads to a favorable upper-level divergence pattern that exports mass in the upper troposphere. Circulation increases in response to this upper-level forcing can be expected in the low-level inward transport associated with the mean mode. The occurrence of mean mode low-level inward transport maxima (Fig. 4.5) after the establishment of eddy mode inward transport maxima (Fig. 4.6) at the upper levels illustrates this relationship. In summary, the mean mode transport is large at both the lower and upper levels, while the eddy mode transport is important only in the upper troposphere.

The vertical vorticity transport serves to vertically redistribute the vorticity brought into the budget volume from lateral transport mechanisms. The divergence of

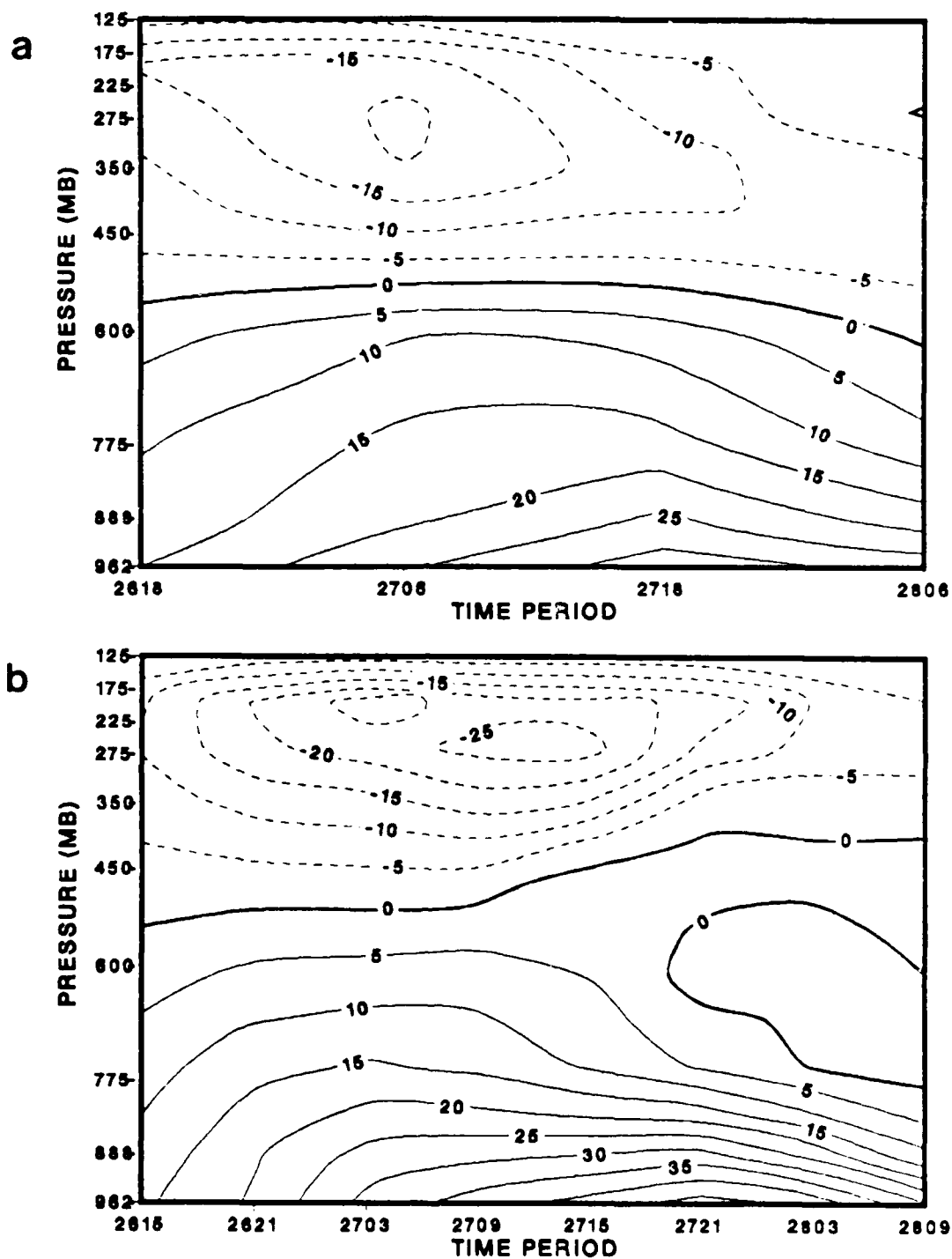


Figure 4.5. Mean mode lateral transport of absolute vorticity for 4° lat. radius in the (a) analysis and (b) forecast. Solid dashed contours indicate inward outward vorticity transport. Contours are $5 \times 10^{10} - 10^{11} \text{ s}^{-2}$.

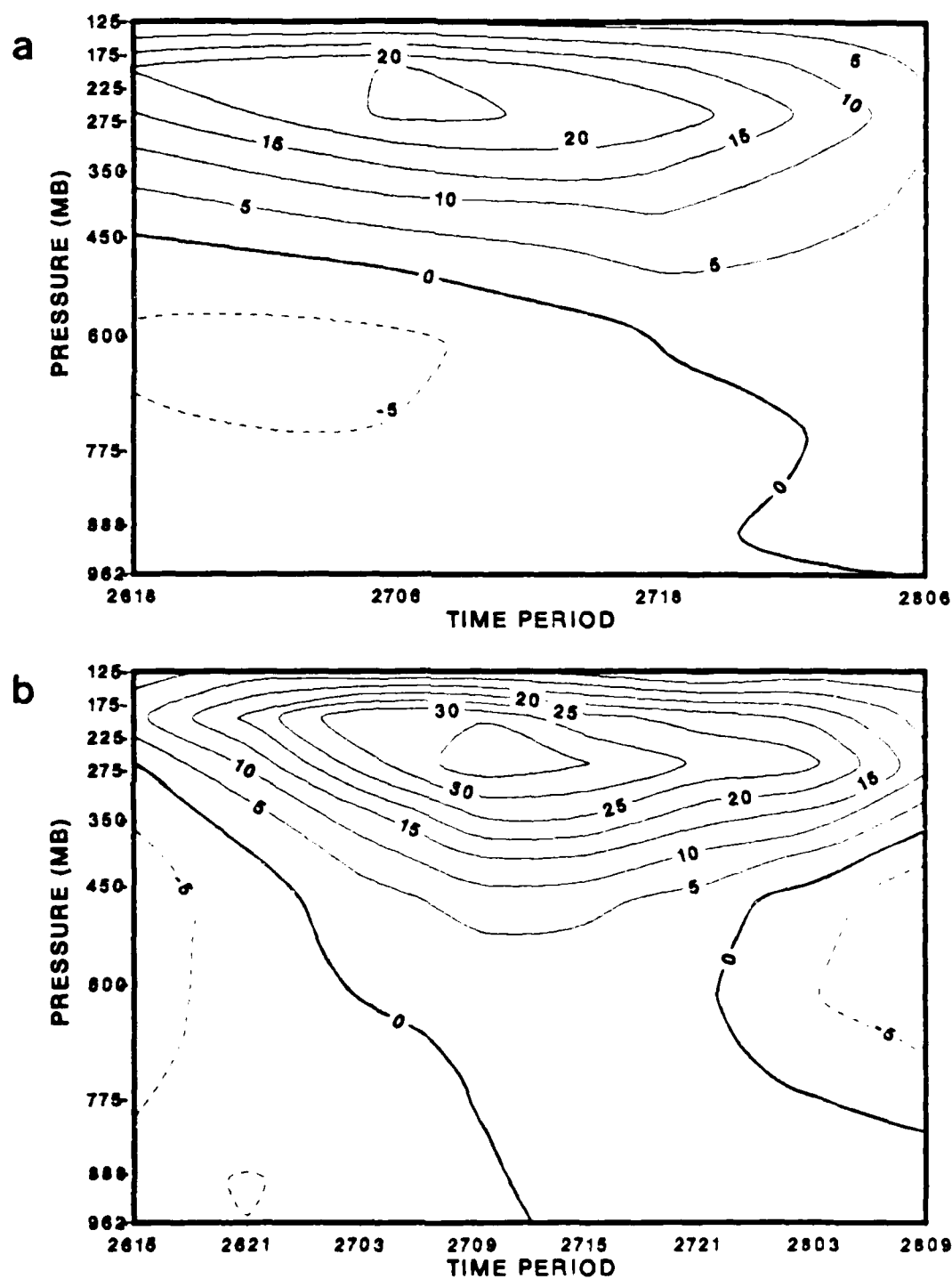


Figure 4.6 Eddy mode lateral transport of absolute vorticity for 4 lat. radius in the (a) analysis and (b) forecast. Solid dashed contours indicate inward outward vorticity transport. Contours are $5 \times 10^{-10} \text{ s}^{-2}$.

the vertical transport (Fig. 4.7) is the main contributor to vertical vorticity redistribution and opposite of the lateral divergence term (Fig. 4.5) discussed above. This term results from the vertical derivative of the transport between levels and represents the redistribution of vorticity upward through the troposphere. The vertical transport of vorticity is a direct consequence of the upper-level divergence, which induces the lower-level circulation and forced vertical ascent in the low and middle troposphere. Thus, the vertical vorticity transport maxima are temporally coincident with periods of maximum vertical motion (Fig. 4.2) and storm development. In both the analysis (Fig. 4.7a) and forecast (Fig. 4.7b), a two-layer structure exists, with a decrease of vorticity below the maximum in vertical motion and an increase above this maximum. The vertical advection component of the vertical transport (not shown) plays a relatively minor role in the budget.

The sources and sinks of vorticity include the divergence and tilting terms, while frictional dissipation acts as a vorticity sink. Generation of vorticity by horizontal convergence is the fluid analog of the conservation of angular momentum in solid body rotation. If horizontal convergence occurs and circulation is conserved, the area enclosed by the fluid decreases and the average vorticity of the parcel must increase. A pattern of low-level convergence and upper-level divergence implies that vorticity is being created (a source) at low levels and destroyed in the upper troposphere (a sink). The divergence term is mathematically very similar to the mean mode component of the lateral vorticity transport discussed above and exhibits the same two-level vertical structure. In both the analysis (Fig. 4.8a) and forecast (Fig. 4.8b), low-level convergence (upper-level divergence) generates positive (negative) vorticity. The forecast magnitudes tend to be considerably larger than the corresponding analysis values, which reflects the greater storm deepening predicted by the model. The analysis (Fig. 4.8a) has a vorticity convergence (generation) maximum at 12 GMT 27 January and a divergence maximum centered at 06 GMT 27 January 1986. By contrast, the forecast (Fig. 4.8b) has the vorticity convergence maximum at 09 GMT 27 January and the vorticity divergence maximum at 03 GMT 27 January 1986. The relatively large magnitudes of the divergence maxima suggest that the divergence term plays a dominant forcing role in the vorticity budget. QLD investigations of cyclogenesis by Cailand (1983) and Rau (1986) support this conclusion.

The tilting term arises from vertical vorticity components generated by the tilting of horizontally oriented vorticity elements in a non-uniform vertical motion field.

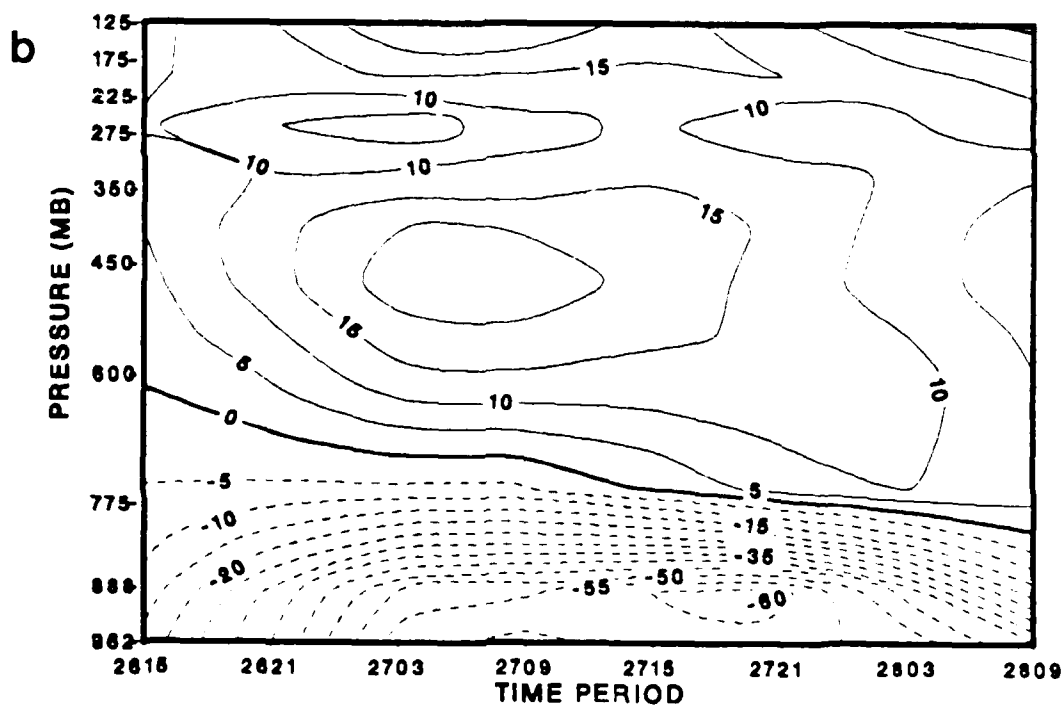
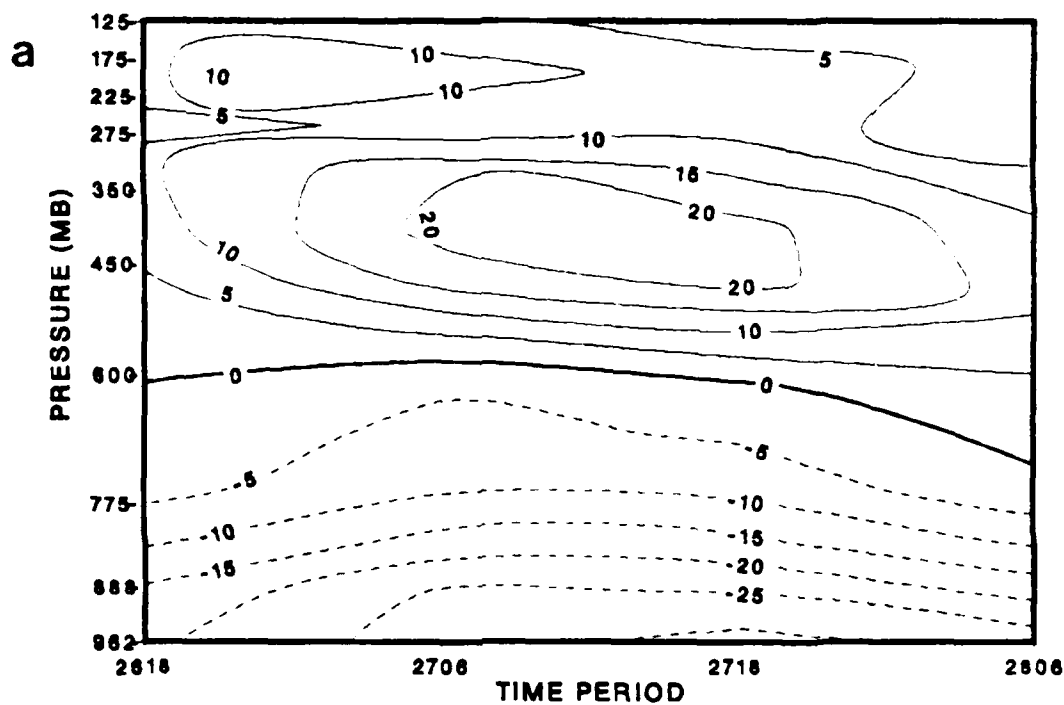


Figure 4.7. Vertical transport of absolute vorticity for 4° lat. radius in the (a) analysis and (b) forecast. Solid dashed contours indicate positive negative vorticity transport. Contours are $5 \times 10^{10} - 10^{11} \text{ s}^{-2}$.

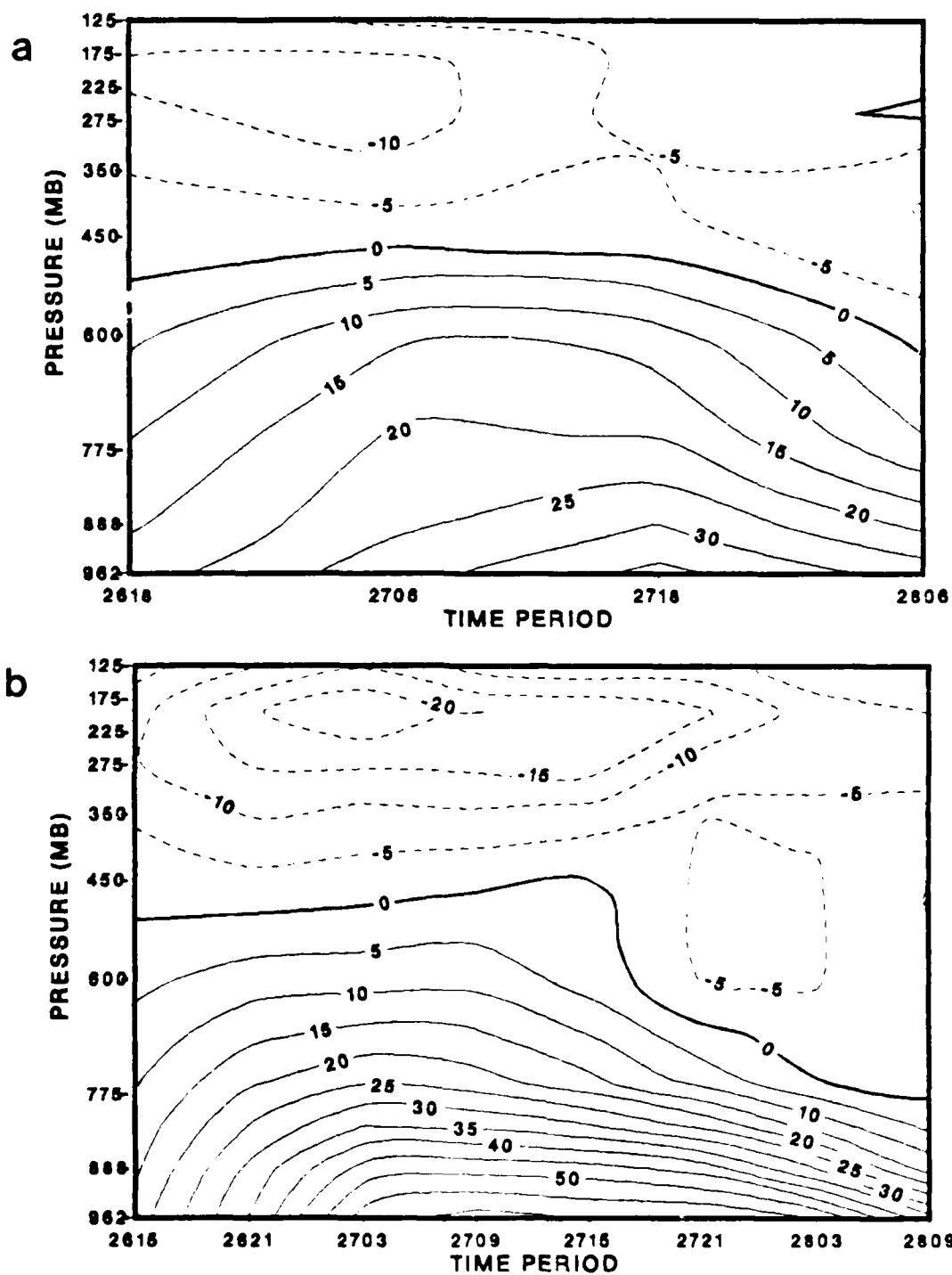


Figure 4.8. Vorticity divergence term for 41 lat. radius in the (a) analysis and (b) forecast. Solid dashed contours indicate vorticity convergence (source) divergence (sink). Contours are $5 \times 10^{-10} \text{ s}^{-2}$.

Therefore, strong vertical shear and a horizontally varying omega field are requirements for contributions from this source. The tilting term in the analysis (Fig. 4.9a) has a weak negative contribution in the low and upper troposphere over most time periods. For the forecast case (Fig. 4.9b), the same general pattern exists, although the magnitude of the negative contribution is substantially greater and is centered at 03 GMT 27 January 1986. However, the tilting term contribution to the vorticity tendency is still small compared to the lateral transport and divergence terms.

Frictional dissipation is assumed to occur only in the PBL and is parameterized using a stability dependent scheme (Johnson and Downey, 1975). In both the analysis (Fig. 4.10a) and forecast (Fig. 4.10b), the vorticity lost through frictional dissipation is minimal until 06 GMT 27 January 1986, when the circulation has become well organized. These results suggest that frictional dissipation of vorticity is important during the mature stage of a cyclone, when the surface winds have reached maximum velocity and surface drag has become a significant factor.

The residual term contains the accumulated computational errors from the budget calculations and any sources and sinks not explicitly resolved. A small residual implies that the forcing has been captured by the resolved terms in the budget and that computational errors are negligible. A positive negative residual in the vorticity budget indicates an apparent vorticity source sink in which the observed increases decreases in the budget volume are larger than can be explained from the computed terms. Observational errors in the vertical motion and horizontal wind fields contribute to the residual components. Computational error contributions to the residual include spatial and temporal finite differencing and interpolation from the NORAPS grid to the budget volume. Additionally, the residual term will contain errors due to differences between the model and budget PBL parameterization scheme.

In the analysis case (Fig. 4.11a), the residual is positive in the middle troposphere throughout the 48 h, with a maximum at 06 GMT 27 January 1986. This positive vorticity may be the result of inaccuracies in the observed wind field that affects the computation of lateral and vertical vorticity transport. Additionally, the residual can be expected to be greater than normal in areas of significant jet streak activity where the horizontal wind fields are generally the least accurate. Negative residuals occur above 200 mb and from the surface to 600 mb after 06 GMT 27 January 1986. The large negative maximum at 18 GMT 27 January may be partially due to improper parameterization of the PBL in the budget formulation. The forecast residual (Fig.

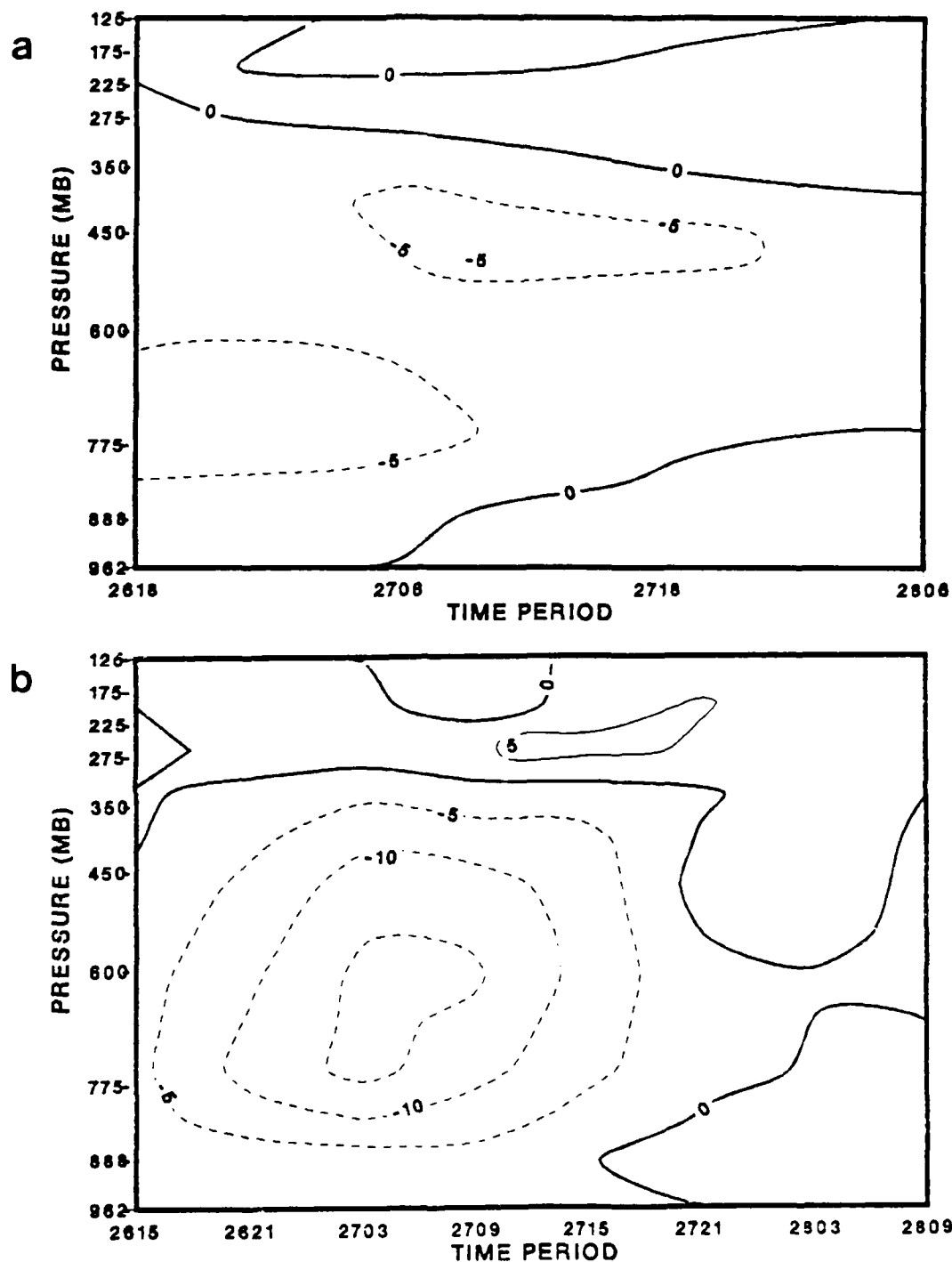


Figure 4.9 Vorticity tilting term for 4° lat. radius in the (a) analysis and (b) forecast. Solid dashed contours indicate positive, negative vorticity contribution. Contours are $5 \times 10^{**}-10 \text{ s}^{-2}$.

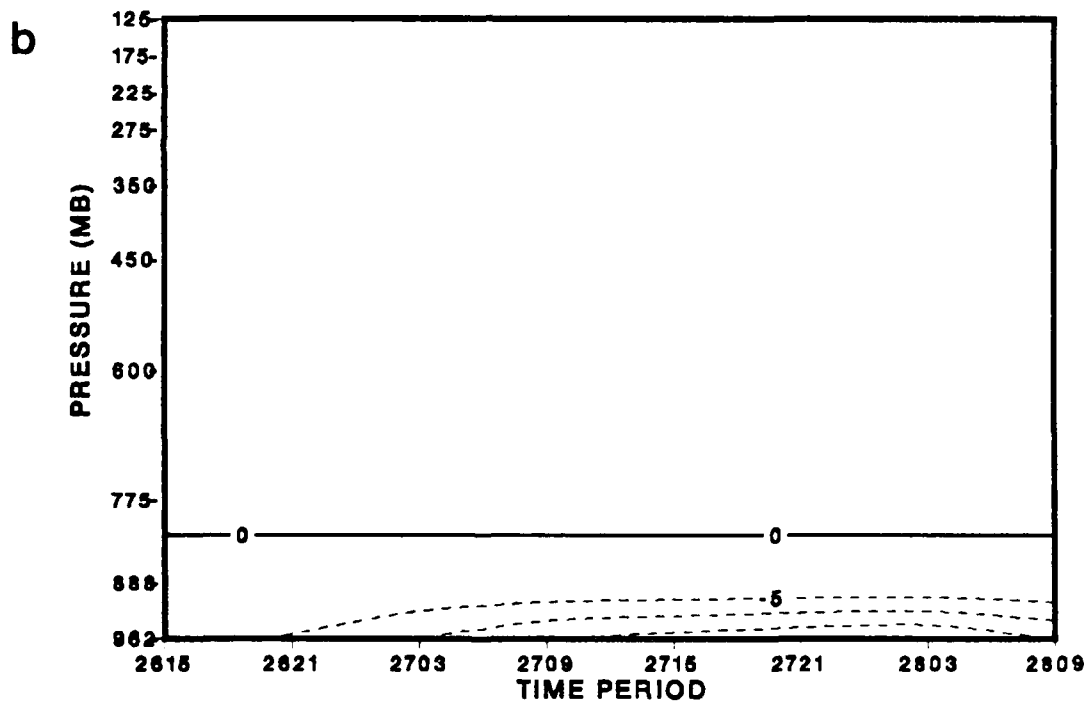
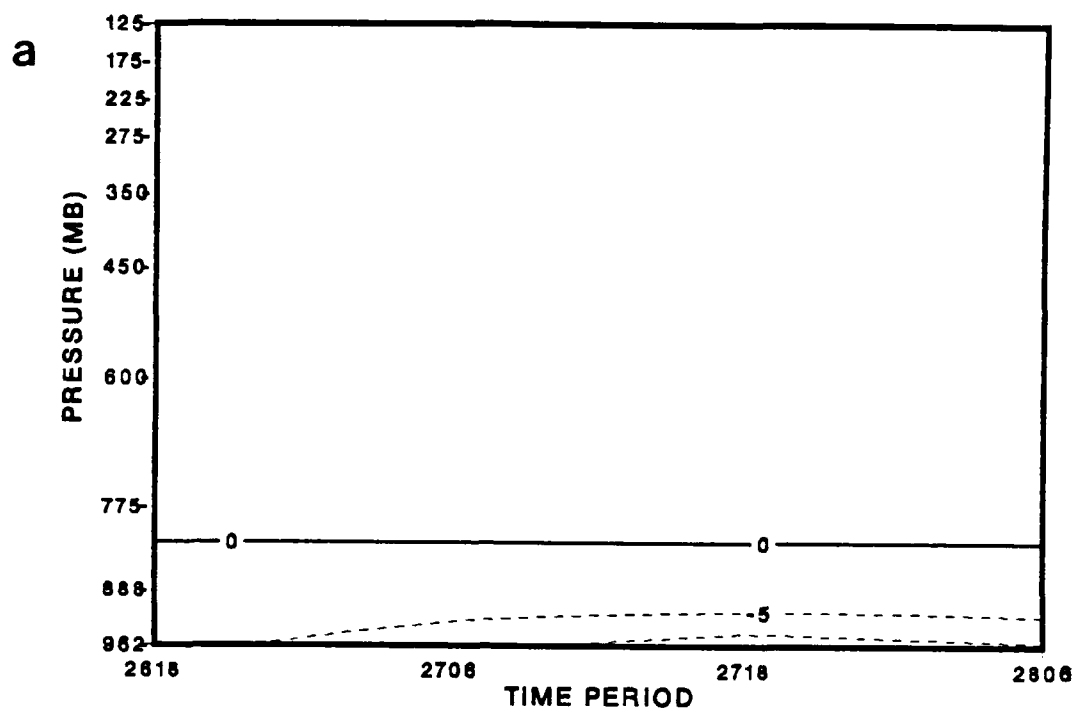


Figure 4.10 Frictional dissipation of absolute vorticity for 4° lat. radius in the (a) analysis and (b) forecast. Dashed contours indicate a negative (sink) vorticity contribution. Contours are $5 \times 10^{-10} \text{ s}^{-2}$.

4.11b) shows general agreement with the analysis throughout most of the atmosphere. The large positive residual maximum at 03 GMT 27 January 1986 and negative maximum at 21 GMT 27 January 1986 are in close agreement with the corresponding analysis.

The terms of the vorticity budget are vertically averaged over the lower troposphere (1000-500 mb) to obtain a clearer understanding of the relative importance of each term in the spin-up of the low-level vortex. Because the friction term plays a relatively minor role in the budget, it is not included with these results. The positive vorticity tendency in the analysis (Fig. 4.12) is concentrated at 06 GMT 27 January, whereas the positive tendency in the forecast (Fig. 4.13) extends from 21 GMT 26 January to 15 GMT 27 January. For both the analysis and forecast, the leading forcing term in the lower troposphere is vorticity generation by low-level convergence, and the second term is the (inward) transport of vorticity. The vertical transport of vorticity generally ranks as the third leading term in the budget. The tilting term and residual are generally smaller in magnitude than the two leading terms. The relatively small magnitude of the residual over the early period of rapid storm development suggests that the primary forcing was resolved. However, the residual term increases significantly during the mature stage of the cyclone. Evidently, the simple formulation of vorticity dissipation used in the budgets does not represent the actual dissipation in nature or in the NORAPS model. Based on these results, the vorticity divergence term appears to be the leading source of vorticity to the budget volume in the lower troposphere through strong low-level convergence.

F. SUMMARY

The mass budget illustrates a two-layer vertical structure with strong low-level convergence below a layer of upper-level divergence. The shallow inflow layer combined with a deeper outflow layer results in a net vertically-integrated mass loss in the atmospheric column that is consistent with the surface pressure falls during the rapid deepening phase of the coastal system. The level of maximum vertical velocity (ω) remains relatively constant at 500 mb throughout the period of rapid intensification.

The increase of absolute vorticity tendency at low levels during the rapid development phase of the storm (00-12 GMT 27 January) can be related to the vorticity convergence (generation) and lateral mass transport. In the upper

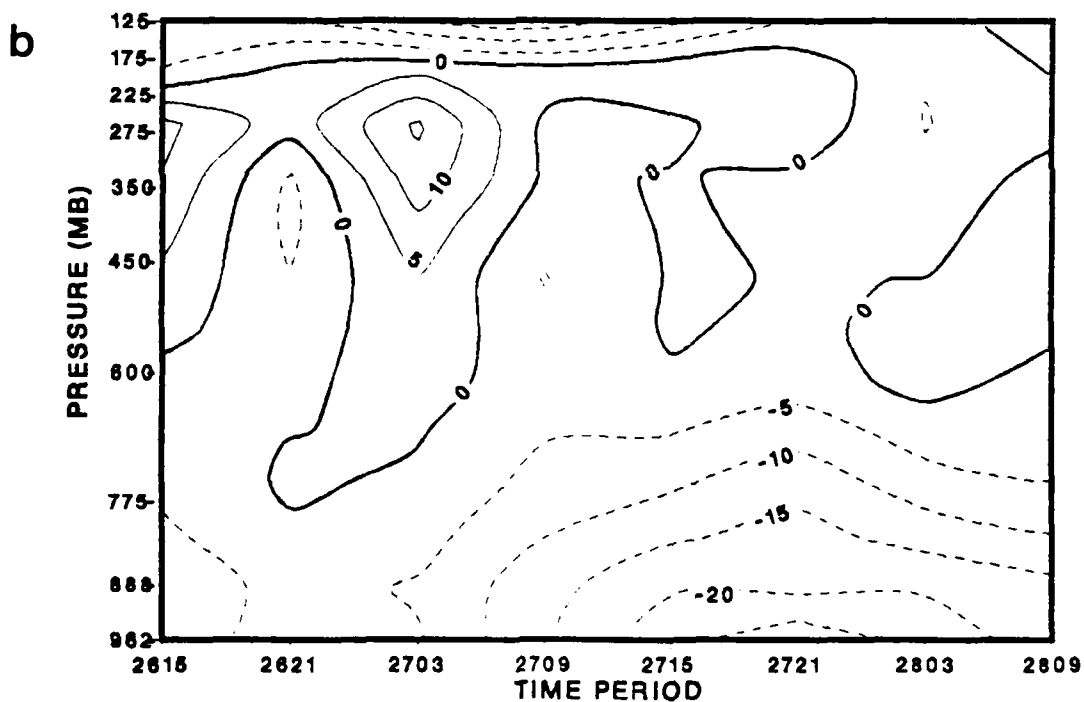
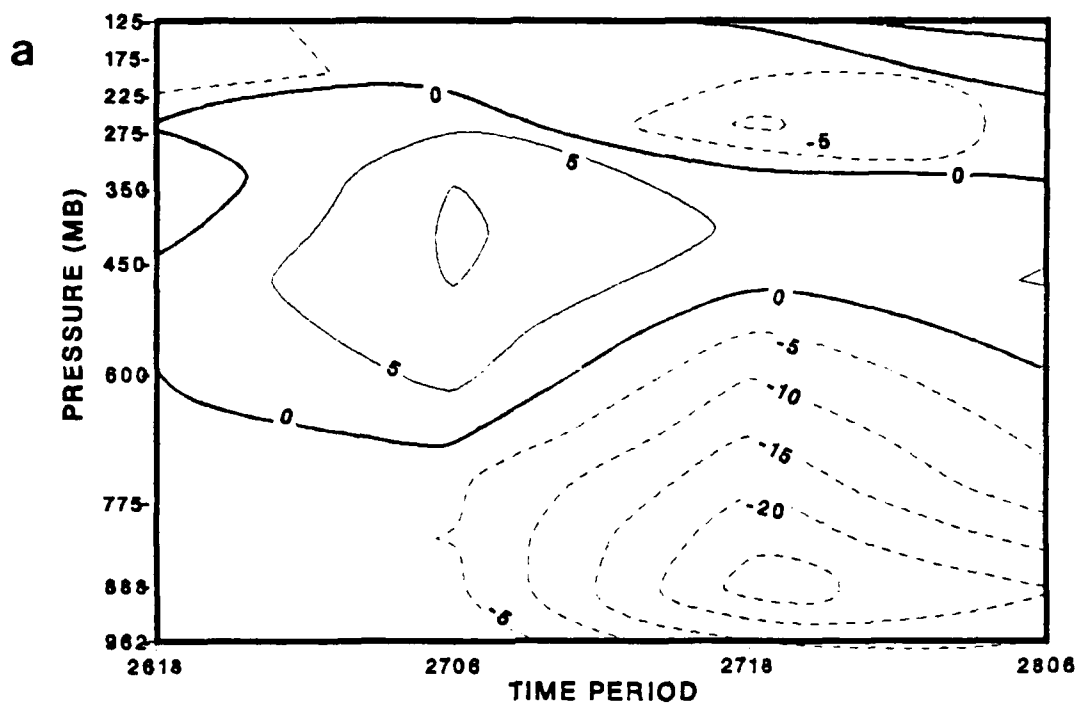


Figure 4.11. Residual of absolute vorticity for 4° lat. radius in the (a) analysis and (b) forecast. Solid dashed contours indicate positive negative vorticity contribution. Contours are $5 \times 10^{-10} \text{ s}^{-2}$.

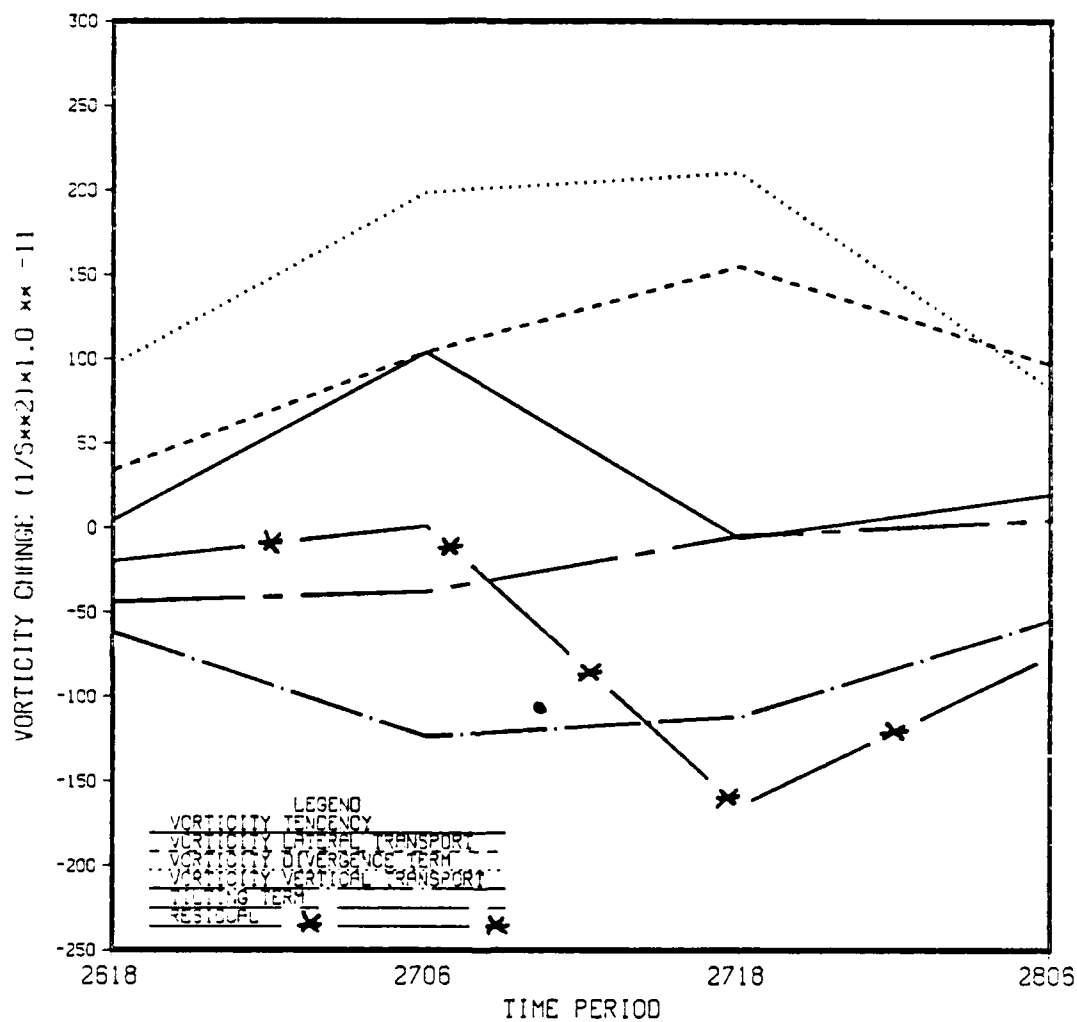


Figure 4.12 Analyzed 1000-500 mb average vorticity budget terms (radius 4):
Lateral transport (dash), tendency (solid), divergence (dot), vertical
transport (chain-dot), residual (chain-*), and tilting term (chain-dash).

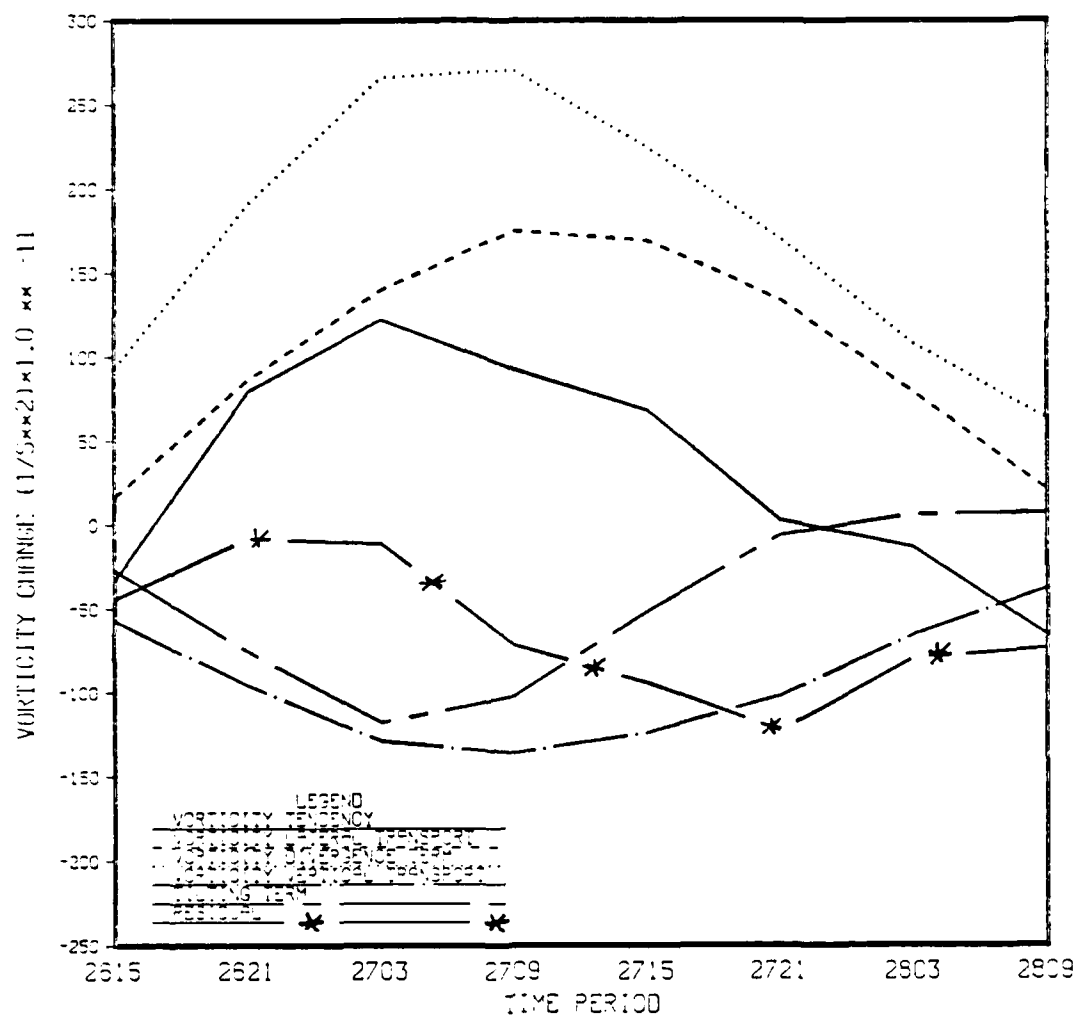


Figure 4.13 Forecast 1000-500 mb average vorticity budget terms (radius 4): Lateral transport (dash), tendency (solid), divergence (dot), vertical transport (chain-dot), residual (chain-), and tilting term (chain-dash).

troposphere, positive lateral transport into the budget volume results from the eddy mode (PVA) contribution offsetting the mean mode (divergence) contribution. Large amounts of cyclonic shear vorticity are advected into the budget volume after 18 GMT 26 January 1986, when it is in the right rear (entrance) region of a strong jet streak. A favorable upper-level divergence pattern is created that exports mass aloft and promotes low-level convergence and spin-up of the low-level vortex. In the lower troposphere, the induced low-level convergence provides the major source of vorticity. The vertical vorticity transport term serves to redistribute vorticity created in the lower layers through vorticity convergence (generation) into the middle and upper troposphere. The tilting term acts as a vorticity sink over most of the atmosphere, particularly in the lower levels. Frictional dissipation of vorticity is important in the PBL during the mature phase of the cyclone and acts to partially offset some of the low-level vorticity spin-up. Therefore, the net vorticity increase in the lower troposphere results from the excess of the vorticity convergence (generation) over frictional dissipation and a negative contribution from the tilting term. As the upper-level forcing weakens and the storm track moves inland, frictional dissipation assumes a more prominent role and the cyclone weakens slightly after 12 GMT 27 January 1986.

V. HEAT AND MOISTURE BUDGET RESULTS

A. GENERAL

The heat and moisture budgets are used to quantitatively evaluate the importance of diabatic heating and moistening in maritime explosive cyclogenesis development. Identification of the leading terms in each budget equation and the vertical distribution of heating and moistening in the atmosphere will provide valuable insight into the interaction between upper-level forcing and diabatic effects. In the analysis and forecast, the diabatic heating and moistening rates are available only as a residual in the budget equation. A direct comparison can be made between the rates diagnosed from the forecast fields in the budget formulation and the actual NORAPS model-predicted rates. Additionally, a direct comparison can be made of the level and phase of the maximum heating and moistening rates.

The moisture budget is available only for the forecast fields since NORAPS does not produce a moisture analysis. The moisture residual at each level, which corresponds to moisture sources/sinks at that level, is vertically integrated and compared with the area-averaged 6-h precipitation amounts from the NORAPS model. The 4° lat. radius is selected to evaluate the various terms of each budget equation as this radius most nearly represents the inner core of the cyclone where heating and moistening tend to be concentrated. After comparing the heating and moistening rates diagnosed from the budget calculations with the corresponding NORAPS model-predicted rates, the column-integrated results will be presented.

B. DESCRIPTION OF THE HEAT BUDGET

The area-averaged flux form of the thermodynamic equation is

$$\overline{\delta T / \delta t} = -1/A \oint T (V_n - V_o) dl - \partial / \partial p (\overline{\omega T}) + \overline{\omega \alpha} c_p + \overline{Q}, \quad (5.1)$$

where T is the temperature, α is the specific volume, c_p is the specific heat capacity at constant pressure and the overbar denotes the area-average of the term. The term on the left side of (5.1) is the quasi-Lagrangian temperature tendency. The first term on the right side of (5.1) is the horizontal heat flux, while the second term is the vertical

heat flux. The third term is the energy conversion term and the final term is the residual. The residual is a measure of the diabatic heating plus computational errors in the budget calculation. Use of the flux form of the equation (as opposed to the advective form) reduces computational errors and attaches increased physical significance to the inferred diabatic heating term.

The vertical-time display of each term in the thermodynamic equation is presented in the advective form of the equation to permit easier interpretation of the physical processes involved. The energy conversion and the vertical advection terms are shown individually and then later combined to form the adiabatic cooling term. The area-averaged advective form of the thermodynamic equation is

$$\overline{\delta T \delta t} = - \overline{(V - V_0) \cdot \nabla T} - \overline{\omega \partial T \partial p} + \overline{\omega \alpha c_p} + \overline{\dot{Q}}. \quad (5.2)$$

The term on the left side of (5.2) is the quasi-Lagrangian temperature tendency. The first term on the right side of (5.2) is the horizontal temperature advection, while the second term is the vertical temperature advection. The third term is the energy conversion term and the final term is the residual. Each term of (5.2) can be vertically integrated to obtain column-averaged heating rates. This permits identification of the most important physical processes involved in heating or cooling the budget volume during the rapid intensification of the storm.

C. HEAT BUDGET RESULTS

The quasi-Lagrangian tendency (Fig. 5.1a) for the analysis depicts mid-tropospheric temperature increases over the initial 12-h period, with decreases in the lower and upper troposphere. From 06 GMT 27 to 03 GMT 28 January 1986, the analysis has cooling from the surface to 300 mb and heating above that level. Beyond 03 GMT 28 January 1986, temperature increases occur over the entire depth of the budget volume. Temperature decreases are largest at 200 mb (18 GMT 26 January), near the surface (06 GMT 27 January) and near 400 mb (18 GMT 27 January). The temperature tendency in the forecast case (Fig. 5.1b) shows the same general pattern but with much larger increases and decreases. Particularly significant are the large temperature decreases near the surface during the period 09 GMT 27 January to 09 GMT 28 January 1986.

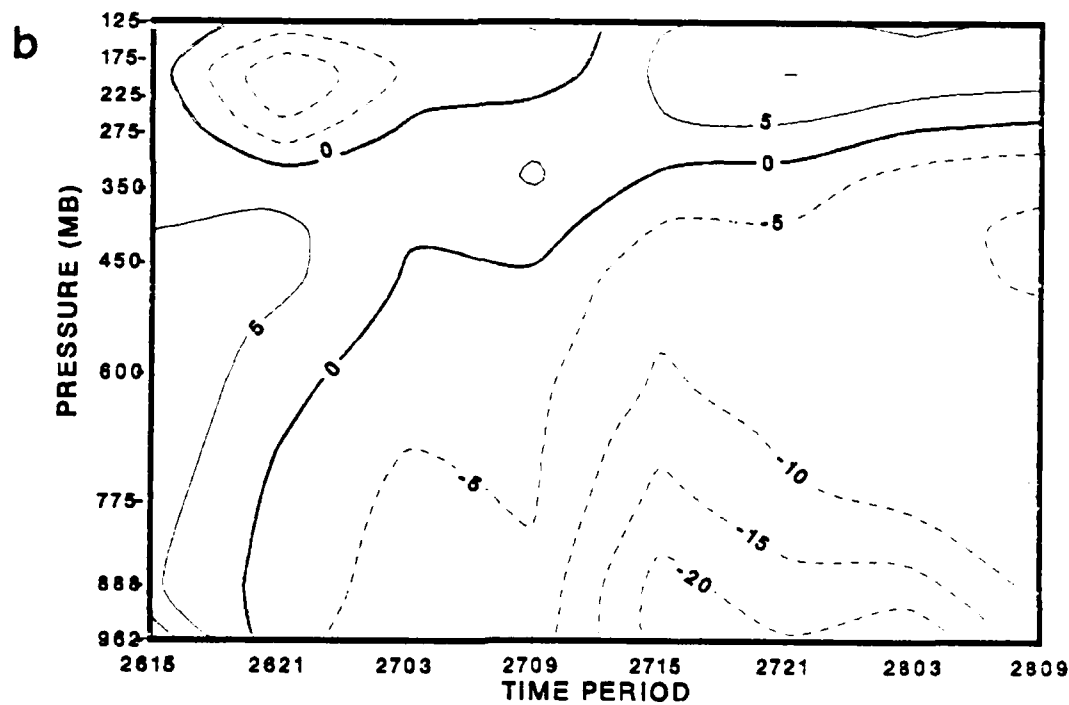
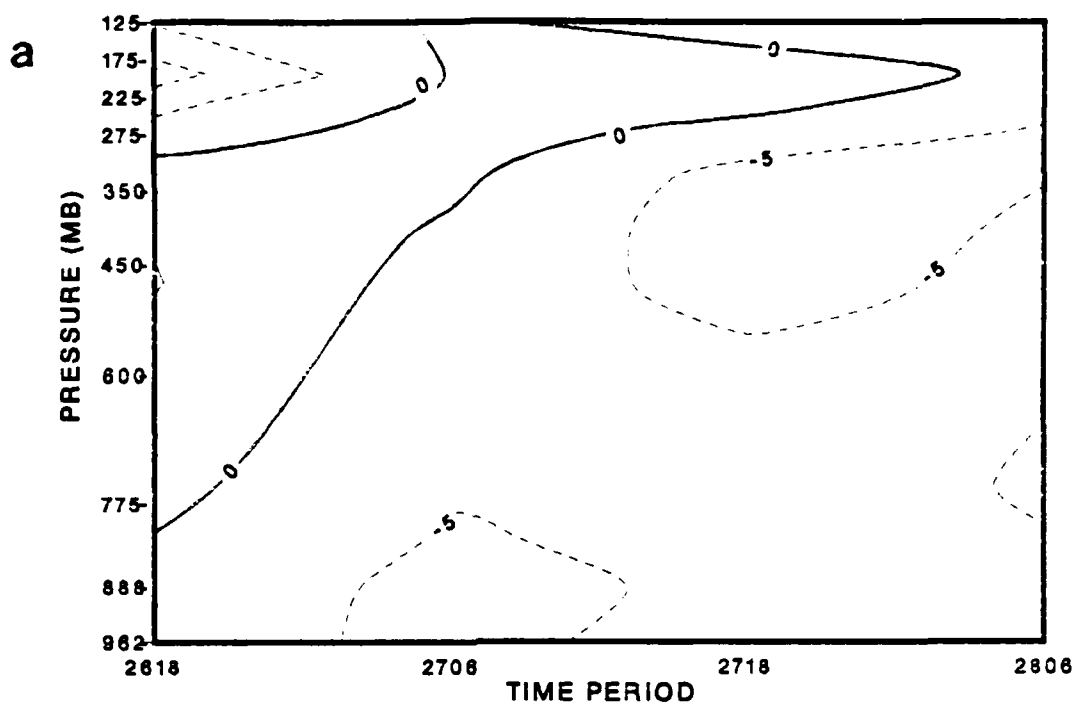


Figure 5.1 Quasi-Lagrangian temperature tendency for 4° lat. radius in the (a) analysis and (b) forecast. Positive negative values indicate heating cooling of the budget volume. Contour interval is 5°C day .

The quasi-Lagrangian formulation of the horizontal advection term removes the effects due to cyclone velocity. Therefore, only the purely development effects of the horizontal temperature advection that influence storm development are presented. This term is computed by subtracting the velocity convergence divergence multiplied by temperature from the total horizontal temperature flux. The horizontal temperature advection in the analysis (Fig. 5.2a) depicts warming throughout the atmosphere with significant warming above 350 mb ($10\text{--}20^\circ\text{C day}$). The horizontal advection in the forecast case (Fig. 5.2b) shows good agreement in the middle and upper troposphere. The magnitude of the warm advection in the upper levels ($10\text{--}30^\circ\text{C day}$) is much greater during the period of rapid development centered at 06 GMT 27 January 1986. Additionally, the cold advection maximum (-10 to -20°C day) shown at 18 GMT 27 January 1986 is not consistent with the corresponding analysis. This forecast low-level cold advection and related cooling maximum in the tendency term can be interpreted with respect to the predicted primary storm track (Fig. 3.10a). After 12 GMT 27 January 1986, the predicted storm track moved ashore across New England and into Quebec, Canada. As a result, cold continental air is advected into the predicted storm which causes the relatively warm budget volume to experience cooling. The relatively weak warm advection in the low to middle troposphere and strong warm advection in the upper levels (200 mb) agrees very well with the synoptic discussion of this storm in Chapter III.

The vertical temperature advection (Fig. 5.3a) in the analysis has a maximum of 55°C day at 400 mb at 06 GMT 27 January 1986. The forecast vertical temperature advection (Fig. 5.3b) also has a warming maximum near 400 mb with a much greater magnitude of 80°C day . Notice that the maximum warming rate occurs during the period of rapid storm intensification (00-12 GMT 27 January) in both the analysis and forecast. As the area-averaged levels of maximum vertical motion are near 500 mb in both the analysis and forecast (Fig. 4.2), a large upper-level vertical temperature gradient should be present to account for the higher levels depicted in the vertical temperature advection profiles.

The area-averaged vertical temperature profile (Fig. 5.4) for both the analysis and forecast appears to support this reasoning. The temperature decreases throughout the depth of the atmosphere (to 100 mb) with a stronger temperature gradient in the upper levels (500-250 mb). Notice that neither the analysis or forecast cases have a distinct tropopause. An examination of individual grid points within the budget volume at 12

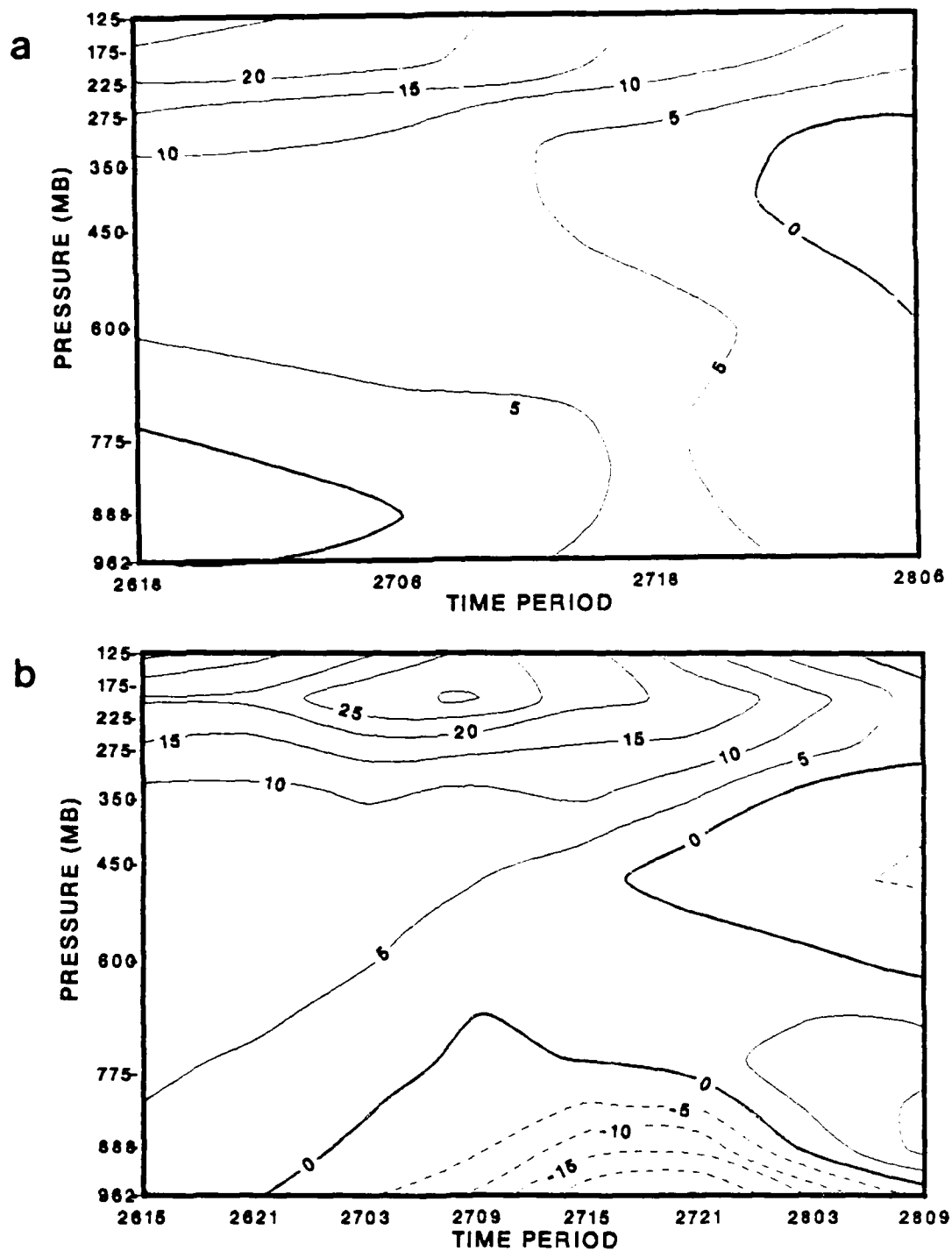


Figure 5.2 Horizontal temperature advection for 4° lat. radius in the
 (a) analysis and (b) forecast. Positive negative values indicate
 warm cold advection. Contour interval is 5° C day.

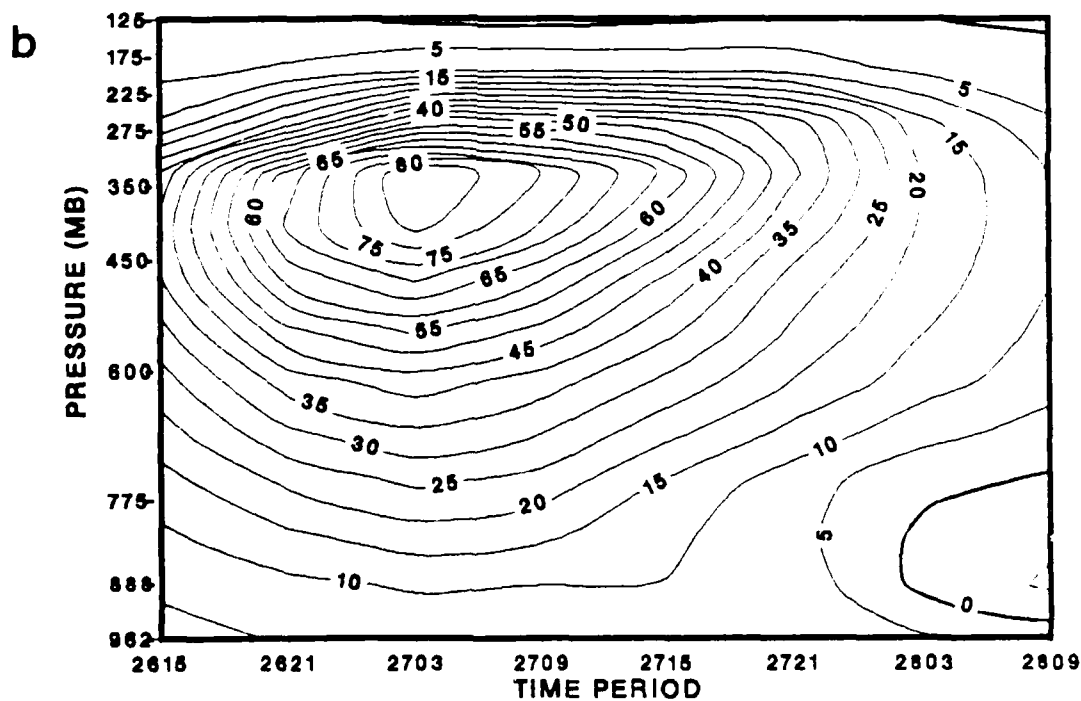
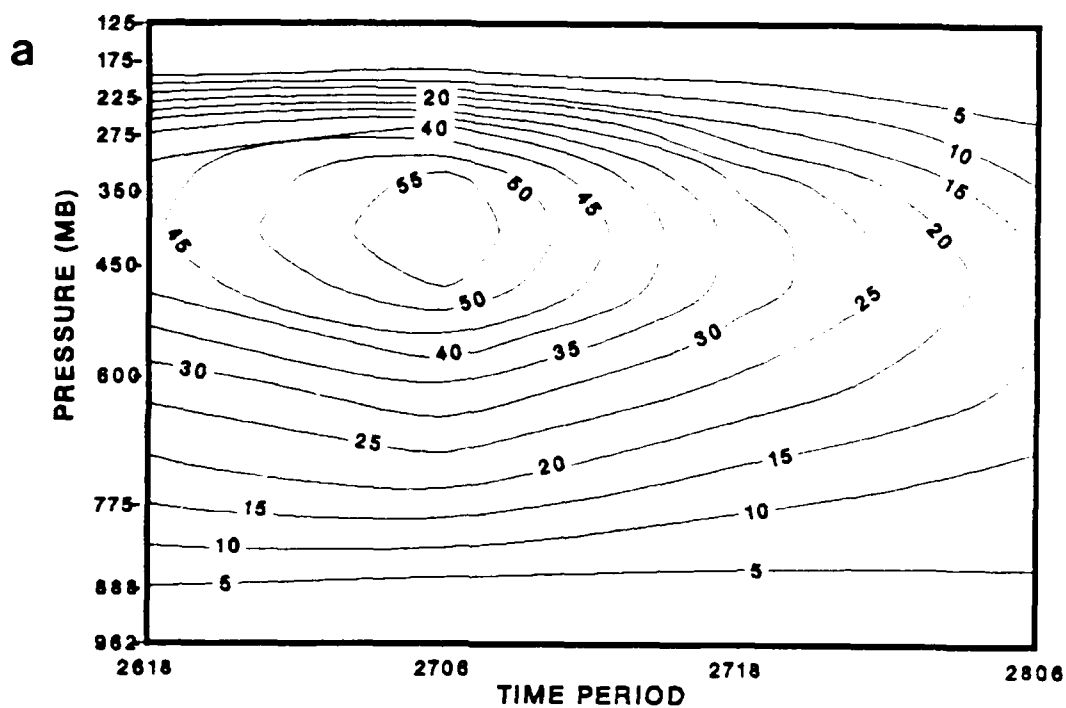


Figure 5.3 Vertical temperature advection for 4° lat. radius in the (a) analysis and (b) forecast. Positive negative values indicate warm cold advection. Contour interval is 5°C day .

GMT 26 January 1986 showed that the NORAPS objective analysis was in agreement with the actual observed soundings. In the actual soundings, the tropopause was delineated by an isothermal layer between 250 and 150 mb. Given the rather weak tropopause, the area-averaging used in the budget calculations and the 5°C day contour interval utilized in Fig. 5.4, a decreasing vertical temperature profile in the upper troposphere should be expected. However, the tropopause can be located at the level where the temperature gradient shows a distinct change. For both analysis and forecast, a tropopause can be identified near the 250 level.

The analyzed energy conversion term (Fig. 5.5a) has a cooling maximum of -75°C day near 450 mb at 06 GMT 27 January 1986. The forecast energy conversion (Fig. 5.5b) shows a higher cooling maximum of -100°C day near 400 mb at 03 GMT 27 January 1986. The general pattern of both the analyzed and forecast energy conversion closely resembles the vertical velocity fields (Fig. 4.2) presented in the mass budget, except the maxima are shifted upward due to the weighting factor of specific volume in the energy conversion term.

The vertical temperature advection and energy conversion terms can be combined to form the adiabatic cooling term. Both terms have omega as a common factor and are of opposite sign. The resulting adiabatic cooling term can thus be written as $\omega(\Gamma_d - \Gamma)$, where Γ_d is the dry adiabatic lapse rate and Γ is the environmental lapse rate or vertical temperature gradient. In the NORAPS model atmosphere, $\Gamma_d - \Gamma$ is always constrained to be greater than zero due to the dry convective adjustment scheme employed. Because the mean vertical motion is upward during cyclone development (negative ω), this term is negative and opposes heating. In effect, this term serves to modulate any heating introduced into the volume by horizontal temperature advection or latent heat release. The analyzed adiabatic cooling (Fig. 5.6a) depicts cooling maxima of -25°C day at 200 mb (18 GMT 26 January) and 600 mb (06 GMT 27 January). The forecast adiabatic cooling (Fig. 5.6b) verifies well, although with significantly greater magnitudes (-30 to -45°C day) between 00-12 GMT 27 January 1986, when the cyclone is rapidly intensifying. The cooling maxima in both the analysis and forecast at 600 mb correlate well with the vertical motion field (omega) discussed earlier.

The surface sensible heat flux (Fig. 5.7) is archived in the forecast but is unavailable for verification since it is not directly observed in the analysis. It shows an alternating pattern of warming (1 to 3°C day) and cooling (-1 to -3°C day) between

AD-A183 333

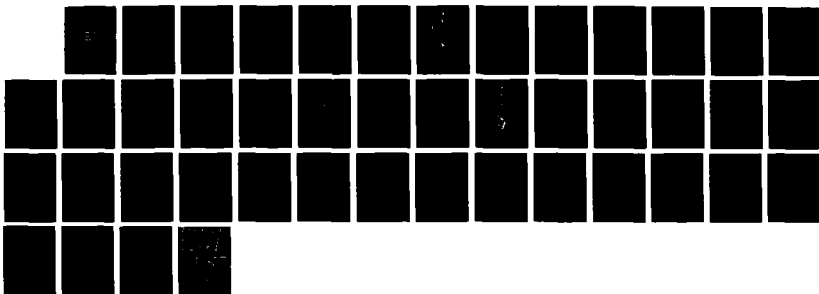
DIAGNOSTIC STUDY OF A GENESIS OF ATLANTIC LOWS
EXPERIMENT (GALE) CYCLOGENESIS EVENT(U) NAVAL
POSTGRADUATE SCHOOL MONTEREY CA D J SOPER MAR 87

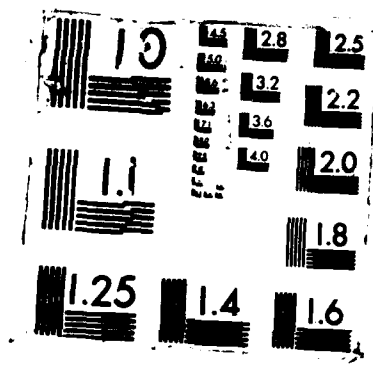
2/2

UNCLASSIFIED

F/G 4/2

NL





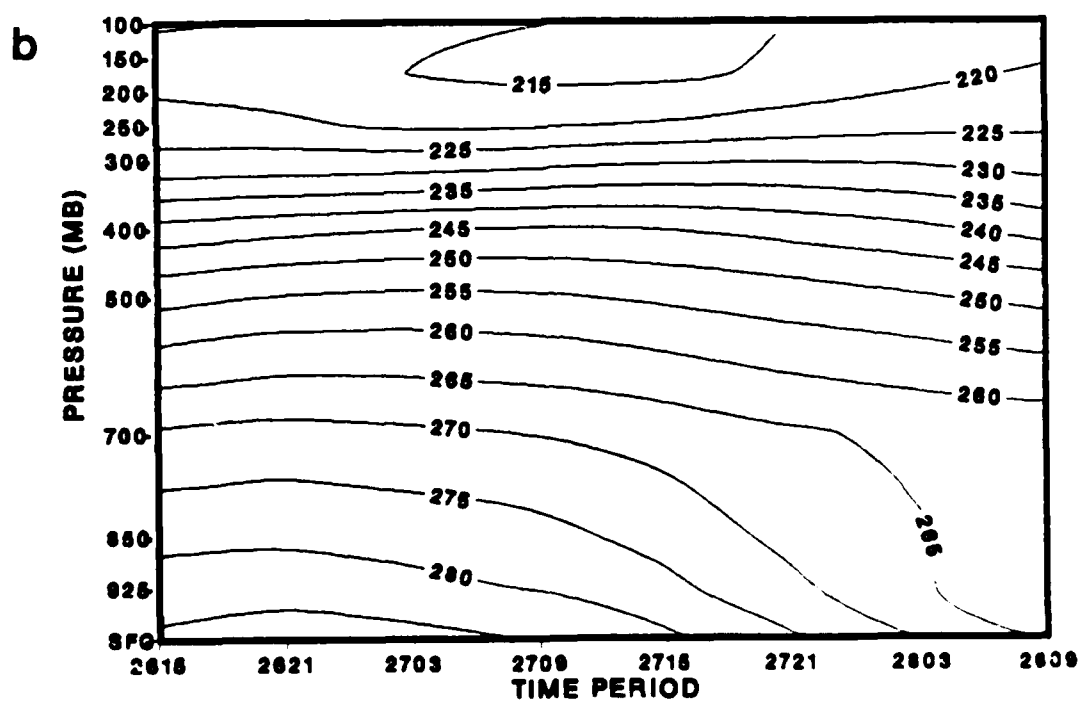
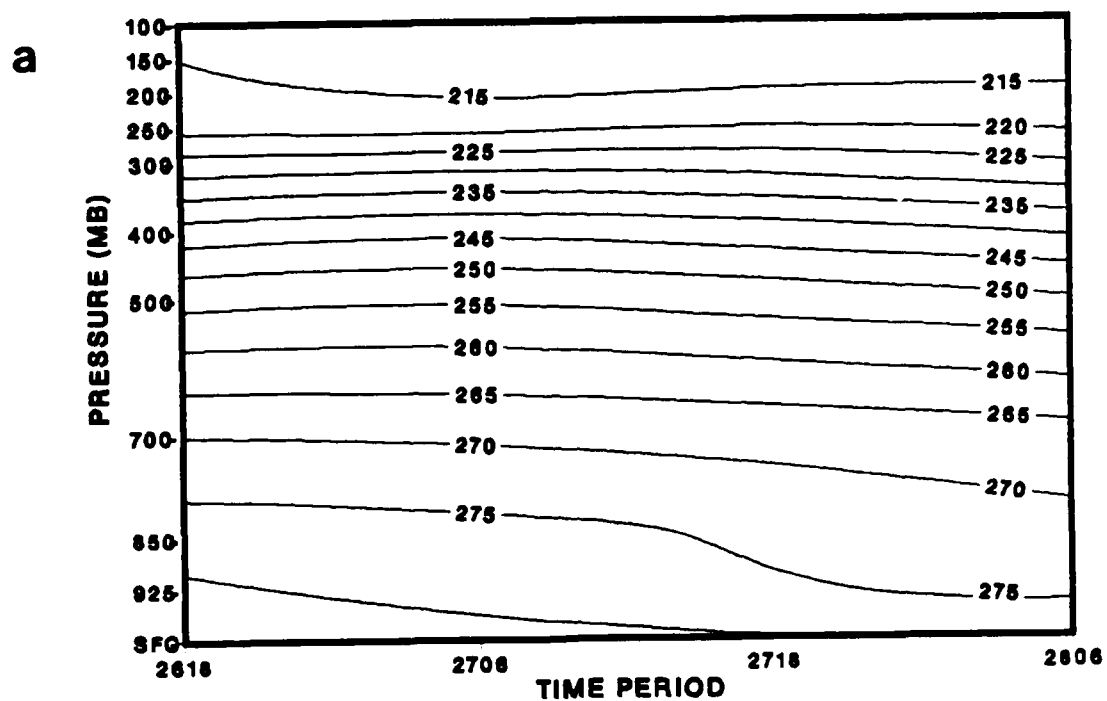


Figure 5.4 Area-averaged temperature for 4° lat. radius in the
(a) analysis and (b) forecast. Contour interval is 5° K.

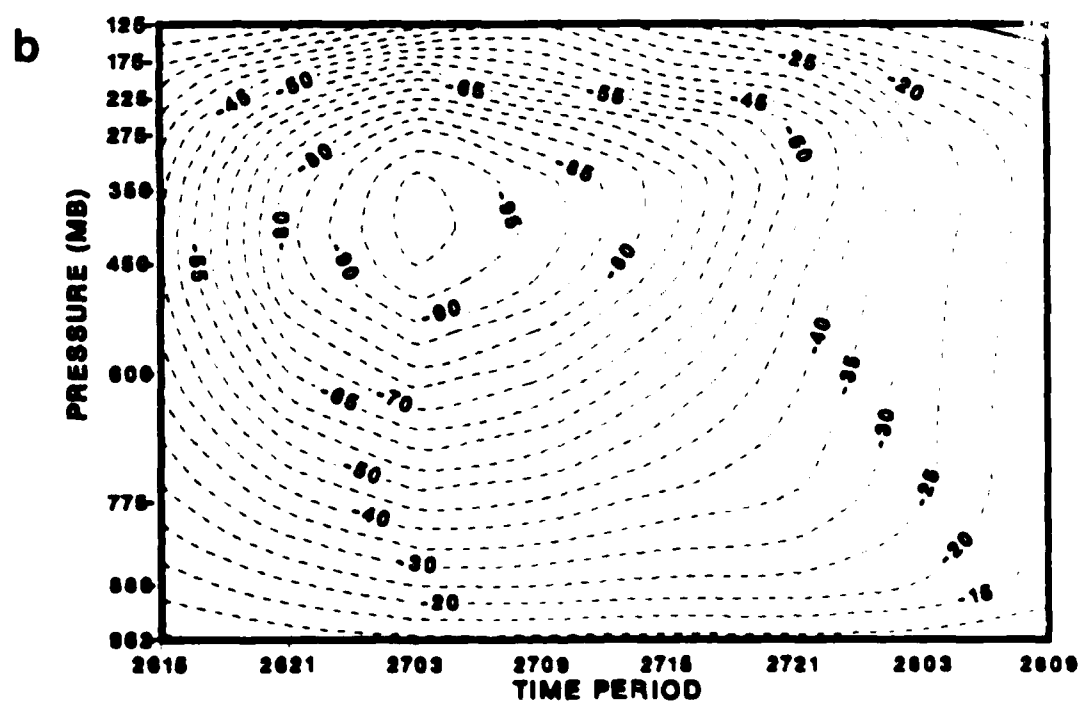
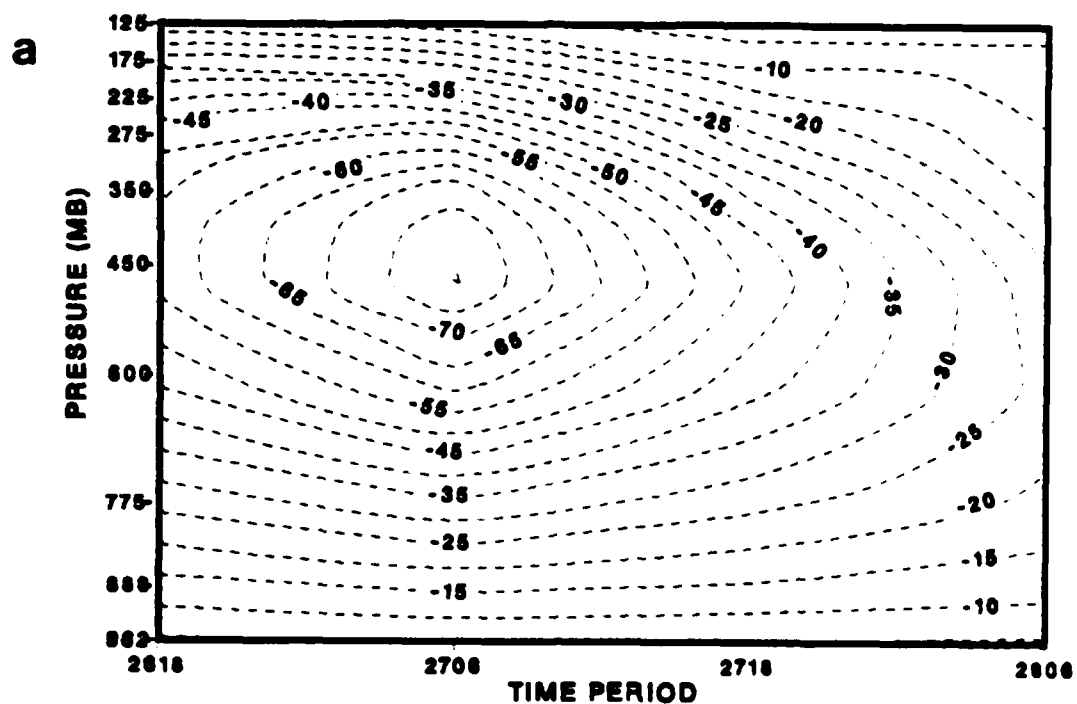


Figure 5.5 Energy conversion term for 4° lat. radius in the (a) analysis and (b) forecast. Negative values indicate cooling of the budget volume. Contour interval is 5°C day .

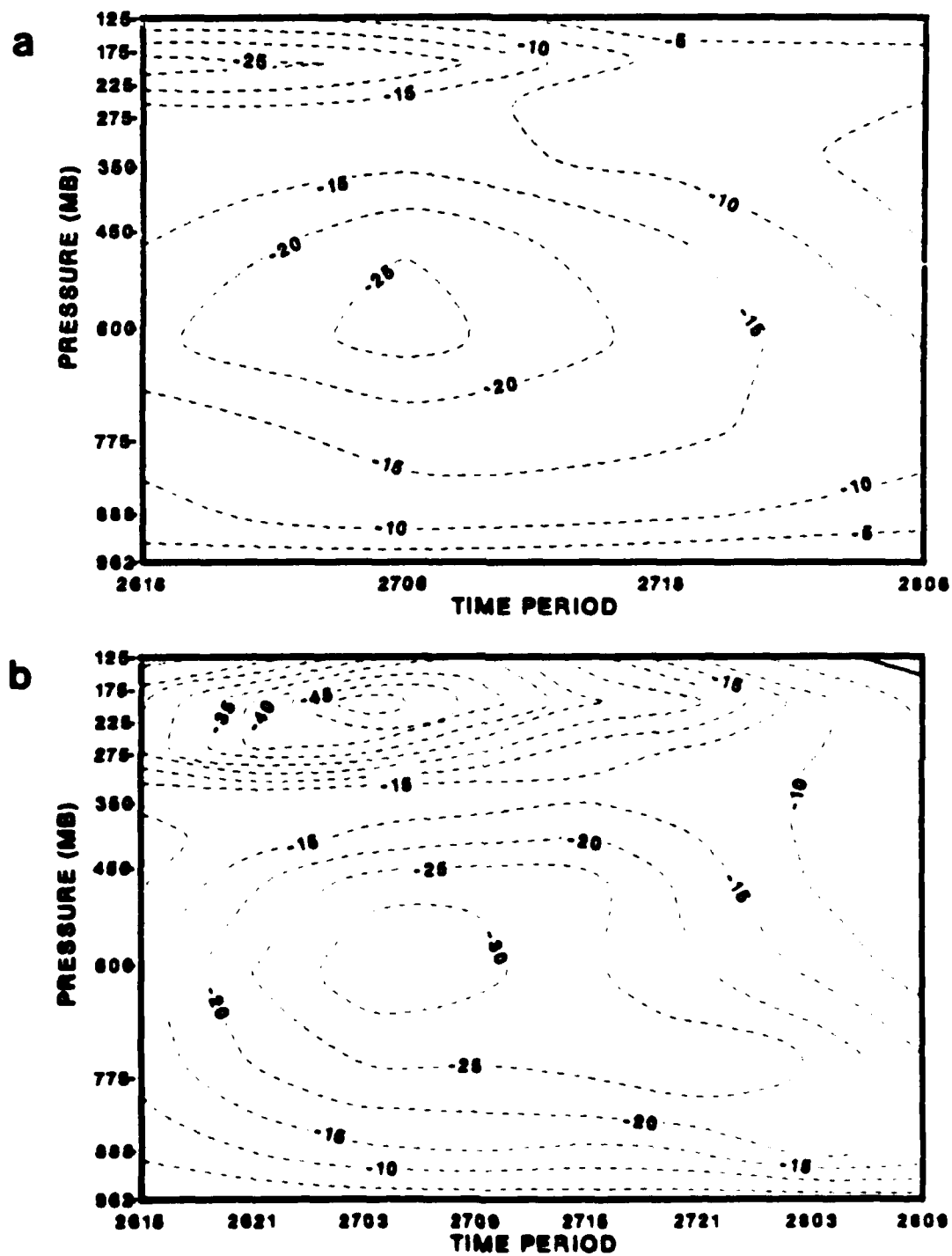


Figure 3.6 Adiabatic cooling term for 4° lat. radius in the (a) analysis and (b) forecast. Negative values indicate cooling of the budget volume. Contour interval is 5°C day .

occurs as the storm moves off the coast at 15 GMT 26 January and comes ashore again at 12 GMT 27 January 1986. In a column and area-averaged sense, this overall contribution to the budget is relatively small. However, its effect can be significant over limited areas because an upward heat flux can destabilize lapse rates and initiate convection, and thus become an important factor in the deepening phase of the storm. The NORAPS model-predicted surface sensible heat fluxes (Fig. 5.8) for the eastern U.S. and adjacent coastal waters are presented for 18 GMT 26 January and 06 GMT 28 January 1986. The positive sensible fluxes in Fig. 5.7 from 15 GMT 26 January to 00 GMT 27 January 1986 correlate well with weak positive sensible fluxes off the Carolina coast (Fig. 5.8) at 18 GMT 26 January 1986. Similar agreement exists for the negative sensible fluxes over the period 03-15 GMT 27 January 1986. After the primary cyclone moves ashore, the variation in the surface fluxes ($1\text{-}2^{\circ}\text{C/day}$) appears to be diurnal in nature.

The residual term is computed as the balance of the other calculated terms in the budget and thus includes diabatic heating, surface sensible heat fluxes and computational errors. Important physical processes such as sensible latent heating and radiational cooling cannot be measured directly and must be inferred as a residual in the computations. Radiational cooling is considered to be small compared to the effects of sensible heat fluxes and latent heat release. The analyzed residual (Fig. 5.9a) shows heating throughout most of the troposphere with a maximum (15°C/day) at 600 mb from 18 GMT 26 January to 06 GMT 27 January 1986. Cooling rates of -5 to -10°C/day occur near the surface and above 200 mb. The level and magnitude of the heating is in agreement with the results of Liou and Elsberry (1985) and Rau (1986). Liou and Elsberry (1985) used European Center for Medium Range Weather Forecasting (ECMWF) analyses for a North Pacific Ocean case study and found a 25°C/day heating rate at 600 mb. Similarly, Rau (1986) found a heating maximum of 20°C/day at 550 mb in his study of extratropical cyclogenesis based on NORAPS analyses. The residual (heating rate) in the forecast case (Fig. 5.9b) has the same general heating pattern in the middle troposphere with a greater heating maximum of 25°C/day near 600 mb between 03-09 GMT 27 January 1986. Secondary maxima of $15\text{-}20^{\circ}\text{C/day}$ are predicted between 175-275 mb that are not consistent with the analysis. The significantly greater predicted mid-level heating is consistent with the greater deepening predicted by the model during 00-12 GMT 27 January 1986. Studies by Anthes *et al.* (1983) and Gyakum (1983b) suggest that a low to mid-level

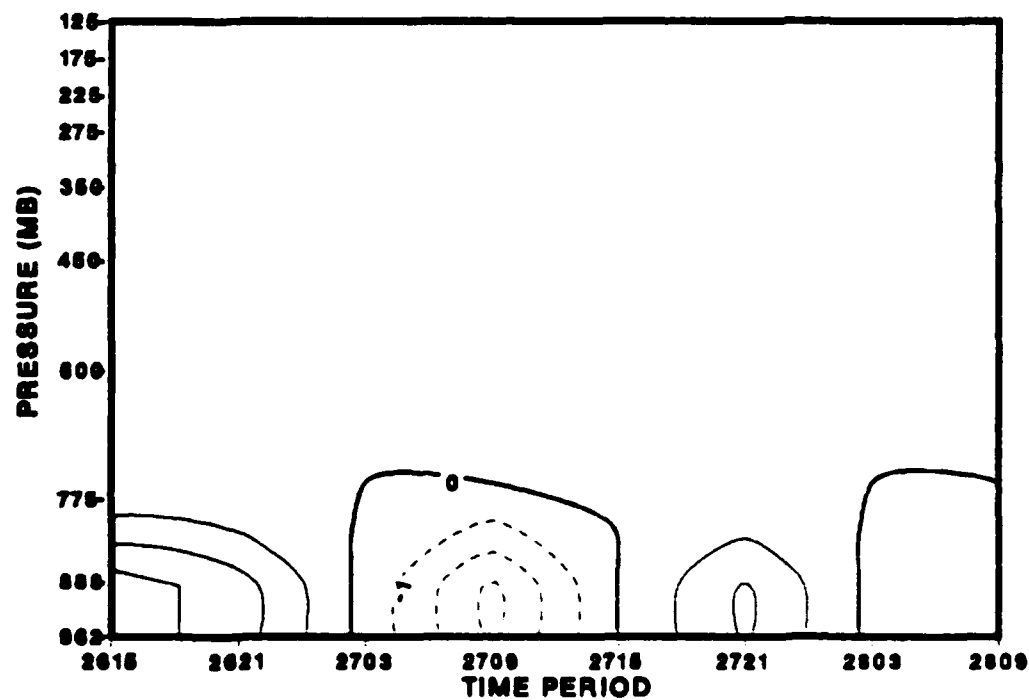


Figure 5.7 Forecast surface sensible heat flux convergence within the lowest 200 mb for 4° lat radius. Contour interval is 1 C day.

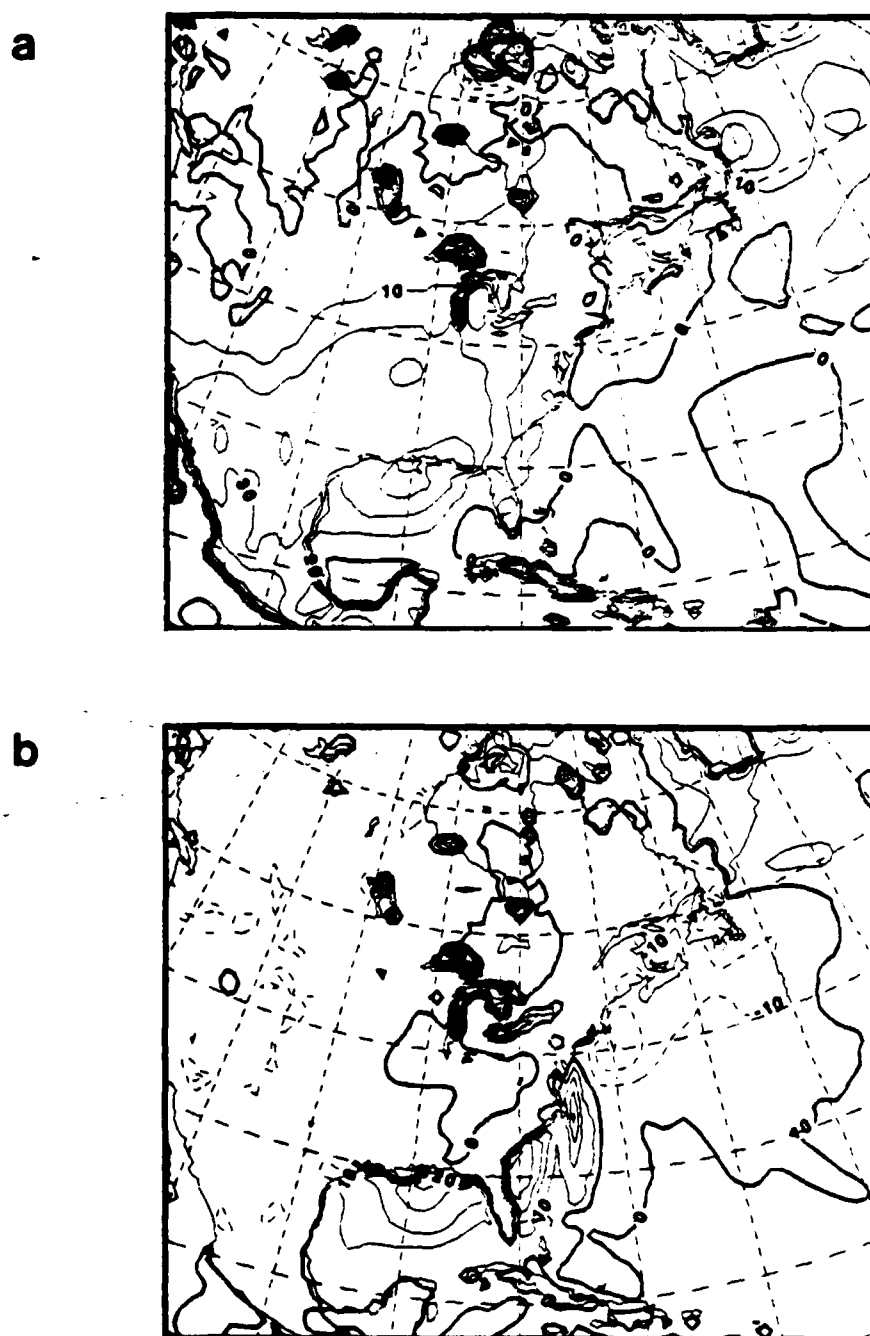


Figure 5.8. NORAPS operational forecast surface sensible heat fluxes for eastern U.S. and adjacent ocean areas at (a) 18 GMT 26 January and (b) 06 GMT 27 January 1986. Contour interval is $10 \text{ cal cm}^{-2}\text{-h}$.

tropospheric maximum in the vertical heating profile is more favorable for cyclone intensification. Qualitatively, this lower heating maximum and associated vertical velocity maximum would imply stronger horizontal convergence in the lower troposphere and a greater vorticity tendency near the surface.

A comparison of the NORAPS diabatic heating rate as archived in the output fields and the diagnosed heating rate from the budget residual derived from the forecast fields is presented in Fig. 5.10. The NORAPS model-predicted heating rate is the 6 h accumulated value during the integration converted to a daily rate ($^{\circ}\text{C}/\text{day}$). These heating rates include net latent heating and short and long-wave radiational cooling. However, the surface sensible heat flux is not included in the NORAPS predicted heating rate since it is not distributed over a constant depth in the model forecast as is assumed in the diagnostic model (lowest 200 mb). The NORAPS predicted heating rate (Fig. 5.10a) has a maximum of $20^{\circ}\text{C}/\text{day}$ at 550 mb between 03-09 GMT 27 January 1986. This is slightly higher than the 600 mb level diagnosed in the analyzed and forecast budget residuals. Additionally, the diagnosed heating maxima in the forecast residual (Fig. 5.9b) above 275 mb are totally absent in the NORAPS archived heating rate (Fig. 5.10a). The difference between the budget residual (forecast) and the NORAPS predicted heating rate (Fig. 5.10b) provides an estimate of the computational errors in the budget. Small differences support the accuracy of the budget results. Throughout most of the low to middle troposphere, a relatively small residual of plus or minus $5^{\circ}\text{C}/\text{day}$ exists. Only above 300 mb do the errors in the budget become significant (differences of $5\text{--}15^{\circ}\text{C}/\text{day}$). These differences in the upper troposphere are related to the unrealistically large values of adiabatic cooling identified in the budget based on the forecast (Fig. 5.6b).

The leading term in the 1000-300 mb column-averaged heat budgets for both the analysis (Fig. 5.11) and forecast (Fig. 5.12) is the adiabatic cooling term, in which the energy conversion term is the major component. The diabatic heating term (residual plus computation errors) is the second leading term and reaches magnitudes of $10^{\circ}\text{C}/\text{day}$ (analysis) and $18^{\circ}\text{C}/\text{day}$ (forecast) during the period of explosive storm deepening. The primary role of diabatic heating is to offset adiabatic cooling and thus allow the budget volume to remain warmer than it would be without the additional source of energy. Hydrostatic considerations then dictate that a warmer column will result in a lower SLP and greater storm intensity. Horizontal temperature advection approaches values of $3\text{--}6^{\circ}\text{C}/\text{day}$ during the period of rapid storm development. In the

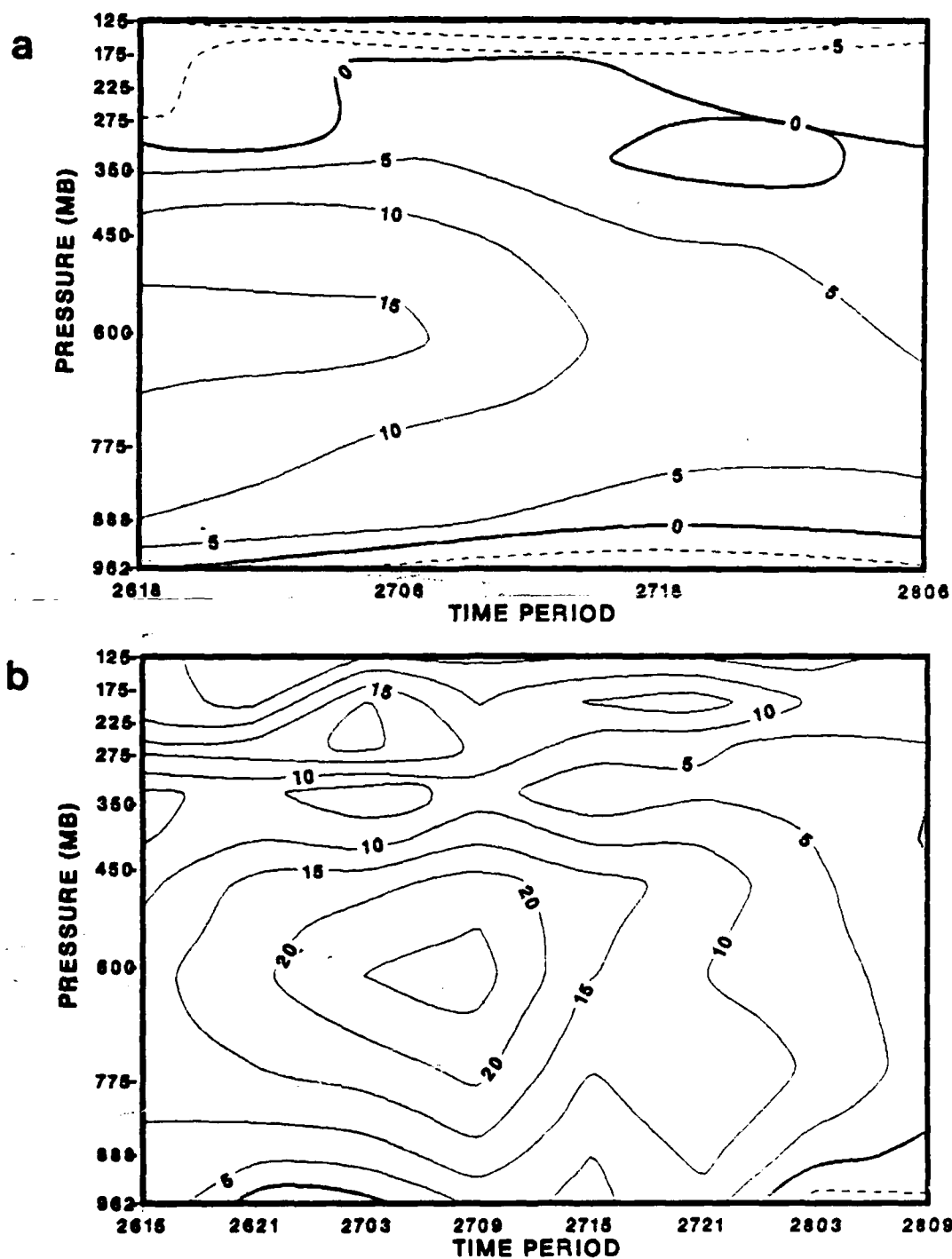


Figure 5.9 Heat budget residual (heating rate) for 4° lat. radius in the (a) analysis and (b) forecast. Positive negative values indicate heating cooling of the budget volume. Contour interval is 5° C day.

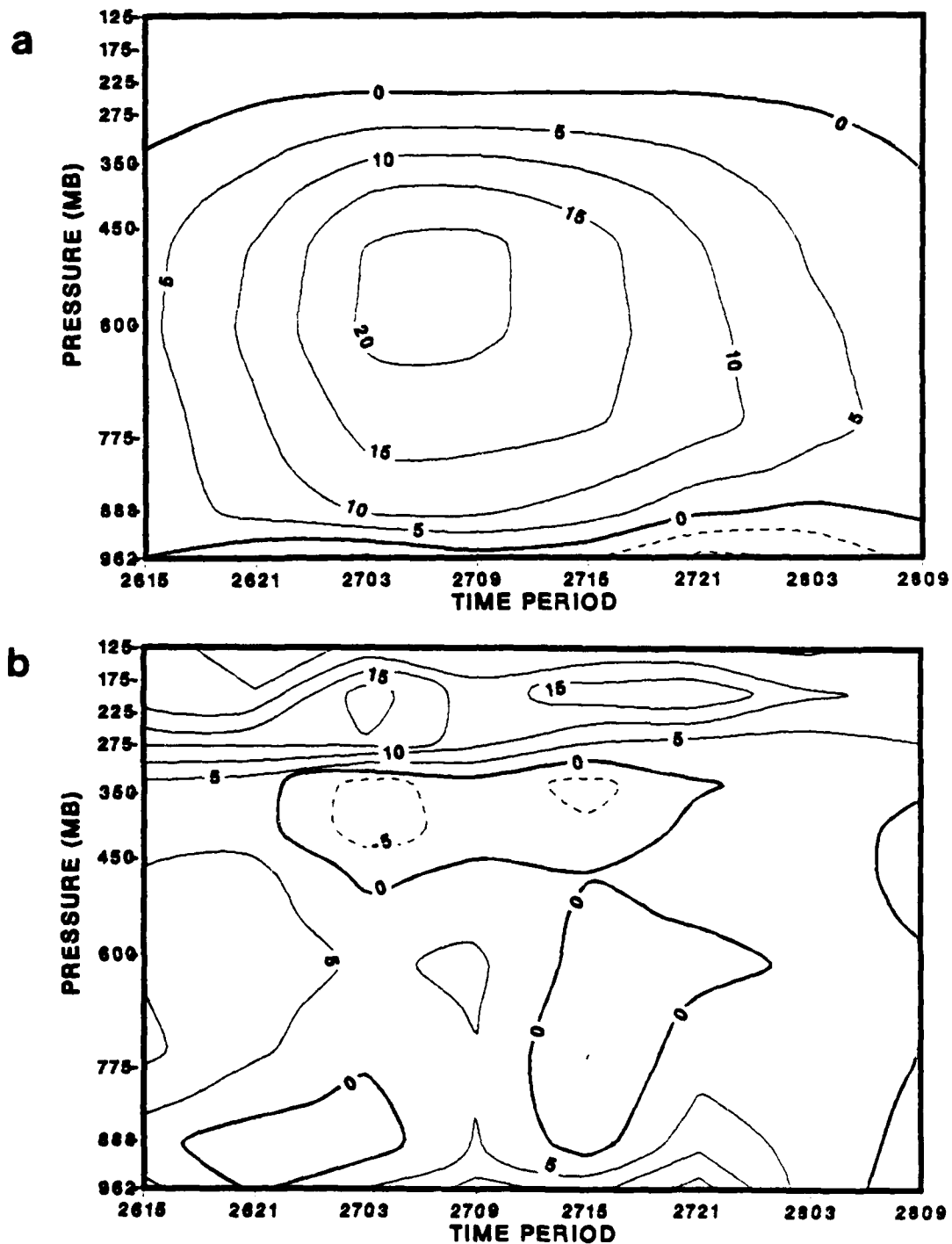


Figure 5.10 (a) NORAPS model-predicted diabatic heating rate. (b) Difference of forecast budget residual and NORAPS model-predicted diabatic heating rate for 4° lat. radius. Contour interval is 5°C day .

forecast, horizontal temperature advection is smaller than diabatic heating at all time periods. The quasi-Lagrangian temperature tendency combines the effects of diabatic and adiabatic heating and horizontal temperature advection averaged over the budget volume. Both analysis and forecast have a positive temperature tendency at the initial period that becomes negative at all other times.

A comparison between the 1000-300 mb column-averaged forecast budget residual (inferred heating rate) and the corresponding NORAPS archived heating rate is presented in Fig. 5.13. Although the initial difference of 7°C/day is rather large, closer agreement (0-4°C/day) exists over the period of explosive development from 03-15 GMT 27 January 1986. Both estimates emphasize the importance of diabatic heating during the explosive phase of cyclone development from 00-12 GMT 27 January 1986. Studies by Liou and Elsberry (1985) and Elsberry *et al.* (1985) also identified a strong correlation between SLP deepening rate and the diabatic heating rate.

In this coastal storm, it appears that both diabatic heating and warm advection played roles in producing a warmer core and stronger cyclone. In the column-averaged analysis and forecast, diabatic heating was a significantly greater factor during the period of greatest storm intensification. During the rapid development phase, the greater forecast deepening of 4 mb appears to be correlated with a much stronger predicted diabatic heating rate (14-18°C/day) than is indicated in the analysis (8-10°C/day).

D. DESCRIPTION OF THE MOISTURE BUDGET

The initial moisture field is specified in the NORAPS model by using the 12-h forecast fields of vapor pressure (moisture content). The forecast vapor pressure is then internally converted into a specific humidity field within the budget program.

The area-averaged flux form of the moisture budget equation is similar to the heat budget,

$$\overline{\delta q} \delta t = -1/A \oint q (V_n - V_o) dl - \partial \partial p (\overline{\omega q}) + \overline{E} - \overline{P}, \quad (5.3)$$

where q is the specific humidity, E is evaporation rate, P is precipitation rate and the overbar denotes the area-average of the term. The term on the left side of (5.3) is the quasi-Lagrangian moisture tendency. On the right side of (5.3), the first two terms are

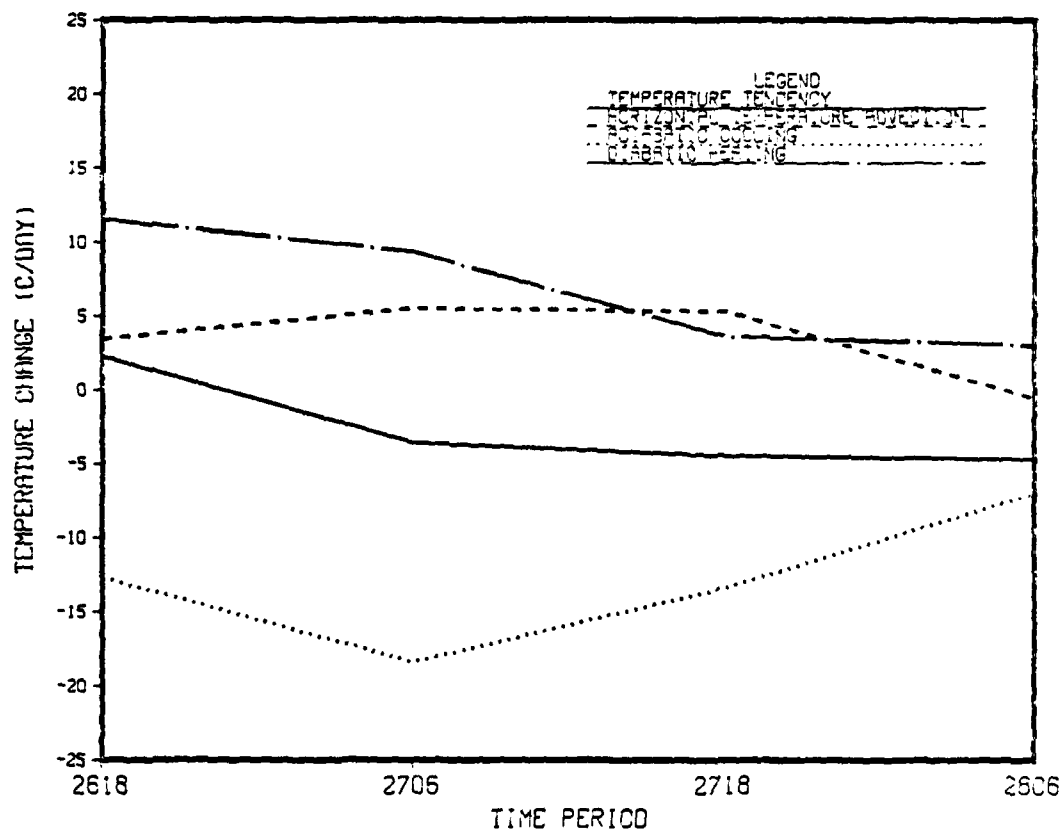


Figure 5.11 Analyzed 1000-300 mb column-averaged heat budget results (radius 4): Temperature tendency (solid), horizontal advection (dash), adiabatic cooling (dot), and diabatic heating (chain-dot). Units are $^{\circ}\text{C day}$.

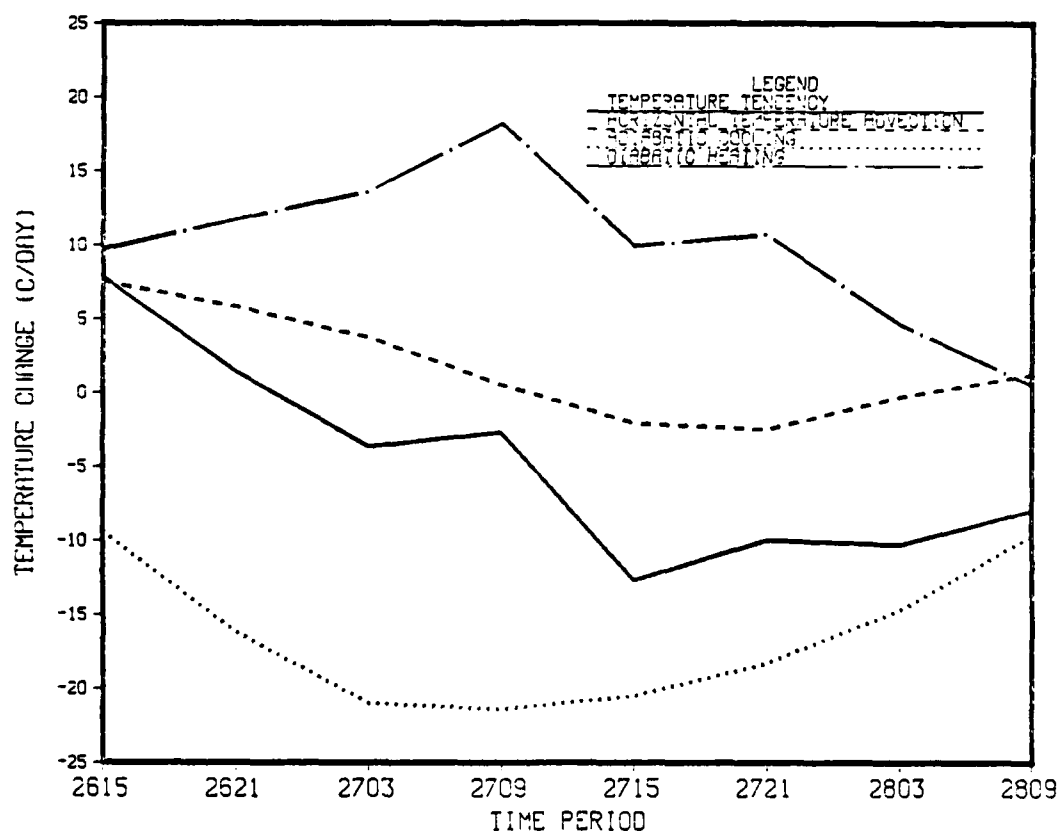


Figure 5.12 Forecast 1000-300 mb column-averaged heat budget results (radius 4): Temperature tendency (solid), horizontal advection (dash), adiabatic cooling (dot), and diabatic heating (chain-dot). Units are °C day.

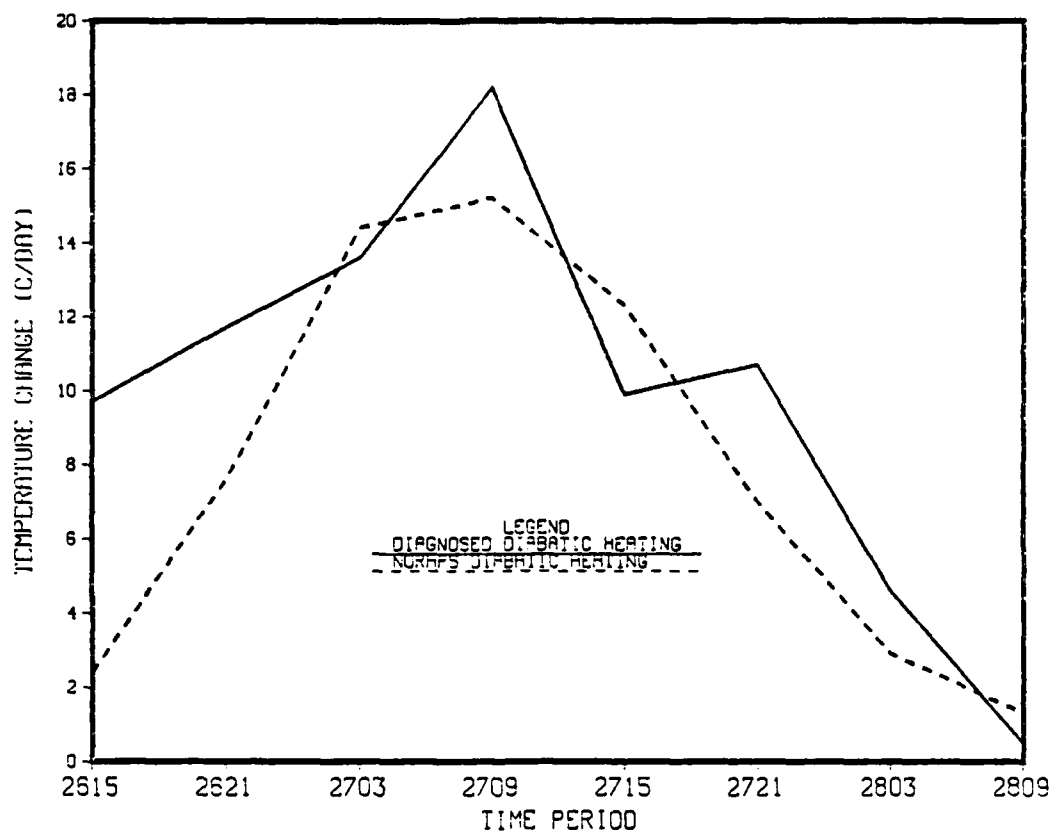


Figure 5.13 Column-averaged heat budget residual (solid) and NORAPS model-predicted diabatic heating rate (dash) for 4° lat. radius. Units are °C day.

the horizontal and vertical moisture fluxes. Evaporation and precipitation are combined in the moisture source/sink term, which includes the effects of moisture fluxes from the surface. Since these terms cannot be observed directly, they must be computed as a budget residual. The sign convention for the residual is negative (positive) if net precipitation (evaporation) is occurring. When precipitation occurs over an area, the phase change causes a decrease in the amount of water vapor in the air. Although precipitation is measured by the synoptic network, surface moisture fluxes and evaporation cannot be measured directly and must be inferred.

The main objective in calculating the moisture budget is to identify correlations with the heat budget with respect to the level and phase of maximum heating and moistening within the budget volume. As in the previous budget studies, the 4° lat. radius is selected as most representative of the inner storm processes. A comparison of analyzed and forecast budget results cannot be made, since a moisture analysis is not performed by NORAPS. A comparison is made between the diagnosed budget residual and the NORAPS moistening rate archived in the NORAPS output files. This moistening rate is the 6-h averaged value during the integration.

Various sources of error can arise in the moisture budget. A bi-cubic spline interpolation scheme is used to interpolate from the NORAPS grid to the budget volume. When the vapor values are very small, especially above 500 mb, small negative values of vapor pressure can be introduced. Errors can also be introduced in the calculation of vertical moisture flux. The NORAPS model employs a linear-p interpolation scheme to interpolate the moisture field at odd sigma levels to even sigma levels where vertical velocity is specified. By contrast, the vertical flux of moisture in the budget is calculated on pressure levels, which can result in large errors due to sharp moisture gradients in the vertical. The moisture prediction in NORAPS currently uses a leapfrog (centered differencing) scheme. One problem with this solution is the omission of a time filter to smooth the large computational modes that cause oscillations in a centered-differencing scheme. As a result, large errors can occur in the quasi-Lagrangian moisture tendency (too small or too large).

E. MOISTURE BUDGET RESULTS

The quasi-Lagrangian moisture time tendency (Fig. 5.14) in the forecast has an initial period of moistening prior to 00 GMT 27 January 1986, which is followed by an extended period of moisture decrease within the budget volume from 00 GMT 27

January to 09 GMT 28 January 1986. The maximum negative tendency value occurs during the period 15-21 GMT 27 January 1986. The forecast moisture time tendency is in general agreement with the NORAPS predicted 6-h precipitation pattern (Fig. 5.15). Periods of negative moisture tendencies tend to correlate with corresponding periods of moderate to heavy precipitation during 06-18 GMT 27 January 1986.

The horizontal moisture flux (Fig. 5.16a) for the forecast has strong moisture convergence from the surface to 600 mb with a maximum during the period 03-09 GMT 27 January 1986. This agrees well with the horizontal convergence layer depicted in the mass budget (Fig. 4.1). Relatively weak moisture divergence is shown aloft from 15 GMT 27 January to 03 GMT 28 January 1986. The horizontal moisture flux term can be decomposed into symmetric (divergence) and asymmetric (advective) components (not shown). In this study, the divergence component accounts for about 80% of the total moisture flux, which is consistent with results found by Rau (1986). However, the negative moisture flux above 600 mb is primarily attributed to the advective component (not shown).

The vertical moisture flux represents the redistribution of moisture in the vertical. From continuity considerations, the horizontal moisture flux convergence below 600 mb must be offset by a corresponding vertical flux divergence. The forecast vertical moisture flux (Fig. 5.16b) has a pattern of low-level moisture divergence below 775 mb and moisture convergence from 775 to 275 mb. Rau (1986) also found that the change from moisture divergence to moisture convergence occurred near 775 mb. These maxima of moisture divergence (below 775 mb) and convergence (above 775 mb) are centered at 03 GMT 27 January 1986, which correlates well with the period of rapid storm intensification.

The surface moisture flux (Fig. 5.17) archived in the forecast is assumed in the QLD budget formulation to decrease linearly to zero over a 200 mb layer. A significant contribution to moistening below 775 mb occurs from 15 GMT 26 January to 15 GMT 27 January 1986. This period corresponds to that part of the forecast cyclone track which was over water. Although smaller in magnitude than either the horizontal or vertical advection terms, this is an important contribution to increasing the potential instability within the budget volume. The release of latent heat by large-scale and organized convective processes is an important factor in the explosive phase of the storm. The NORAPS surface latent heat fluxes (Fig. 5.18) for the Atlantic coastal areas are presented for 18 GMT 26 January and 06 GMT 27 January 1986.

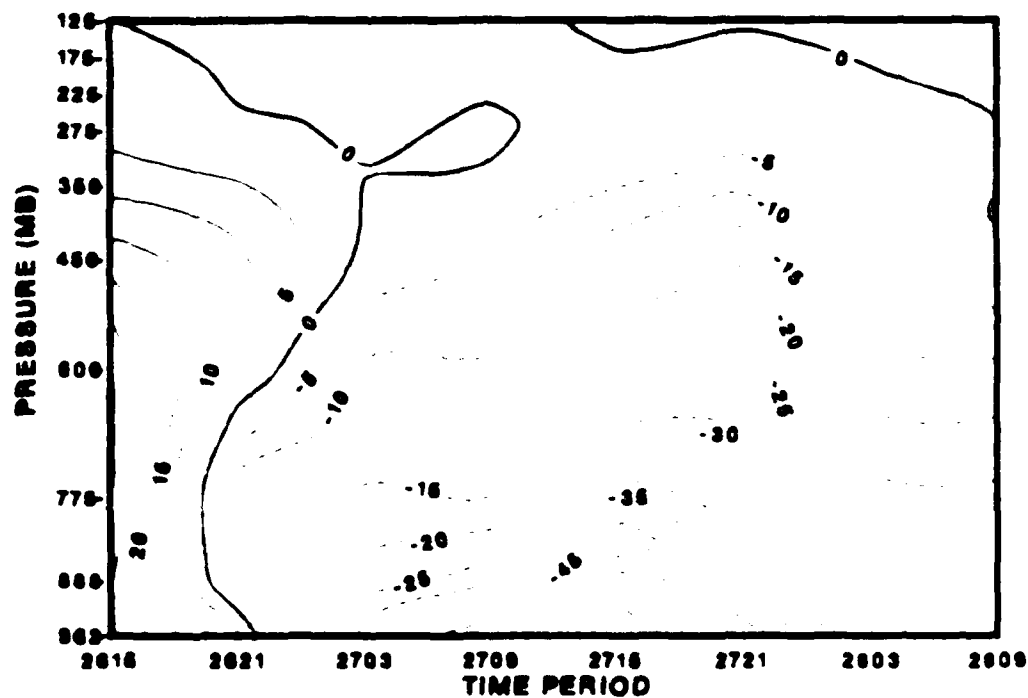


Figure 5.14 Quasi-Lagrangian moisture tendency in the forecast for 4-latitude radius. Positive/negative values indicate moistening/drying of the budget volume. Contour interval is 4×10^{-12} g/g/day.

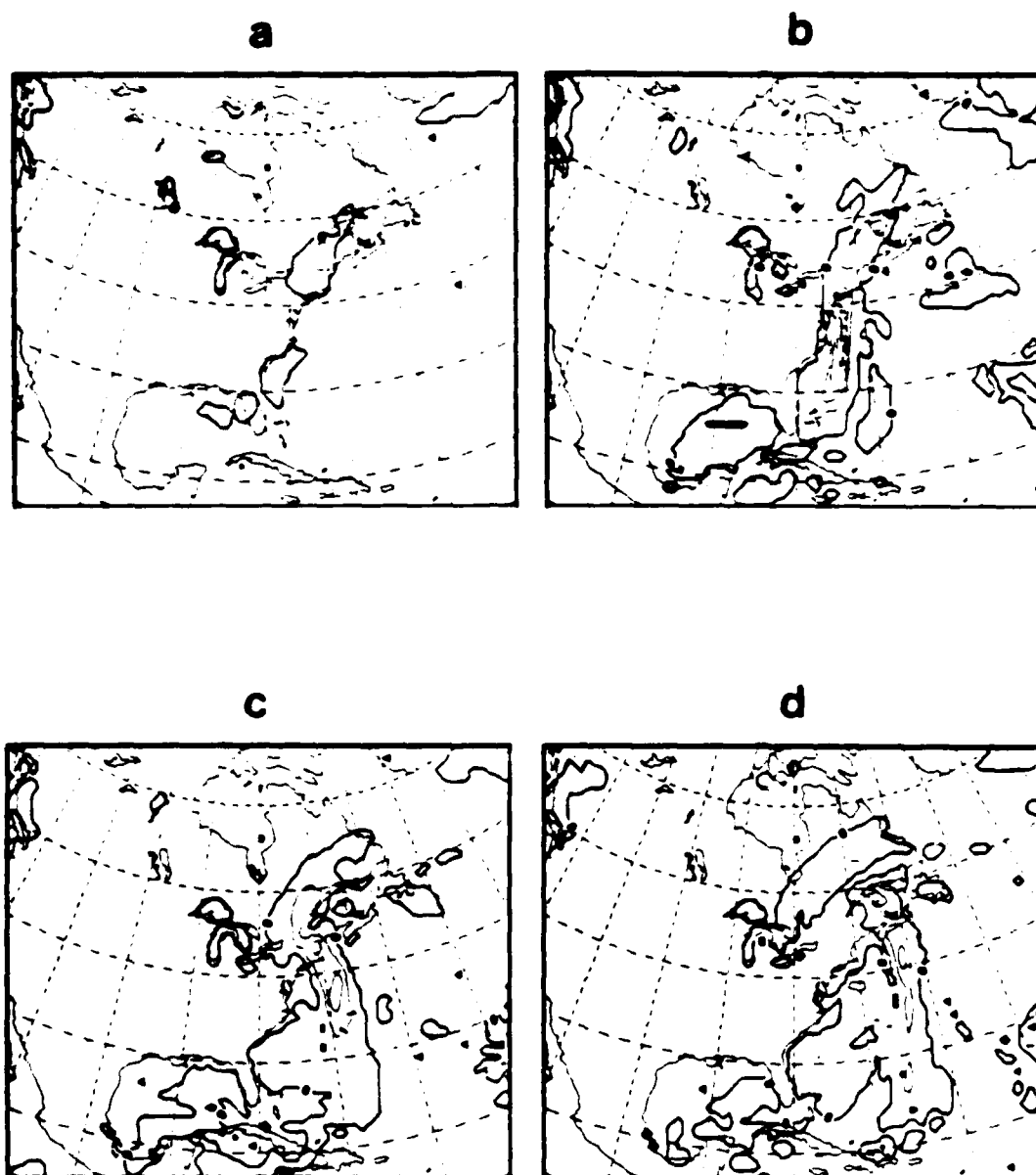


Figure 5.15. NORAPS predicted 6 h total precipitation (cm 6 h) for 4° lat. radius.
 (a) 18 GMT 26 January, (b) 06 GMT 27 January, (c) 18 GMT 27 January,
 and (d) 06 GMT 28 January. Contour interval is 1.0 cm 6 h.

which is during the positive moisture flux in Fig. 5.17. These positive moisture fluxes during the cyclone's 'over water' track are associated with the cold outbreak of dry continental air over the Atlantic coastal areas as the storm moved up the coast.

The moisture budget residual includes the effects of evaporation, precipitation, surface moisture fluxes and computational errors. A positive negative value indicates a moisture source sink (evaporation is greater smaller than precipitation). The forecast moisture budget residual (Fig. 5.19a) has a negative moisture tendency maximum (sink) centered near 500 mb at 03 GMT 27 January 1986. This negative maximum is associated with the relative maximum in the moisture tendency term at 03 GMT 27 January (Fig. 5.14) and shows that precipitation exceeded evaporation in the mid troposphere during the storm intensification period. The strong moisture sink (precipitation) also correlates well with the large NORAPS forecast precipitation rates (Fig. 5.15) depicted at 06 GMT 27 January 1986. The small residuals above 275 mb are the result of the negligible amount of moisture in the upper troposphere.

The archived NORAPS moistening rate (Fig. 5.19b) has a very similar structure and shows excellent agreement with the diagnosed budget residual. A moisture sink is again depicted near 500 mb with a $-90 \times 10^{-2} - 4$ g/g/day maximum centered at 03 GMT 27 January 1986. These moistening rates agree very closely in level and phase with the diabatic heating rates (Fig. 5.9), which is expected if latent heat release is the primary contributor to the diabatic term.

The difference between the moisture budget residual (forecast) and the archived NORAPS model-predicted moistening rate is presented in Fig. 5.20. As in the heat budget, this difference provides a estimate of the computational error in the budget. The extremely small differences throughout the middle and upper troposphere give strong support to the accuracy of the budget results. The only significant differences occur in the lower troposphere below 800 mb. The archived NORAPS model output includes a positive moisture tendency (source) below 900 mb after 15 GMT 27 January 1986. However, the forecast budget residual only has a small positive maxima below 900 mb before 00 GMT 27 January 1986. The temporal differences in the locations of these relatively small moisture sources in the PBL appear to be responsible for most of the differences below 800 mb.

The column-averaged (forecast) budget residual, NORAPS archived moistening rate and the NORAPS area-averaged 6-h precipitation rates are presented in Fig. 5.21. Whereas the NORAPS moistening rate is a 6-h averaged value, the NORAPS

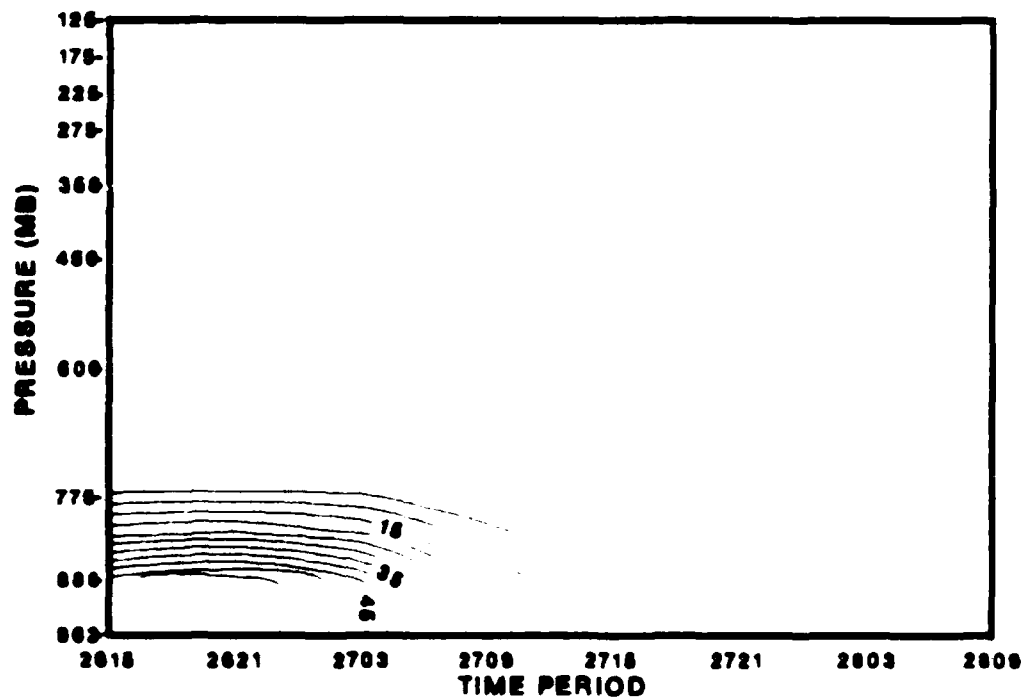
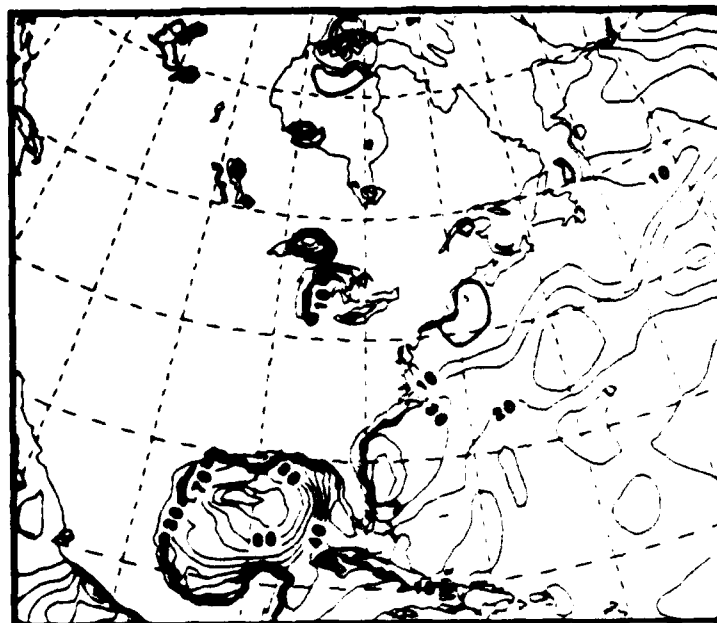


Figure 5.17. Forecast surface moisture flux convergence within the lowest 200 mb for 4° lat radius. Time interval is 5×10^{-4} g/g day.

a



b

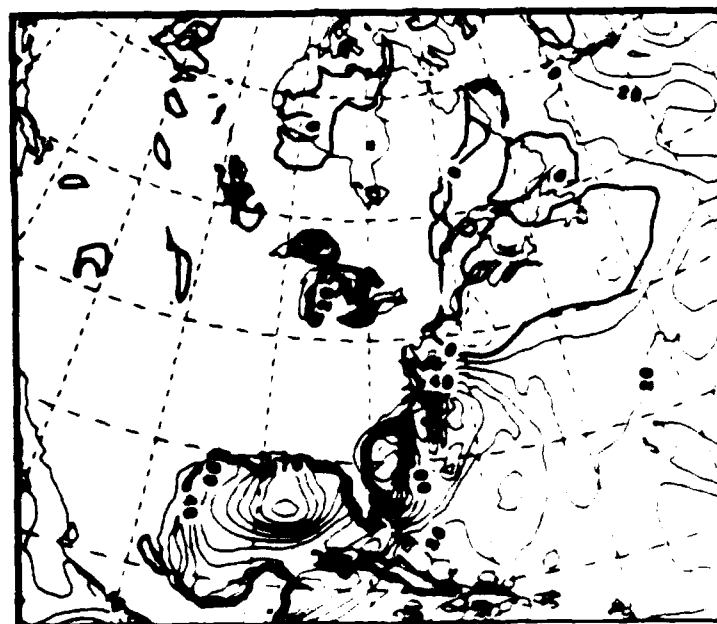


Figure 5.18. NORAPS operational forecast surface latent heat fluxes for eastern U.S. and adjacent coastal areas at (a) 18 GMT 26 January and (b) 06 GMT 27 January. Contour interval is $10 \text{ cal cm}^{-2}\text{-h}$.

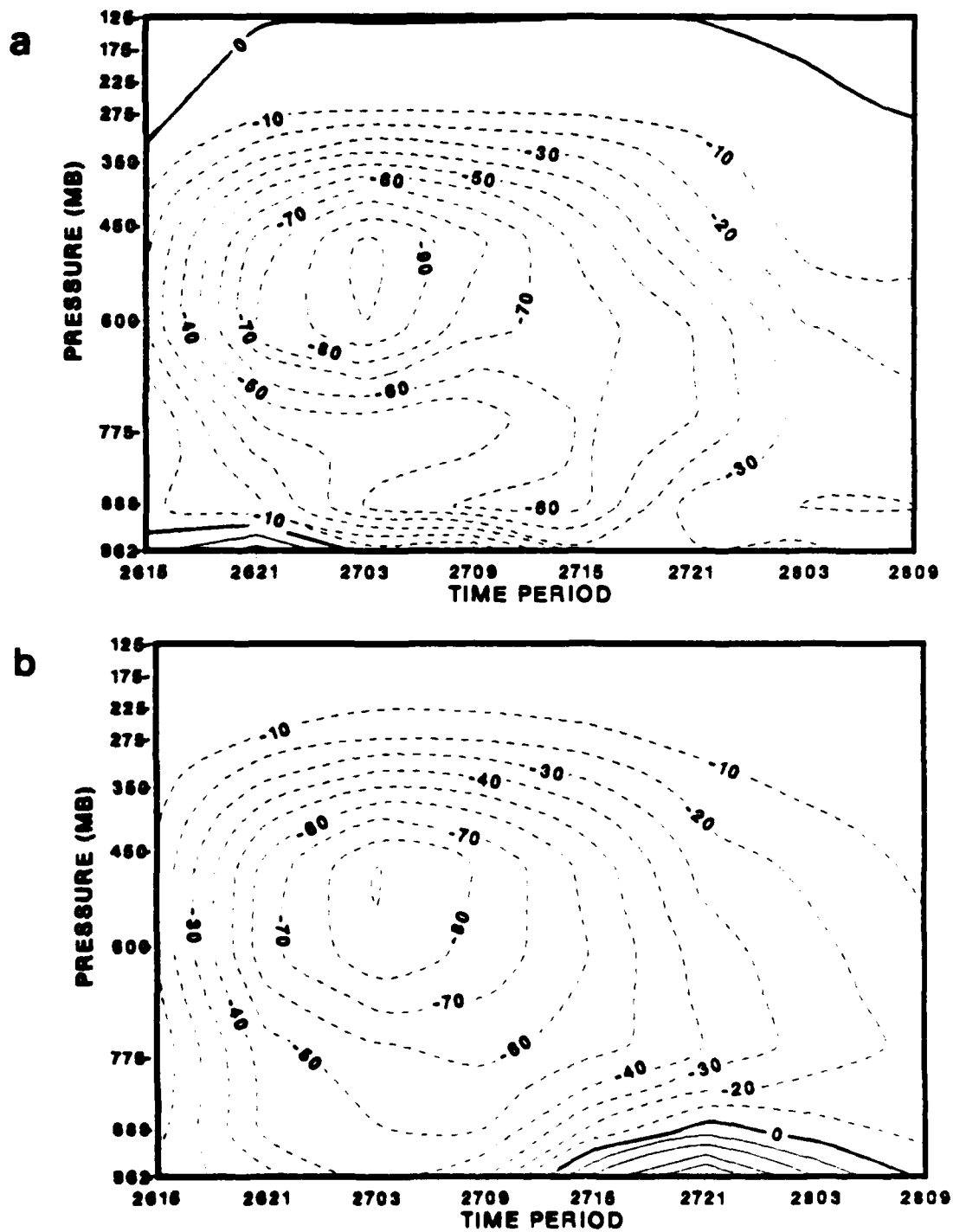


Figure 5.19 (a) Forecast moisture budget residual and (b) NORAPS archived moistening rate for 4 lat. radius. Positive negative values indicate moisture convergence divergence. Contour interval is $10 \times 10^{10} \text{ g day}^{-1}$.

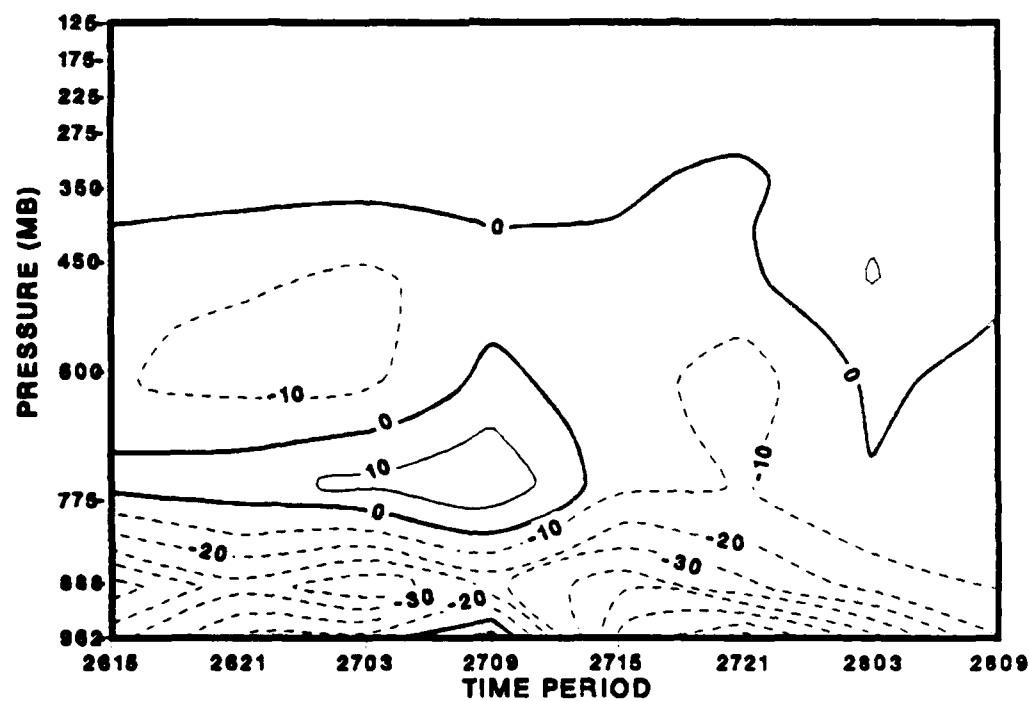


Figure 5.20 Difference of forecast moisture budget residual and
NORAPS archived moistening rate for 4° lat. radius.
Contour interval is 10×10^{-4} g g day.

precipitation rate is an accumulated 6 h total that does not include surface moisture fluxes. The diagnosed budget residual agrees very well with both the moistening rate and the area-averaged total precipitation prior to 12 GMT 27 January and after 03 GMT 28 January 1986. Peak values of 5 cm/day averaged over 4° lat. radius occur during the rapid intensification period of the storm. The diagnosed residual overpredicts the average precipitation by about 1 cm/day from 15 GMT 27 January to 03 GMT 28 January 1986.

F. SUMMARY

In summary, the heat budget demonstrates the importance of both diabatic heating and warm advection in creating a more intense surface low pressure system through warming of the budget volume. During the period of rapid storm intensification, diabatic heating appears to be the dominant factor in both the analysis and forecast. The stronger diabatic heating depicted in the NORAPS forecast case can be related to the greater predicted deepening of 4 mb during the explosive stage of the primary cyclone from 00-12 GMT 27 January 1986.

The moisture budget shows strong horizontal moisture flux convergence near the surface that is modulated by the vertical velocity field. The upward flux of heat and moisture in the PBL is also quite significant as the storm moves northward over the Atlantic coastal waters. The moisture is then transported upward through the vertical moisture flux and condenses. The latent heat released in the phase change from water vapor to liquid water is a major contributor to the energetics of the cyclone. The level in the troposphere at which latent heat is released is also an extremely important variable. A low to mid-level tropospheric maximum in the vertical heating profile, as identified in this study, should set up conditions more favorable for an explosive response. Investigations of the QE-II storm by Anthes *et al.* (1983) and Gyakum (1983b) support this reasoning. Additionally, studies by Liou and Elsberry (1985) and Elsberry *et al.* (1985) also identify a strong correlation between SLP deepening rate and the diabatic heating rate. The level and phase of the forecast diabatic heating and moistening rates are very strongly correlated. Latent heat release appears to account for a major portion of the heating in the middle troposphere during the period of explosive development offshore.

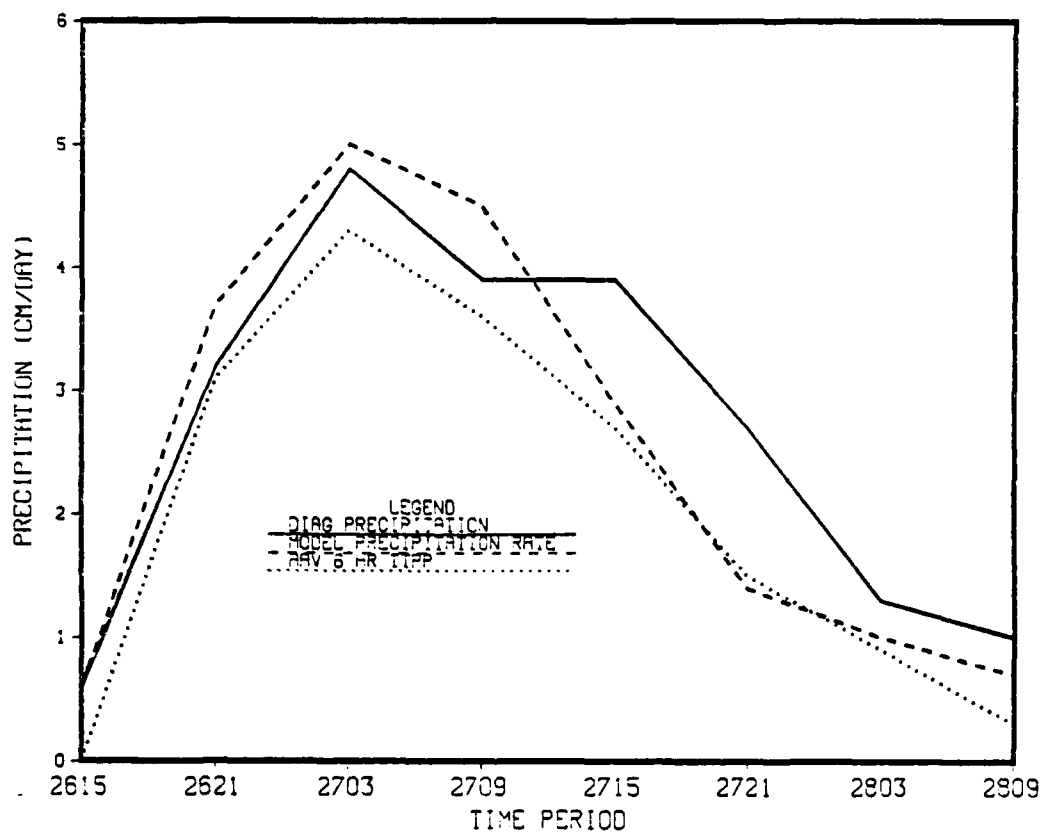


Figure 5.21. Area and column-averaged moisture budget results for 4° lat. radius. Moisture budget residual (solid), NORAPS moistening rate (dash), NORAPS area-averaged 6 h precipitation (dot). Units are cm day.

VI. CONCLUSIONS AND RECOMMENDATIONS

A. CONCLUSIONS

Physical processes that influence the formation and development of extratropical cyclogenesis occur over a broad spectrum of space and time scales. Several previous studies have suggested that mesoscale features play a leading role in distinguishing explosive cyclones from the typically less intense mid-latitude cyclone cases. The Genesis of Atlantic Lows Experiment (GALE) conducted during the winter of 1986 offered the first real opportunity to gather a research-quality data set with the spatial and temporal resolution adequate to study most mesoscale phenomena and important air-sea interaction processes. A small subset of the data collected from the GALE project was used in this study to begin addressing the question of data impact on forecast skill.

In this study, the small set of GALE data added to the initial conditions provided no significant improvement in forecast skill over the control forecast. This lack of improvement in forecast skill can be related to the fact that the 14 additional GALE soundings were downstream of the storm center in the initial conditions, rather than upstream. It is also important to note that this was a very limited data impact study. No attempt was made to improve upon the original 12-h update cycle or utilize GALE soundings that were available every 3 h. Therefore, no firm conclusions concerning the effectiveness of enhanced spatial and temporal resolution in the initial conditions can be stated with confidence.

Several of the synoptic and mesoscale physical processes identified by earlier investigators to be important in explosive cyclogenesis are evident in IOP-2. Upper-level jet streak forcing, cold-air damming with a well-defined coastal front, a pre-existing low along the front, significant sensible and latent heat fluxes and strong latent heating all play important roles in creating conditions for an explosive response. The importance of emphasizing explosive cyclogenesis as a scale-interaction problem cannot be overemphasized. Quasi-Lagrangian diagnostics were utilized as a means to assess quantitatively the relative importance of the physical processes believed to be significant in maritime explosive cyclogenesis in IOP-2. QLD budgets of mass, vorticity, heat and moisture seem to capture quite well the dynamical and thermodynamical forcing on the cyclone scale.

The mass budget reveals a two-layer structure with strong low-level convergence below a deep layer of upper-level divergence. The shallow inflow layer combined with a deeper outflow layer results in a net-vertically integrated mass loss within the atmospheric column that is consistent with the surface pressure falls during the rapid deepening phase of the coastal cyclone. The level of maximum vertical velocity remains near 500 mb throughout the developing and mature stages of the storm.

The increase of absolute vorticity at low levels during the period of rapid development (00-12 GMT 27 January) is related to vorticity convergence by the low-level lateral mass transport. In the upper troposphere, positive vorticity lateral transport into the budget volume results from the eddy mode contribution (PVA) offsetting the mean mode contribution (divergence). Large amounts of cyclonic shear vorticity are advected into the budget volume after 18 GMT 26 January 1986, when it is in the right-rear (entrance) region of a strong jet streak. A favorable upper-level divergence pattern is created that exports mass aloft and promotes the low-level convergence and spin-up of the low-level vortex discussed above. In the lower troposphere, this induced low-level convergence provides the major source of vorticity. Frictional dissipation of vorticity becomes important in the PBL during the mature phase of the cyclone and partially offsets some of the low-level vorticity spin-up. The net vorticity increase in the lower troposphere is due to the excess of vorticity convergence (generation) over frictional dissipation and a negative contribution from the tilting term. As the upper-level forcing weakens and the storm moves inland, frictional dissipation becomes more important and the cyclone weakens slightly after 12 GMT 27 January 1986.

The heat budget demonstrates the importance of both diabatic heating and warm advection in creating a more intense surface low pressure system. Upper-level warm advection and mid-level diabatic heating maxima are strongly correlated with the period of rapid intensification from 00-12 GMT 27 January 1986. The primary role of the diabatic heating is to offset adiabatic cooling and thus allow the budget volume to remain warmer than it would be without the additional source of energy. Hydrostatic considerations then dictate that a warmer column will result in a lower SLP and greater storm intensity. The greater diabatic heating in the NORAPS forecast case can be related to the greater predicted deepening of 4 mb during the explosive stage of the primary cyclone. This diabatic forcing of the vertical/lateral circulation appears to be a distinguishing feature of explosive cyclogenesis cases.

In the moisture budget, the strong horizontal moisture flux convergence near the surface is due to strong mass convergence. The upward flux of heat and moisture as the storm moves northward over the Atlantic coastal waters is also quite pronounced. These upward fluxes reduce the static stability and increase the potential instability of the atmospheric column, which permits a significantly greater response to the upper-level forcing. The moisture is transported upward through the vertical moisture flux. The latent heat released in the phase change from water vapor to liquid water is a major contributor to the energetics of the cyclone. The low to mid-level tropospheric maximum in the vertical heating profile in this study is associated with a maximum in the vertical velocity, which leads to stronger convergence and vorticity generation in the low levels of the cyclone. Investigations of the QE-II storm by Anthes *et al.* (1983) and Gyakum (1983b) support this reasoning. Additionally, studies by Liou and Elsberry (1985) and Elsberry *et al.* (1985) also identify a strong correlation between SLP deepening rate and the diabatic heating rate. Latent heat release appears to account for a major portion of the heating in the middle troposphere during the period of explosive development offshore.

In the verification of the NORAPS "operational" forecast discussed in Chapter II, SLP errors over the cold continental land mass were quite significant (4-16 mb) after only 24 h. Surface highs in these areas tended to be overpredicted (too high) while the lows were underpredicted (too high). These excessive SLP's appear to be due to poor handling of the surface processes in the cold air over land and may be responsible for significantly degraded forecast low positions beyond 36 h.

B. RECOMMENDATIONS

A better understanding of the effects of diabatic heating on mesoscale time and space scales is still required. The use of the higher spatial resolution NORAPS model is important in modeling the evolution of mesoscale features that affect the cyclone scale. Unfortunately, the small subset of mesoscale data extracted from the GALE data base for this study was insufficient to provide any positive impact.

Recommendations for future research include:

- Increase the temporal resolution of the initial conditions by using a 3-h or 6-h update cycle. Both intervals are available for the GALE data base.
- Enhance the initial conditions upstream of the storm center so the impact of the additional data can be felt downstream at the cyclone position.

APPENDIX A

NAVY OPERATIONAL REGIONAL ATMOSPHERIC PREDICTION SYSTEM-NORAPS

1. MODEL CHARACTERISTICS

NORAPS, which includes an analysis and a regional forecast model, produces high spatial resolution (typically 80 km in the western Atlantic version), short-term (36-48 hr) numerical forecasts over a limited domain. NORAPS was developed by Dr. Rich Hodur of the Naval Environmental Prediction Research Facility (NEPRF), who kindly provided the system for this research. The principle advantage of using NORAPS as opposed to a global or hemispheric model is the small spatial scale features that are resolved. This model has the additional asset of flexibility as the grid is globally relocatable, and the user may specify the dimensions and horizontal vertical resolution. Three different projections (Mercator, Lambert conformal, or polar stereographic) are available to minimize distortion in the tropics, mid-latitudes or polar regions. An additional feature is the "terrain enveloping" concept in which topography is calculated at a high horizontal resolution to incorporate the effects of the sub-grid scale features into the topographic field. A thorough discussion of NORAPS is provided by Hodur (1982, 1984).

The four major components of NORAPS are the analysis, initialization, forecast and output. The analysis component consists of acquiring different types of data (radiosonde, satellite, land and ship reports) and applying quality control checks to determine data validity. A single bad observation can have an adverse effect on the regional model if not removed prior to initialization. The next step in the analysis is to interpolate the observations to the grid. The data fields for the model are the u and v wind components, temperature, geopotential, specific humidity, surface pressure, sea-surface temperature and terrain height. A regional update cycle is used in which the 12-h NORAPS forecast, which serves as the first guess, and the latest observations are analyzed with a successive corrections technique. An exponential weighting function takes into account the distance from the observation to the grid point. The analyses are performed at 1000, 925, 850, 700, 500, 400, 300, 250, 200, 150 and 100 mb.

The purpose of the initialization phase is to approximately balance the mass and wind fields and thus suppress the growth of large amplitude inertial-gravity waves that

would contaminate the forecast fields. The static initialization procedure uses diagnostic constraints to balance the wind and mass fields by setting the horizontal divergence to zero.

The forecast component is the heart of the NORAPS model and this phase requires the majority of the computation time. The model uses the flux form of the primitive equations on a staggered grid scheme C (Arakawa and Lamb, 1977). This grid scheme has excellent geostrophic adjustment properties and group velocity characteristics (Haltiner and Williams, 1980). The vertical coordinate is sigma, which orients all coordinate surfaces parallel to the surface terrain. Thus, the vertical velocity is identically zero at the lower boundary, even in the vicinity of mountainous terrain. The vertical structure of the atmosphere is normally represented in 12 discrete layers, although as many as 19 layers may be specified. All variables (u , v , q and T) except vertical velocity are carried at the middle of each layer. A split-explicit time integration scheme is used to permit larger time steps for the slower meteorological modes, while still being able to predict all the gravity modes. The size of the time step is governed by the computational stability criterion for the horizontal resolution selected. Fourth-order advection is used for the prediction equation set to reduce errors in phase speed.

One-way influence boundary conditions are used to specify the time-dependent lateral boundary conditions on the finer mesh NORAPS model from the NOGAPS predictions. The one-way influence refers to the NOGAPS solution forcing the fine-mesh model, without the fine grid affecting the coarse grid solution. For timeliness required in operational use, these boundary conditions must be derived from an earlier forecast rather than utilizing the corresponding NOGAPS forecast from the same time. A method developed by Perkey and Kreitzberg (1976) is used to spatially interpolate the solutions near the boundary of the finer mesh. The NOGAPS time tendencies are blended with the NORAPS time tendencies over a distance of five grid points to dampen spurious reflections at the regional model boundary due to the change in grid spacing.

The output phase of NORAPS prepares the forecast data for interpolation to the standard pressure levels. The output fields can include winds, temperature, specific humidity, surface pressure, relative humidity, absolute vorticity, divergence, surface sensible and latent heat flux, and precipitation.

2. MODEL PHYSICS

The model physics contained in NORAPS constitute a crucial component in this experiment. The treatment of diabatic processes is important to simulate the effect on the atmosphere of the surface fluxes across the air-sea interface. NORAPS includes representations of the following physical processes: (i) dry convective adjustment; (ii) surface friction; (iii) cumulus parameterization; (iv) large-scale precipitation; and (v) radiative transfer processes.

a. Planetary Boundary Layer

The effects of the PBL should be included in any numerical model to physically simulate maritime cyclogenesis on the time scales of more than a few hours (Anthes *et al.*, 1983). The NORAPS planetary boundary layer (PBL), which is constrained to be within the bottom three layers of the model atmosphere, is well mixed in temperature, momentum and moisture. Interactions occurring between the lower boundary and overlying atmospheric layer provide sources and sinks for momentum, heat and moisture.

The NORAPS PBL parameterization follows Deardorff (1972). After the later mean values of V , θ and q are known, a bulk Richardson number (Ri_B) is computed to determine the stability of the PBL.

$$Ri_B = gh(\theta_{vm} - \theta_{vs})/U_m^2, \quad (A.1)$$

where g is the gravitational constant, h is the PBL height, θ_v is the virtual potential temperature, subscript s denotes surface values and subscript m denotes mean PBL values. For unstable conditions ($Ri_B < 0$), i.e., strong winds, daytime heating over land surfaces and strong mixing, a predictive equation for the PBL height (h) proposed by Stull (1976) is used. The rate of change of the PBL height is related to the surface sensible heat flux, mean PBL wind speed, the large-scale vertical motion and cloud-induced subsidence. For stable or neutral conditions ($Ri_B > 0$), i.e., light winds, nighttime over land with weak mixing, a predictive equation for the PBL height after Nieuwstadt and Tennekes (1981) is used. Transfer (drag) coefficients for heat (C_θ) and friction (C_u) are computed from empirical formulas that include the stability dependence via the Ri_B . Surface fluxes of moisture, heat and momentum (A.2, A.3, and A.4) are computed using the bulk aerodynamic formulas, which assume the transfer coefficients are functions of Ri_B and h :

Sensible heat flux,

$$H_s = \rho c_p \overline{(w\theta)} = \rho c_p u_* c_\theta (\theta_s - \theta_m) \quad (A.2)$$

Latent heat flux,

$$H_l = L_v \overline{(wq)} = \rho c_p u_* c_\theta (q_s - q_m) \text{ and} \quad (A.3)$$

Surface stress,

$$\tau = \rho u_*^2 = \rho u_m^2 c_u^2 \quad (A.4)$$

where ρ is the density of air, u_* is the frictional velocity, θ is the potential temperature, L_v is the latent heat of vaporization, w is the vertical velocity, q is the specific humidity, c_p is the specific heat of dry air at constant pressure, subscript m denotes the mean PBL value and subscript s denotes the surface value. The PBL is constrained to extend through at least the bottom layer of the model (approximately 40 mb) to avoid extrapolation problems in determining mean PBL quantities.

Another feature of the NORAPS PBL is that seasonally dependent climatological values of albedo, sea ice, ground wetness and surface roughness are specified. A predictive equation for the ground temperature after Blackadar (1979) is used to model the lower boundary condition for the temperature over land. The sea-surface temperatures are assumed to be constant over the forecast period, which is valid for short-range forecasts.

b. Cumulus Parameterization

The NORAPS model uses a modified version of the Kuo (1965) cumulus parameterization scheme. This version links the convection to the PBL by requiring moisture convergence in the PBL. By contrast, the original Kuo version required net moisture convergence in the entire column before convection was initiated. The moisture convergence is

$$M_t = 1/g \nabla \cdot (q_m \pi V_m) (1 - \sigma_{pbl}) + \rho_s \overline{(wq)}_s \quad (A.5)$$

where the first term on the right side is the vertically-integrated moisture convergence and the second term is the surface moisture flux. Convection is assumed to occur when $M_t > 4.0 \times 10^{-6} \text{ gm m}^{-2} \text{ s}^{-1}$ and the equivalent potential temperature decreases with height (conditionally unstable) from the PBL to the first model layer above the

PBL The final constraint is that deep convection cannot occur if the lifting condensation level (LCL) is above the PBL. This scheme partitions the moisture transport into two fractions: the first (hM_q) serves to moisten the environment to saturation conditions through the cloud layer, and the second ($(1-h)M_q$) condenses and falls instantaneously as rain.

In addition to large-scale advection, temperature and moisture changes at any level are caused by convective clouds. It is assumed that the temperature of the cloud is warmer than the environment. Cloud production, which is the ratio of the water vapor available to the water vapor needed to form the cloud, is computed for each gridpoint. The fractional cloud area is used to adjust the layer mean temperature and moisture to account for the presence of clouds.

c. Large-Scale Precipitation

Large-scale precipitation (non-convective) can occur when supersaturation is achieved at any level. The excess moisture is allowed to fall into the next layer and increase the moisture content of that layer, or continue to fall if that layer is already supersaturated. Precipitation occurs only when the air is saturated from the cloud to the ground. Convective precipitation occurs according to the modified Kuo cumulus convection scheme discussed in the previous section. The precipitation routines are only called every four time steps for computational efficiency. The heating and moistening rates are then spread evenly over subsequent time steps until the next call to these routines.

d. Radiation

The incorporation of solar radiation into numerical models is essential for prediction of surface temperatures and the cooling rates at cloud tops that may deepen cloud layers. The radiation parameterization in NORAPS follows Katayama (1974) for short-wave radiation and Sasamori (1968) for long-wave radiation.

APPENDIX B

DATA ACQUISITION AND PROCESSING

1. DATA ACQUISITION

The NORAPS analyses and forecast fields for this budget study were obtained from Dr. C.-S. Liou at the Naval Postgraduate School through liaison with the Naval Environmental Prediction and Research Facility (NEPRF). Dr. Liou is also responsible for developing the data acquisition and processing programs discussed below. The data on 9-track tape are transferred to the mass storage device on the NPS IBM 3033. The unprocessed NORAPS data fields are on a 109×82 grid at 12 sigma levels. A horizontal grid spacing of 80 km is used. A slightly smaller window (79×69 with 11 pressure levels) is extracted to accommodate easier storage and access from the disk. The analysis base time for the model run is 12 GMT 26 January 1986. A 48-hour model forecast is produced with output fields generated every six hours to 12 GMT 28 January 1986. NORAPS analyses are available every 12 hours from 00 GMT 26 January until 12 GMT 28 January 1986.

The Lambert conformal projection used for the output fields is ideally suited for mid-latitudes since there is minimum distortion between the true parallels of 30° and 60° N. The Lambert conformal map is a bi-conic, secant type of projection that preserves angles when projecting the earth's surface onto a plane surface.

To obtain the data for the budget programs, several preliminary steps are necessary. First, surface and upper air fields are plotted using DISSPLA, which is a software package available on the NPS IBM 3033 mainframe. The user must be aware that DISSPLA requires a rectangular region of latitude longitude points to be specified. Because NORAPS output fields are specified in Lambert conformal coordinates, DISSPLA would perform what amounts to a double transformation and produce a distorted and inaccurate field. Three separate steps are incorporated in a program called DISPLA NORAPS to produce a plot with correct positioning on the map projection. First, a subplot area is specified and a blanking routine is used to truncate the lower curved boundary that is standard for the Lambert conformal plot. This step merely serves to ensure a rectangular plot is produced. Second, the contouring and a border are drawn that is separate from the projection and geography routines. Third, the Lambert conformal projection, i.e., the latitude and longitude

lines, and the geography are added. Integral to each of these three separate steps is the statement, `CALL ENDGR(0)`, which terminates that particular block of code. This statement ends a subplot but remains on the same physical page, which allows other plots, such as the contouring and projection in this case, to be drawn on the same physical page.

It is sometimes necessary to retrieve data from the output grid to determine the center of a low center in the (i,j) Lambert conformal coordinates. The `NDATA FORTRAN` program can be easily modified to retrieve output data for any user-specified field and level. Once the appropriate data fields are obtained, a program called `TRANS FORTRAN` is used to transform the (i,j) Lambert conformal coordinate to a latitude and longitude on the earth's surface. The corresponding latitude and longitude of the low center are entered into an interactive program (called `STORMO FORTRAN`) at each time period to compute the speed and direction of the cyclone center. A forward difference is used to compute the speed for the first and last time periods, while a centered difference is used for the other time periods. The low center location, direction and speed are then entered at the end of the budget programs as required parameters for the budget calculations.

2. DESCRIPTION OF WIND ADJUSTMENT

Because all `NORAPS` output fields are given in Lambert conformal coordinates, the wind directions will be distorted from the true direction away from the central meridian of the conformal grid. This central or true meridian, which is 80°W in this case, is parallel to the y-axis in a Cartesian coordinate system. A subroutine called `WNDADJ` makes the necessary transformations to provide the true wind direction on the earth's surface. The only information required to make this transformation is the Lambert conformal coordinates of the pole point, which are 40.0 (x-coordinate) and -44.986 (y-coordinate). Equations (B.1) and (B.2) are used to transform the Lambert conformal wind direction components, denoted u' and v' :

$$U = u' \cos(\theta) - v' \sin(\theta) \quad (\text{B.1})$$

$$V = v' \cos(\theta) + u' \sin(\theta) \quad (\text{B.2})$$

where U and V are the true horizontal wind direction components and the angle $\theta = \tan^{-1}(x_p - x, y - y_p)$, where x_p, y_p are the Lambert conformal pole point coordinates and x, y are the Lambert conformal (i,j) grid point that is being transformed. The convention for the angle (θ), which is the angle that the Lambert conformal coordinate axes must be rotated to become true directional axes, is positive for a counter-clockwise direction and negative for a clockwise rotation.

3. CONVENTIONS FOR NORAPS FIELDS AND BUDGET PROGRAMS

The NORAPS output fields are presented in a right-hand coordinate system with the (1,1) grid point being the southwest corner of the grid. The column value increases eastward and the row value increases northward. However, these NORAPS data fields are read in for the budget programs in a different manner. A left-hand coordinate system is used for reading in the fields in the HOJO subroutine, with the (1,1) grid point at the northwest corner. The column value increases eastward and the row value increases southward. The pole point is referenced in this coordinate system since wind adjustments are performed after the data fields have been read in.

The latitude convention in the budget program is positive north and negative south; longitude is positive west of Greenwich and (360-longitude) east of Greenwich. The convention for the normal wind components in the budget programs are positive outward and negative inward.

Another convention the user should be aware of is the method of defining latitude and longitude in the DISSPLA software package for plotting the NORAPS output fields. Longitudes west (east) of Greenwich are negative (positive). The latitudes are positive for north and negative for south. These are arguments to be included in the subroutines GRAF and MAPGR.

APPENDIX C

"OPERATIONAL" NORAPS MODEL SPECIFICATIONS

Problems identified in the existing NORAPS model by this study and in an earlier study by Rau (1986) have resulted in several modifications to make the model output more realistic. To distinguish this model from the previous NORAPS model output, the new output fields are referred to as the "operational" analysis and forecasts respectively. In this study, the "operational" NORAPS output is utilized as the control study for quasi-Lagrangian diagnostics and in the evaluation of model forecast skill. The updated NORAPS model includes the following modifications:

- Corrections to the time-step errors of adding only half of the diabatic heating and moistening rates to the thermodynamic and moisture prognostic equations;
- Changes to the vertical interpolation scheme for computing vertical fluxes from a harmonic-mean scheme to a vertical linear-p interpolation in σ ;
- The PBL adjustment routine is now called every time step;
- Corrections to errors in the PBL adjustment so that the adjustment will be applied to current time variables;
- The convergence criterion has been made more restrictive in the large-scale precipitation computation; and
- The physical package is called every 4 time steps rather than every 8 time steps;

LIST OF REFERENCES

- Anthes, R. A., and D. Keyser, 1979: Tests of a fine-mesh model over Europe and the United States. *Mon. Wea. Rev.*, **107**, 963-984.
- , N. L. Seaman and T. T. Warner, 1980: Comparisons of numerical simulations of the planetary boundary layer by a mixed-layer and a multi-level model. *Mon. Wea. Rev.*, **108**, 363-376.
- , Y. H. Kuo and J. R. Gyakum, 1983: Numerical simulation of a case of explosive maritime cyclogenesis. *Mon. Wea. Rev.*, **111**, 1174-1188.
- Arakawa, A., and V. R. Lamb, 1977: Computational design of the basic dynamic process of the UCLA general circulation models. *Methods in Computational Physics*, **17**, Academic Press, 173-265.
- Austin, J. M., 1941: Favorable conditions for cyclogenesis near the Atlantic coast. *Bull. Amer. Meteor. Soc.*, **22**, 270-272.
- Baker, D. G., 1970: A study of high pressure ridges to the east of the Appalachian mountains. Ph.D. dissertation, Massachusetts Institute of Technology, Cambridge, Ma., 127 pp.
- Blackadar, A. K., 1979: High resolution models of the planetary boundary layer. *Advances in Environmental Science and Engineering*, Vol. 1, Gordon and Breach, 30-85.
- Bosart, L. F., C. J. Vaudo and J. H. Helsdon, 1972: Coastal frontogenesis. *J. Appl. Meteor.*, **11**, 1236-1258.
- , 1975: New England coastal frontogenesis. *Quart. J. Roy. Meteor. Soc.*, **101**, 957-978.
- , 1981: The Presidents' Day snowstorm of 18-19 February 1979: A subsynoptic scale event. *Mon. Wea. Rev.*, **109**, 1542-1566.
- , and S. C. Lin, 1985: A diagnostic analysis of the Presidents' Day storm of February 1979. *Mon. Wea. Rev.*, **112**, 2148-2177.
- Budyko, M. I., 1974: *Climate and Life*. Academic Press, New York, N.Y., 508 pp.
- Calland, W. E., 1983: Quasi-Lagrangian diagnostics applied to an extratropical explosive cyclogenesis in the North Pacific. M.S. Thesis, Naval Postgraduate School, Monterey, Ca., 152 pp.
- Chang, C. B., D. J. Perkey and C. W. Kreitzberg, 1984: Latent heat induced energy transformations during cyclogenesis. *Mon. Wea. Rev.*, **112**, 357-366.
- Chen, T. -S., C. -B. Chang and D. J. Perkey, 1985: Synoptic study of a medium-scale oceanic cyclone during AMTEX '75. *Mon. Wea. Rev.*, **113**, 349-361.

- Colucci, S.J., 1976: Winter cyclone frequencies over the eastern United States and adjacent western Atlantic, 1964-1973. *Bull. Amer. Meteor. Soc.*, 57, 548-553.
- Conant, P. R., 1982: A study of east-coast cyclogenesis employing quasi-Lagrangian diagnostics. M.S. Thesis, Naval Postgraduate School, Monterey, Ca., 102 pp.
- Cook, W. A., 1983: A quasi-Lagrangian diagnostic investigation of rapid cyclogenesis in a polar air stream. M.S. Thesis, Naval Postgraduate School, Monterey, Ca., 147 pp.
- Deardorff, J. W., 1972: Parameterization of the planetary boundary layer for use in general circulation models. *Mon. Wea. Rev.*, 100, 93-106.
- Elsberry, R. L., C. H. Wash, C-S. Liou and J. E. Peak, 1985: Observational-numerical study of maritime extratropical cyclones using FGGE data. Department of Meteorology, Naval Postgraduate School, Monterey, Ca., Report Number NPS-63-85-001, 40 pp.
- Forbes, G. S., R. A. Anthes and D. W. Thomson, 1984: Synoptic and mesoscale aspects of an Appalachian ice storm associated with cold-air damming. (unpublished manuscript).
- Gyakum, J. R., 1983a: On the evolution of the QE-II Storm. I: Synoptic aspects. *Mon. Wea. Rev.*, 111, 1137-1155.
- , J. R., 1983b: On the evolution of the QE-II Storm. II: Dynamic and thermodynamic structure. *Mon. Wea. Rev.*, 111, 1156-1173.
- Haltiner, G. J., and R. T. Williams, 1980: *Numerical Prediction and Dynamic Meteorology, Second Edition*, John Wiley and Sons, 226-230.
- Harrold, T. W., 1973: Mechanisms influencing the distributions of precipitation within baroclinic disturbances. *Quart. J. Roy. Meteor. Soc.*, 99, 232-251.
- Hodur, R. M., 1982: Description and evaluation of NORAPS: The Navy Operational Regional Atmospheric Prediction System. *Mon. Wea. Rev.*, 110, 1591-1602.
- , 1984: A numerical study of the Pacific polar low. Ph.D. Thesis, Department of Meteorology, Naval Postgraduate School, Monterey, Ca., 125 pp.
- Johnson, D. R., and W. K. Downey, 1975: Azimuthally averaged transport and budget equations for storms: QuasiLagrangian Diagnostics. *Mon. Wea. Rev.*, 103, 967-979.
- Kaplan, M., J. W. Zack, V. C. Wong and J. J. Tuccillo, 1982: A sixth order mesoscale atmospheric simulation system applicable to research and real-time forecasting problems. In *Collection of Lecture Notes on Mesoscale Models*, Y.K. Sasaki, S. Ray, and L.P. Chang, Eds., Cooperative Institute for Mesoscale Meteorological Studies, University of Oklahoma, Norman, 35-82.
- Kocin, P. J., and L. W. Uccellini, 1984: A review of major East Coast snowstorms. *Preprints, 10th Conference on Weather Forecasting and Analysis*, Amer. Meteor. Soc., Clearwater Beach, Fl., 189-198.

- Kuo, H. L., 1965: On formation and intensification of tropical cyclones through latent heat release by cumulus convection. *J. Atmos. Sci.*, 22, 40-63.
- LeMoyné, J., 1982: The Ocean Ranger's night of death. *Newsweek*, Mr 1, 99, 48.
- Liou, C.-S., and R. L. Elsberry, 1985: Physical processes in prediction of explosive maritime cyclogenesis. *Preprints of Seventh Conference on Numerical Weather Prediction*, Amer. Meteor. Soc., Boston, Ma., 212-218.
- O'Brien, J. J., 1970: Alternative solutions to the classical vertical velocity problem. *J. Appl. Meteor.*, 2, 197-203.
- Pagnotti, V., and L.F. Bosart, 1984: Comparative diagnostic case study of east coast secondary cyclogenesis under weak versus strong synoptic-scale forcing. *Mon. Wea. Rev.*, 112, 5-30.
- Petterssen, S., 1956: *Weather Analysis and Forecasting, Vol. 1*. 2nd Ed., McGraw-Hill, New York, N.Y., 428 pp.
- Rau, R. E., 1986: Heat and moisture budgets of an extratropical cyclone based on NORAPS analysis and forecasts. M.S. Thesis, Naval Postgraduate School, Monterey, Ca., 136 pp.
- Roebber, P. J., 1984: Statistical analysis and updated climatology of explosive cyclogenesis. *Mon. Wea. Rev.*, 112, 1577-1589.
- Rogers, E., and L. F. Bosart, 1986: An investigation of explosive deepening oceanic cyclones. *Mon. Wea. Rev.*, 114, 702-717.
- Sanders, F., and J. R. Gvakum, 1980: Synoptic-dynamic climatology of the "Bomb". *Mon. Wea. Rev.*, 108, 1589-1606.
- Sasamori, T., 1968: The radiative cooling calculation for application to general circulation models. *J. Appl. Met.*, 7, 721-729.
- Shapiro, M. A., 1983: Mesoscale weather systems of the Central United States. *The National Storm Program, Scientific and Technological Bases and Major Objectives*, UCAR, Boulder, Co., Section 3.1.
- Stull, R. B., 1976: Mixed-layer depth model based on turbulent energetics. *J. Atmos. Sci.*, 33, 1268-1278.
- Uccellini, L. W., R. A. Peterson, P. J. Kocin, M. J. Kaplan, J. W. Zack and V. C. Wong, 1983: Mesoscale numerical simulations of the Presidents' Day cyclone: Impact of sensible and latent heating on the pre-cyclogenetic environment. In *Preprints, Sixth Conference on Numerical Weather Prediction*, Omaha, Nebraska, Amer. Meteor. Soc., Boston, Ma., 45-52.
- , 1984: Comments on "Comparative diagnostic case study of east coast secondary cyclogenesis under weak versus strong synoptic-scale forcing." *Mon. Wea. Rev.*, 112, 2540-2543.

- , P. J. Kocin, R. A. Peterson, C. H. Wash and K. F. Brill. 1984: The Presidents' Day cyclone of 18-19 February 1979: Synoptic overview and analysis of the subtropical jet streak influencing the pre-cyclogenetic period. *Mon. Wea. Rev.*, 112, 31-55.
- , D. Keyser, K. F. Brill and C. H. Wash. 1985: The Presidents' Day cyclone of 18-19 February 1979: Influence of upstream trough amplification and associated tropopause folding on rapid cyclogenesis. *Mon. Wea. Rev.*, 113, 962-988.
- Wash, C. H.. 1978: Diagnostics of observed and numerically simulated extratropical cyclones. Ph.D. Thesis, Department of Meteorology, University of Wisconsin. 215 pp.

INITIAL DISTRIBUTION LIST

	No. Copies
1. Defense Technical Information Center Cameron Station Alexandria, VA 22304-6145	2
2. Library, Code 0142 Naval Postgraduate School Monterey, CA 93943-5002	2
3. Chairman, Code 63Rd Department of Meteorology Naval Postgraduate School Monterey, CA 93943-5000	1
4. Chairman, Code 68 Department of Oceanography Naval Postgraduate School Monterey, CA 93943-5000	1
5. Professor R. Elsberry, Code 63Es Department of Meteorology Naval Postgraduate School Monterey, CA 93943-5000	4
6. Professor C.-S. Liou, Code 63Lq Department of Meteorology Naval Postgraduate School Monterey, CA 93943-5000	2
7. Professor C. Wash. Code 63Wx Department of Meteorology Naval Postgraduate School Monterey, CA 93943-5000	1
8. LT Daniel J. Soper Naval Western Oceanography Center Box 113 Pearl Harbor, HI 96860-5050	2
9. Director, Naval Oceanography Division Naval Observatory 34th and Massachusetts Avenue NW Washington, DC 20390	1
10. Commander Naval Oceanography Command NSTL Station Bay St. Louis, MS 39522	1
11. Commanding Officer Naval Oceanographic Office NSTL Station Bay St. Louis, MS 39522	1
12. Commanding Officer Fleet Numerical Oceanography Center Monterey, CA 93943	1

13. Commanding Officer
Naval Ocean Research and Development Activity
NSTL Station
Bay St. Louis, MS 39522 1
14. Commanding Officer
Naval Environmental Prediction Research Facility
Monterey, CA 93943 1
15. Chairman, Oceanography Department
U.S. Naval Academy
Annapolis, MD 21402 1
16. Chief of Naval Research
Naval Ocean Research and Development Activity
800 N. Quincy Street
Arlington, VA 22217 1
17. Commanding Officer
Naval Eastern Oceanography Center
Naval Air Station
Norfolk, VA 23511 1
18. Commanding Officer
Naval Western Oceanography Center
Box 113
Pearl Harbor, HI 96860-5050 1
19. Commanding Officer
Naval Oceanography Command Center, Rota
Box 31
FPO San Francisco, CA 09540 1
20. Commanding Officer
Naval Oceanography Command Center, Guam
Box 12
FPO San Francisco, CA 96630 1
21. Dr. R. Hodur
Naval Environmental Prediction Research Facility,
Monterey, CA 93943 1

END

9-87

Dtic